AD-A153 262 RUNWAY RUBBER REMOVAL SPECIFICATION DEVELOPMENT: FIELD 1/2
EVALUATION PROCEDU..(U) AIR FORCE ENGINEERING AND
SERVICES CENTER TYNDALL AFB FL ENGI..
UNCLASSIFIED R G MCKEEN ET AL. JUL 84 AFESC/ESL-TR-84-40 F/G 1/5 NL

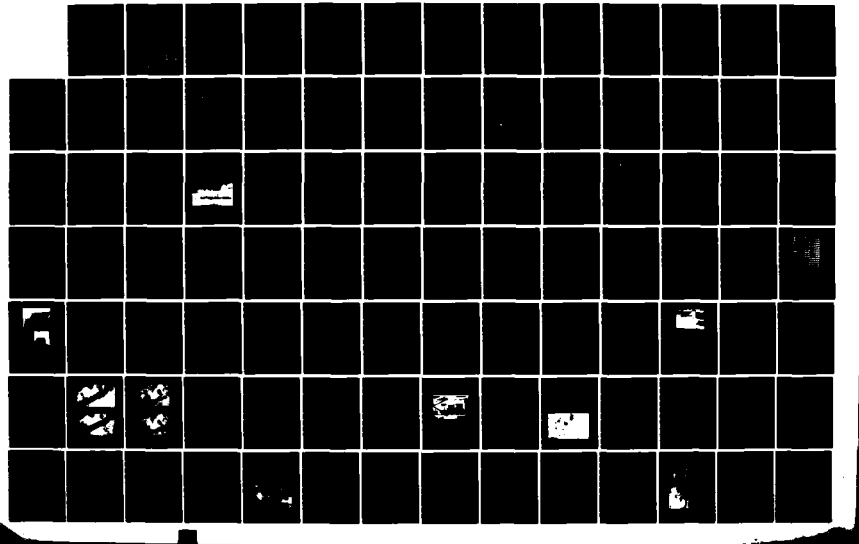

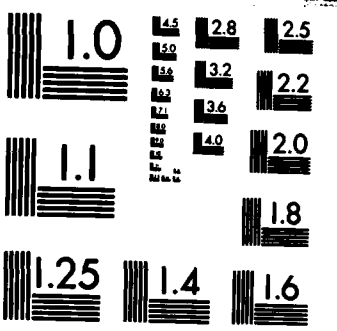

(6)

DOT/FAA/PM-84/27
ESL-TR-84-40

and Maintenance Service
Washington, D.C. 20591

Runway Rubber Removal Specification Development: Field Evaluation Procedures Development

R. Gordon McKeen
Lary R. Lenke
Richard A. Graul

New Mexico Engineering
Research Institute
Box 25, University of New Mexico
Albuquerque, New Mexico 87131

July 1984

U.S. Department of Transportation
Federal Aviation Administration

Department of Defense
USAF Engineering & Services Center

NOTICE

This document is disseminated under the sponsorship of the Department of Transportation in the interest of information exchange. The United States Government assumes no liability for the contents or use thereof.

The United States Government does not endorse products or manufacturers. Trade or manufacturer's names appear herein solely because they are considered essential to the object of this report.

Technical Report Documentation Page

1. Report No.	2. Government Accession No.	3. Recipient's Catalog No.
DOT/FAA/PM-84/27	AD-A153262	

4. Title and Subtitle	5. Report Date
Runway Rubber Removal Specification Development: Field Evaluation Procedures Development	July 1984
	6. Performing Organization Code
	8. Performing Organization Report No.
7. Author(s)	ESL-TR-84-40
Larry Lenke, Gordon McKeen, Richard Graul	
9. Performing Organization Name and Address	10. Work Unit No. (TRAIS)
New Mexico Engineering Research Institute and Air Force Engineering Services Center Tyndall Air Force Base, Florida 32402	11. Contract or Grant No.
	13. Type of Report and Period Covered
12. Sponsoring Agency Name and Address	
U.S. Department of Transportation Federal Aviation Administration Program Engineering and Maintenance Service Washington, D.C. 20591	14. Sponsoring Agency Code APM-740

15. Supplementary Notes

16. Abstract

The phenomenon of runway touchdown zone rubber buildup is a potentially hazardous problem. Rubber buildup covers the runway surface and occludes the surface texture. This results in reduced wet friction coefficient between the runway pavement and the aircraft tires.

Methods and equipment are available for evaluating the wet friction coefficient; however, these methods are expensive and require highly trained personnel. Therefore, most airport and airbase managers rely exclusively on visual impressions on rubber buildup in lieu of quantitative measurements.

Nonetheless, quantitative evaluation techniques are desireable for evaluating rubber buildup. An extensive literature review suggests that pavement surface texture measurement techniques may be indicative of rubber buildup and resultant reduction in wet friction coefficient. Rubber buildup alters the texture properties of a runway as well as the frictional coefficient.

A suggested field evaluation experiment is described in this report to ascertain which of five selected texture measurement techniques are indicative of reduced friction values in pavement areas with rubber buildup. This field experiment is designed to provide quantitative methods for ascertaining rubber buildup. This experiment will also aid in the development of contract specifications for rubber removal.

17. Key Words		18. Distribution Statement
Runway Pavement	Texture Measurement	This document is available to the public through the National Technical Information Service Springfield, Virginia 22161.
Friction	Friction Measurement	
Rubber Buildup	Mu-Meter	
Rubber Removal	Stereophotography	
Specification		

19. Security Classif. (of this report)	20. Security Classif. (of this page)	21. No. of Pages	22. Price
UNCLASSIFIED	UNCLASSIFIED	135	

Form DOT F 1700.7 (8-72) Reproduction of completed page authorized

PREFACE

The authors extend their appreciation to the following individuals at the New Mexico Engineering Research Institute for their contributions during this effort. The authors wish to thank: Dr. Badru Kiggundu, Ms. Betty Humphrey, and Dr. Dennis Zallen for their initial efforts; Dr. Ray Pavlovich for his assistance in the statistical design of the field experiment; Mr. Steven Scales for all his technical efforts during the development phase of the Mu-Meter support equipment and water distribution equipment; Mr. Vince Cassino, Mr. Dean Hitzelberger, Mr. Tommy Escobedo, and Ms. Ginger Kiscaden for their support during laboratory evaluation of the various field test procedures; Ms. Kelly Lovelady and Mr. Scott Royster for their technical support; Mr. Bruce Moore for his aid in the evaluation of the stereophotographic techniques; Mr. Bill LaRue, Mr. Rick Yaple, and Mr. Jack Malm for their administrative and editorial support.

Additional apreciation is extended to: Mr. Tom Morrow of the FAA Engineering and Specifications Division and to Mr. H. Daiutolo and Mr. H. Jackson at the FAA Technical center for the use of the Mu-Meter and tow vehicle during this research effort; Mr. James Murfee and Mr. Fred Horn, project managers for AFESC and FAA, for their help and encouragement.

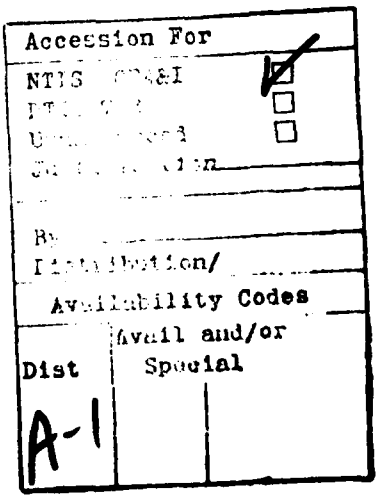

METRIC CONVERSION FACTORS

Approximate Conversions to Metric Measures

Symbol	When You Know	Multiply by	To Find	Symbol
	LENGTH			
in	inches	*2.5	centimeters	cm
ft	feet	30	centimeters	cm
yd	yards	0.9	meters	m
mi	miles	1.6	kilometers	km
	AREA			
in^2	square inches	6.5	square centimeters	cm^2
ft^2	square feet	0.09	square meters	m^2
yd^2	square yards	0.8	square meters	m^2
mi^2	square miles	2.6	square kilometers	km^2
	acres	0.4	hectares	ha
	MASS (weight)			
oz	ounces	28	grams	g
lb	pounds	0.45	kilograms	kg
	short tons (2000 lb)	0.9	tonnes	t
	VOLUME			
tsp	teaspoons	5	milliliters	ml
Tbsp	tablespoons	15	milliliters	ml
fl oz	fluid ounces	30	milliliters	ml
c	cups	0.24	liters	l
pt	pints	0.47	liters	l
qt	quarts	0.95	liters	l
gal	gallons	3.8	liters	l
ft^3	cubic feet	0.03	cubic meters	m^3
yd^3	cubic yards	0.76	cubic meters	m^3
	TEMPERATURE (exact)			
°F	Fahrenheit temperature	5/9 (after subtracting 32)	Celsius temperature	°C

*1 in = 2.54 (exactly). For other exact conversions and more detailed tables, see NBS Misc. Publ. 286, Units of Weights and Measures, Price $2.25, SD Catalog No. C13.10:286.

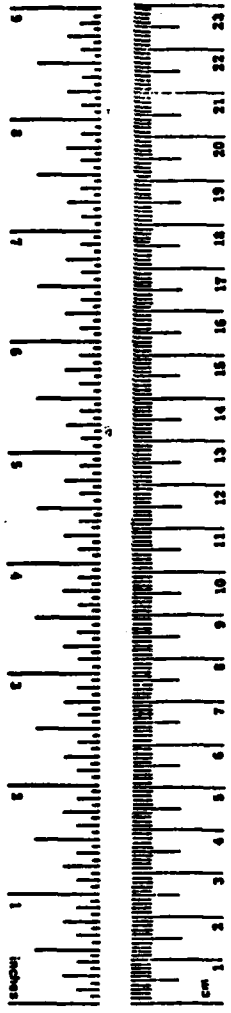

Approximate Conversions from Metric Measures

Symbol	When You Know	Multiply by	To Find	Symbol
	LENGTH			
mm	millimeters	0.04	inches	in
cm	centimeters	0.4	inches	in
m	meters	3.3	feet	ft
m	meters	1.1	yards	yd
km	kilometers	0.6	miles	mi
	AREA			
cm^2	square centimeters	0.16	square inches	in^2
m^2	square meters	1.2	square yards	yd^2
km^2	square kilometers	0.4	square miles	mi^2
ha	hectares (10,000 m^2)	2.5	acres	
	MASS (weight)			
g	grams	0.035	ounces	oz
kg	kilograms	2.2	pounds	lb
t	tonnes (1000 kg)	1.1	short tons	
	VOLUME			
ml	milliliters	0.03	fluid ounces	fl oz
l	liters	2.1	pints	pt
l	liters	1.06	quarts	qt
l	liters	0.26	gallons	gal
m^3	cubic meters	35	cubic feet	ft^3
m^3	cubic meters	1.3	cubic yards	yd^3
	TEMPERATURE (exact)			
°C	Celsius temperature	9/5 (then add 32)	Fahrenheit temperature	°F

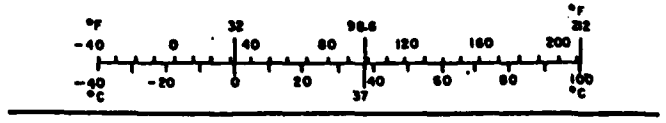

CONTENTS

CONTENTS (CONCLUDED)

ILLUSTRATIONS

ILLUSTRATIONS (CONTINUED)

ILLUSTRATIONS (CONCLUDED)

TABLES

I. INTRODUCTION

With the advent of high-speed and heavy gross weight aircraft, the phenomenon of runway touchdown zone rubber buildup has become a potentially hazardous problem. Rubber buildup tends to cover the surface and occlude the surface voids of the pavement. This buildup is of little consequence during normal airfield operations when the pavement is dry. However, during wet pavement operations, the friction developed between the aircraft tires and the pavement surface is adversely affected. Rubber on rubber yields a high coefficient of friction when dry, but is markedly reduced when wet.

Normal operation of an aircraft at landing requires an adequate frictional value between tire and pavement to provide proper spin-up of the aircraft tires. Spin-up is the process of rotating the tires from zero velocity to touchdown velocity during the immediate moment following touchdown. It is this rapid spin-up which causes rubber buildup.

Aircraft brake design is such that braking efficiency is reduced if the tires are not spinning at a velocity equal to that of the aircraft. This brake design is termed an antiskid device. Insufficient friction between tire and pavement, resulting in a lack of spin-up or tire rotation during landing, can result in a lack of sufficient braking for the aircraft. This in turn can lead to a skidding accident whereby the pilot is unable to brake the aircraft resulting in a departure from the runway. Considerable damage and/or loss of life can result in these instances.

Methods are available to remove rubber from runways (Refs. 1, 2, and 3); these include high-pressure water blast and chemical techniques. Methods are also available for evaluating the pavement friction (or traction) characteristics (Refs. 1, 4, and 5). The Federal Aviation Administration (FAA), United States Air Force (USAF), and National Aeronautics and Space Administration

---

1. Horne, W. B., **Evaluation of High-Pressure Water Blast With Rotating Spary Bar for Removing Paint and Rubber Deposits From Airport Runways, and Review of Runway Slipperiness Problems Created by Rubber**, NASA TMX-72797, National Aeronautics and Space Administration, Hampton, Virginia, 1975.

2. Carpenter, S. H., and Barenberg, E. J., **Rubber Removal From Porous Friction Coarse**, DOT/FAA/PM-83/31, U.S. Department of Transportation, Federal Aviation Administration, Washington, D.C., 1983.

3. McKeen, R. G., and Lenke, L. R., **Alternatives for Rubber Removal From Porous Friction Surfaces**, DOT/FAA/PM-84/28, U.S. Department of Transportation, Federal Aviation Administration, Washington, D.C., 1984.

4. Burk, D. O., **Effectiveness of Rubber Removal Processes at Six Air Force Bases**, AFCEC Memorandum 4-77, Air Force Civil Engineering Center, Tyndall Air Force Base, Florida, 1977.

5. Grisel, C., **A Summary of Runway Friction Changes Due to High-Pressure Water-Jet Cleaning Operations at Four Airports**, FAA-RD-75-218, U.S. Department of Transportation, Federal Aviation Administration, Washington, D.C., 1976.

(NASA) have evaluated numerous devices for determining the frictional value of a runway pavement surface. These include the Mu-Meter, the Diagonally Braked Vehicle (DBV), the Skiddodmeter, the Saab friction test vehicle, and various types of highway skid trailers. Currently, the Mu-Meter is the standard test equipment for the USAF.

The Mu-Meter can be used to identify potential problems on a pavement surface. Recommendations for improvement of the surface can then be expediently made and implemented. The drawbacks of Mu-Meter testing are the initial cost of the Mu-Meter, tow vehicle, and water distribution equipment for performing wet surface testing. In addition, a trained operational crew and maintenance technicians are required. Because of the high cost and personnel requirements, many airports and airfields cannot afford routine friction evaluation testing with the Mu-Meter. For example, the USAF employs a single crew to perform all Mu-Meter testing worldwide.

The inability of airport managers and airfield engineers to routinely evaluate the frictional levels on their runways, particularly in touchdown areas, precludes any quantitative evaluation of rubber buildup. This lack of a quantitative method limits the capability of the airport engineer or airfield manager to determine when rubber removal is required or when a rubber removal contractor has satisfactorily completed a rubber removal project.

Presently, the airport pavement engineer must rely heavily on limited visual impressions and experience to determine when rubber removal is required and when removal has been adequately conducted. Unfortunately, test results obtained by the USAF (Ref. 4) indicate this visual/experience method of inspecting rubber buildup does not correlate well with the results obtained by Mu-Meter frictional testing. The determination of when to remove rubber and what constitutes a good rubber removal job is so arbitrary that the overall effectiveness of any rubber removal program is questionable.

It is apparent from the above discussion that a quantitative evaluation system is highly desirable. A more efficient rubber removal program will reduce contract costs, improve safety, and ensure better and uniform compliance with contract specifications. Currently, procurement officials are reluctant to pursue claims against contractors because of ambiguous or meaningless specifications. Consequently, a simple quantifiable and inexpensive system for determining runway rubber removal requirements is necessary for determining when to remove rubber and to ascertain when rubber removal specifications have been met. In addition, the development of a specification which incorporates such a quantifiable system is also necessary.

The New Mexico Engineering Research Institute (NMERI) has been tasked to develop a simple quantifiable testing scheme for evaluation of rubber buildup. The following four phases of effort were required of NMERI.

PHASE I--RUBBER BUILD-UP CRITERIA AND EVALUATION PROCEDURE DEVELOPMENT

This phase consisted of a review of existing techniques for evaluation of surface coatings. Based on this review, an evaluation procedure was developed which requires little special training, is insensitive to operator change, and is cost effective (less than $10,000 per installation for implementation).

PHASE II--RUBBER REMOVAL TECHNIQUES AND EQUIPMENT

Phase II required review and research of existing rubber removal techniques. Evaluation of effectiveness, cost, simplicity, safety, and environmental effects was ascertained when the reviewed techniques are applied solely to porous friction surfaces (PFS).

PHASE III--RUBBER BUILD-UP PARAMETERS DEVELOPMENT

Phase III required the field test of the evaluation procedure developed in Phase I. This evaluation was conducted before and after rubber removal at selected airports and airbases. Friction measurements using the Mu-Meter were also obtained for future data analyses and correlation. The field testing was conducted for various surface types including Portland Cement Concrete (PCC), Asphalt Concrete (AC), and PFS pavements.

PHASE IV--DEVELOP RUBBER REMOVAL SPECIFICATIONS

This phase incorporates the results of Phases I and III into a concise specification for rubber removal contracts. The intent of this final product is to eliminate the undesirable attributes of existing specifications previously mentioned.

Phases III and IV are currently in progress at NMERI. The results of these phases are to be published at a later date. Phase II has been completed and is reported elsewhere (Ref. 3). The content of this report is a discussion of Phase I. Included are a review of existing friction measurement techniques, techniques for surface evaluation, final selection of field test techniques, and design of the field evaluation experiment (Phase III). Also included is a discussion on the development of a water distribution nozzle suitable for performing wet friction tests with the Mu-Meter.

II. FRICTION, HYDROPLANING, EFFECTS OF RUBBER DEPOSITS

The development of friction between an aircraft tire and a pavement surface is a complex phenomenon. The theory relating two simple objects such as a tire and a pavement structure is not simple. When factors such as the influences of rain (wet surface), aircraft dynamics, variable pavement surfaces, and pilot operational technique are also considered, a theoretical problem is produced that has become a lifetime study of many researchers in the aerospace and pavements industry.

Yager (Ref. 6) discusses the principal weather, aircraft, runway, and pilot factors which combine to affect aircraft ground-handling performance during wet runway operations. These components are shown in flow-chart form in Figure 1.

Figure 1 shows that atmospheric conditions and the runway geometry control the water depth on a runway. Aircraft tire design, inflation pressure, and ground velocity coupled with the texture characteristics of the pavement surface are shown to control the tire-pavement drainage capability. The water depth and drainage capability govern the amount of tire-pavement friction available. The influence of aircraft design and pilot input are also known to influence the performance of an aircraft on wet runways.

In reviewing the factors which influence aircraft runway performance, Yager (Ref. 6) states that several approaches are needed to alleviate the severity of the problem. These include continued pilot education and training, implementation of procedures for monitoring slippery runway conditions, implementation of procedures for notifying pilots when severe runway conditions exist, improvement of antiskid brake system performance, and prompt remedial treatment of runway surface drainage problems. It is also clear that the quality of the pavement, from a surface texture standpoint, must be ensured at the design, construction (quality control), and maintenance levels during the life of the pavement.

TIRE-PAVEMENT FRICTION THEORY

As previously stated, the theory of tire-pavement interaction with regard to friction is quite involved. A number of major works have been written on the subject of tire-pavement friction. The most notable theoretical discussions of this subject are by Moore (Ref. 7) and by Kummer (Ref. 8). While these authors emphasize the importance of tire and rubber design in friction development, they also note the importance of surface texture, particularly macrotexture and microtexture.

---

6. Yager, T. J., **Factors Influencing Aircraft Ground-Handling Performance**, NASA TM-85652, National Aeronautics and Space Administration, Hampton, Virginia, 1983.

7. Moore, D. F., **The Friction of Pneumatic Tyres**, Elsevier Scientific Publishing Company, New York, New York, 1975.

8. Kummer, H. W., **Unified Theory of Rubber and Tire Friction**, Engineering Research Bulletin B-94, Pennsylvania State University, College of Engineering, University Park, Pennsylvania, 1966.

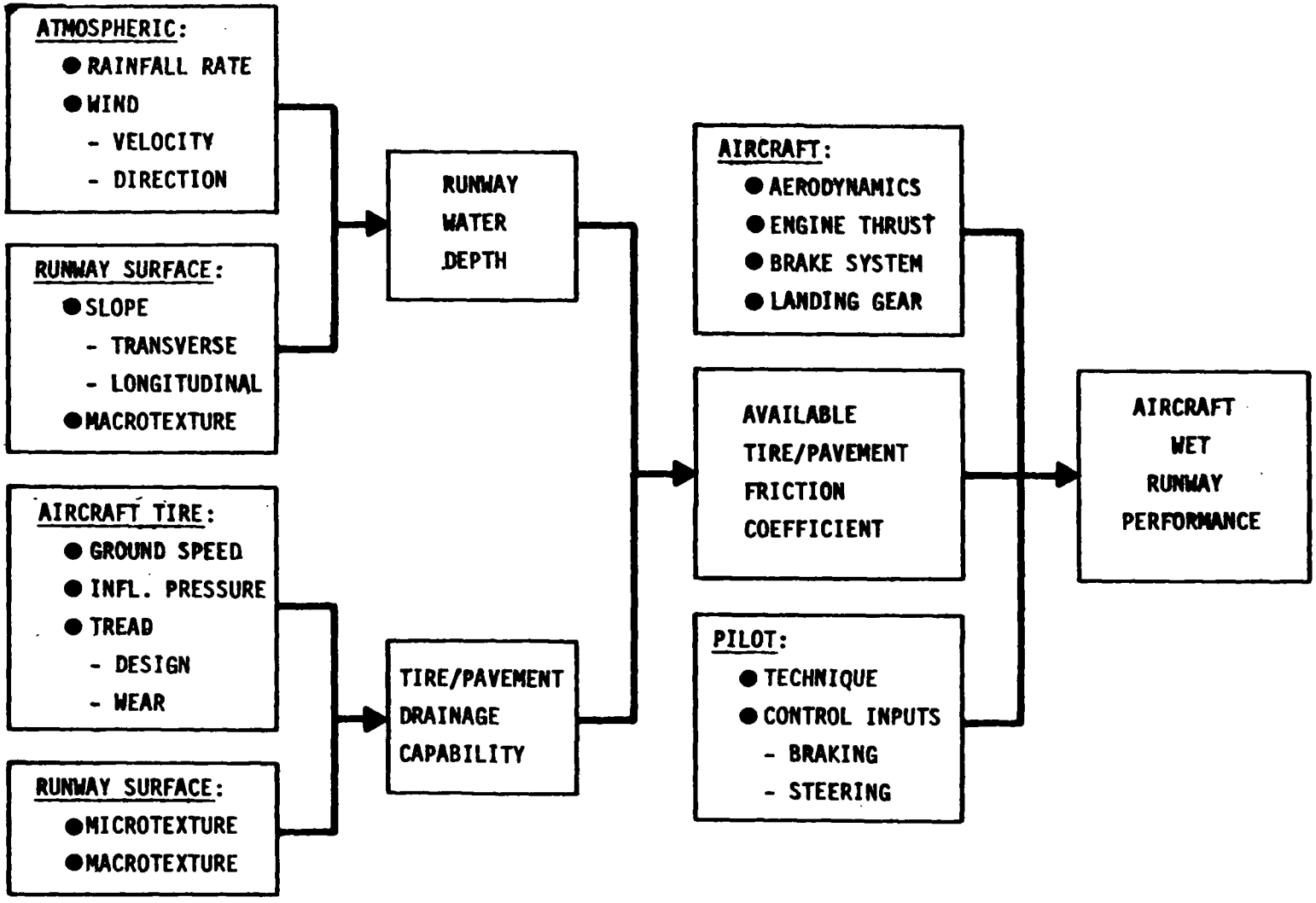

FIGURE 1. FACTORS AFFECTING AIRCRAFT WET RUNWAY PERFORMANCE (REF. 6)

Moore (Ref. 7) differentiates the macrotexture from the microtexture as follows. The individual asperities or stones in a pavement surface constitute the macrotexture, while the finer asperities (or grit) on the larger asperities (macrotexture) constitute the microtexture. Figure 2 illustrates the difference between macro- and microtexture. According to Moore (Ref. 7), typical wavelengths (λ) associated with macrotexture are 6 to 20 mm (0.25 to 0.80 in), and for microtexture are 10 to 100 μm (0.0004 to 0.004 in).

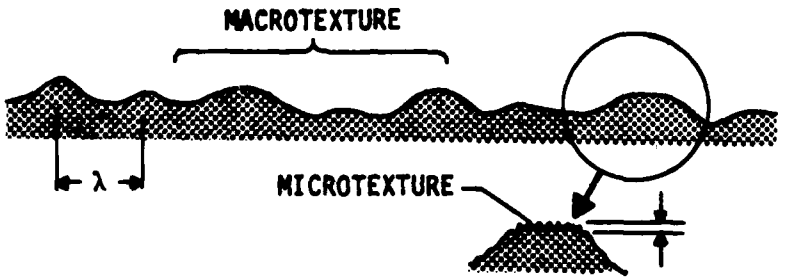

FIGURE 2. PAVEMENT ROUGHNESS INDICATING MACROTEXTURE AND MICROTEXTURE (REF. 7)

The classical laws of friction are often applied to rubber materials. However, materials such as rubber do not conform to these laws. Kummer and Meyer (Ref. 9) illustrate how rubber differs from the four classical laws which state that:

1. Friction coefficient is independent of normal load.
2. Friction coefficient is independent of contact area.
3. Friction coefficient is independent of sliding velocity and temperature.
4. Friction coefficient at rest is higher than that in motion.

Laws 1 and 2 combined indicate that the friction coefficient is independent of normal pressure. Figure 3 compares the friction characteristics of rubber with these classical laws.

Kummer and Meyer (Ref. 9) state that the main components of rubber friction are termed an adhesion component and a hysteresis component. The force required to pull a block of rubber over a surface (Fig. 4) is the sum of adhesional shear forces and hysteresis loss forces. The adhesion component is due to the development of strong molecular forces at the interface of the two materials. The hysteresis losses are attributed to the energy loss due to deformation of the two materials when in contact with each other. Smooth dry surfaces are known to develop strong adhesional forces, while hysteretic forces predominate on coarse textured surfaces.

HYDROPLANING THEORY

The term hydroplaning is understood in general terms by almost anyone who encounters it. A general definition of hydroplaning is the loss of traction

9. Kummer, H. W., and Meyer, W. E., **Measurement of Skid Resistance**, Symposium on Skid Resistance, ASTM STP-326, American Society for Testing and Materials, Philadelphia, Pennsylvania, 1962, pp. 3-28.

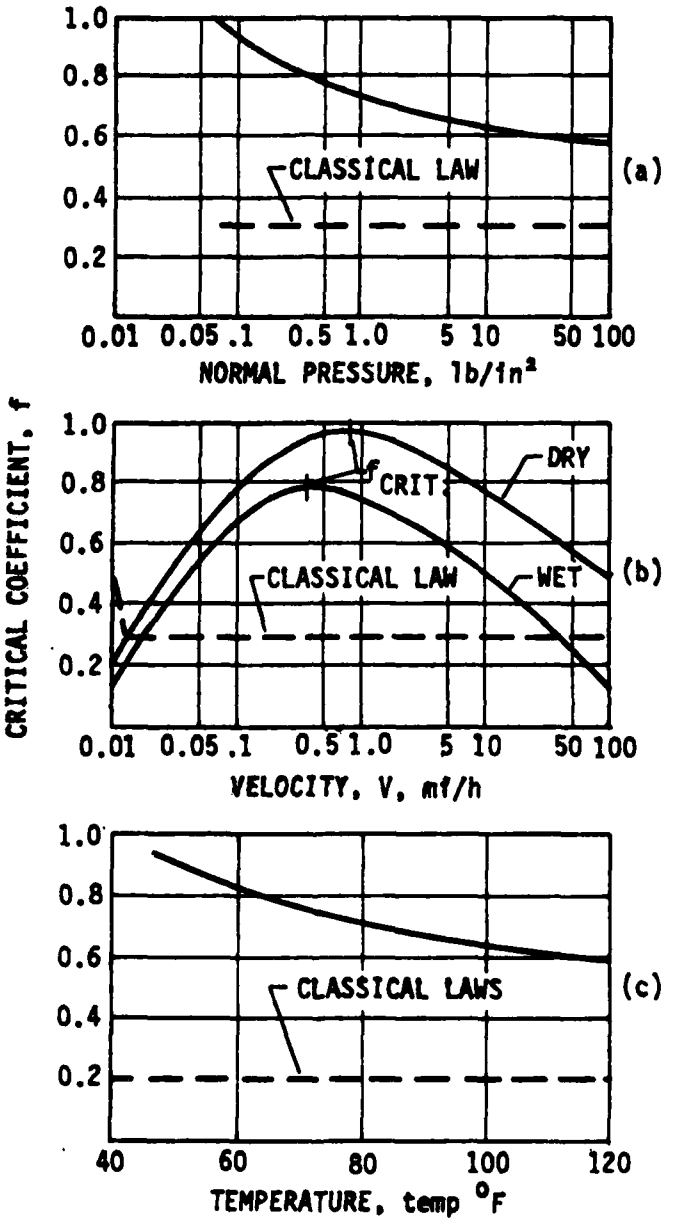

FIGURE 3. RUBBER FRICTION AND THE CLASSICAL LAWS (REF. 9)

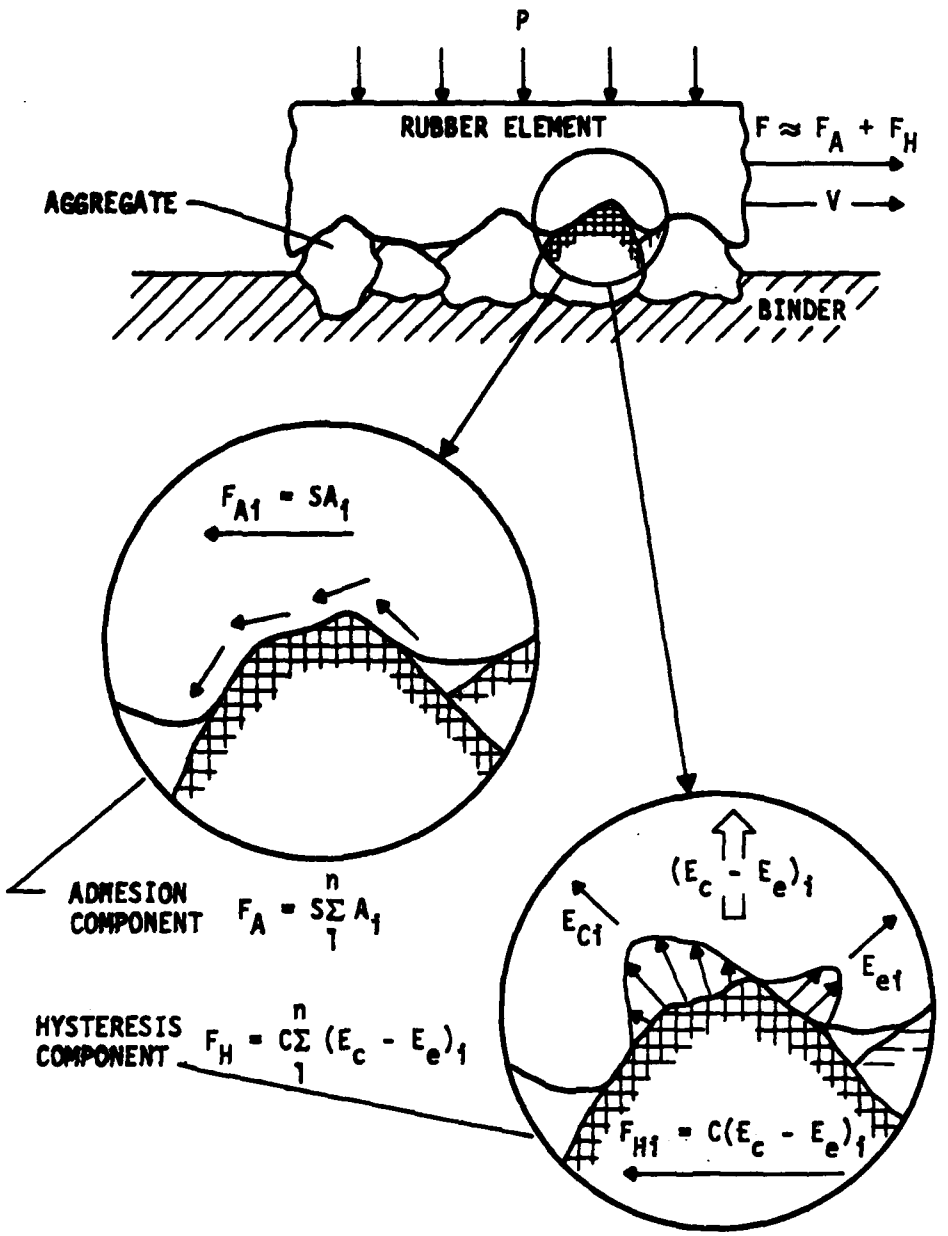

FIGURE 4. MECHANISM OF RUBBER FRICTION (REF. 9)

between tire and pavement due to the presence of a layer of water. Browne, (Ref. 10) on pneumatic tire hydroplaning, states there are three types of hydroplaning, viz., dynamic, viscous, and reverted tire rubber hydroplaning.

Dynamic hydroplaning occurs when the amount of water encountered by the tire exceeds the combined drainage capacity of the tire tread pattern and the pavement macrotexture. It occurs in deep fluid layers where fluid inertial effects predominate. The pressure on the tire surface increases with increasing tire speed until it is greater than the internal tire pressure which results in a complete separation of tire and pavement. It is commonly known that the dynamic hydroplane velocity is proportional to the square root of the tire pressure, Horne and Joyner (Ref. 11) found that

$$V_H = 1.8\sqrt{P_{IN}} \qquad (1)$$

where V_H is in meters per second and P_{IN} is the tire inflation pressure in kilopascals. Refinements of this equation have since been made; however, the point of practical importance is that hydroplane velocity is proportional to the square root of the tire pressure.

Viscous hydroplaning occurs only on surfaces with little microtexture. This lack of microtexture promotes a thin water film between tire and pavement. This type of hydroplaning can occur at any speed and with any fluid depth. Tire pressure is important in that it determines whether viscous hydroplaning will persist at moderate or high speed; the greater the inflation pressure, the more likely viscous hydroplaning will develop rather than dynamic hydroplaning.

Reverted tire hydroplaning occurs when large aircraft lock their wheels (or spin-up at touch down) when moving at high speeds on wet pavement with adequate macrotexture but little microtexture. Heat buildup at the tire-pavement interface due to sliding causes the rubber to melt. The tire then slides on a film of molten rubber, water, and steam.

Browne (Ref. 10) also states that the concept of a tire water skiing with a flat surface is not true. Tires deform under the static and dynamic loadings imposed; if the tire did not deform, the speed at which hydroplaning would occur would be markedly increased.

---

10. Browne, A. L., **Mathematical Analysis for Pneumatic Tire Hydroplaning, Surface Texture Versus Skidding: Measurements, Frictional Aspects, and Safety Features of Tire-Pavement Interactions**, ASTM STP-583, American Society for Testing and Materials, Philadelphia, Pennsylvania, 1975, pp. 75-94.

11. Horne, W. B., and Joyner, U. T., **Pneumatic Tire Hydroplaning and Some Effects on Vehicle Performance**, International Automative Engineering Congress, Society of Automotive Engineers, Detroit, Michigan, January 1965.

A more elaborate discussion of the tire-pavement interaction mechanism during hydroplaning is presented by Moore (Ref. 12). Moore considers the case of a tire rolling on a wet surface at speeds below the hydroplaning limit (or velocity). Hydroplaning upward thrust exists in the wedge just ahead of the contact area of the tire (Fig. 5a). The magnitude of this thrust is dependent on such factors as effective tread width, water layer depth, tire inflation pressure, vehicle velocity, and pavement surface texture. The contact area itself is comprised of three zones (Fig. 5b) as follows:

1. Sinkage, or Squeeze-Film Zone. Under wet conditions, the forward part of what would normally be considered the contact area under dry conditions floats on a thin film of water, the thickness of which decreases progressively as individual tread elements traverse the contact area. Since the tire, water-film, and road surface have virtually no relative motion in the contact area, the tread elements in effect attempt to squeeze out the water between rubber and pavement.

2. Draping, or Transition Zone. The draping zone begins when the tire elements, having penetrated the squeeze film, commence to drape over the major asperities of the surface and to make contact with the lesser asperities.

3. Actual Contact, or Tractive Zone. This is the region where the tire elements, after draping, have attained an equilibrium position vertically on the surface. The length of this region depends on vehicle velocity; it occupies the rear portion of the overall contact area. Tractive effort is developed here.

Horne (Ref. 13) states that the loss of tire friction on wet or flooded pavements with speed is due to the combined effects of viscous and dynamic hydroplaning. As speed increases, a transition occurs from viscous, to combined viscous and dynamic, to full dynamic hydroplaning.

According to Horne (Ref. 13), the pavement macrotexture plays the important role of providing escape channels for drainage of bulk water. Bulk water drainage delays to much higher speeds the build-up of fluid dynamic pressures which cause dynamic hydroplaning. A pavement with good microtexture combats viscous hydroplaning. A good microtexture has a sharp-harsh-gritty feel to the touch. A good microtexture penetrates the thin water-film coating of a pavement surface; this penetration maintains dry contact between tire and pavement, preventing viscous hydroplaning.

Yager (Ref. 6) cites the three principal causes of hydroplaning, discusses the contributing factors of each, and suggests methods for alleviating or preventing them. Figure 6 shows Yager's (Ref. 6) discussion in tabular form.

---

12. Moore, D. F., **Prediction of Skid-Resistance Gradient and Drainage Characteristics for Pavements,**, Highway Research Record 131, Highway Research Board, Washington, D.C., 1966, pp. 181-203.

13. Horne, W. B., **Status of Runway Slipperiness Research**, Presented at NASA Conference on Aircraft Safety and Operating Problems, Hampton, Virginia, October 18-20, 1976.

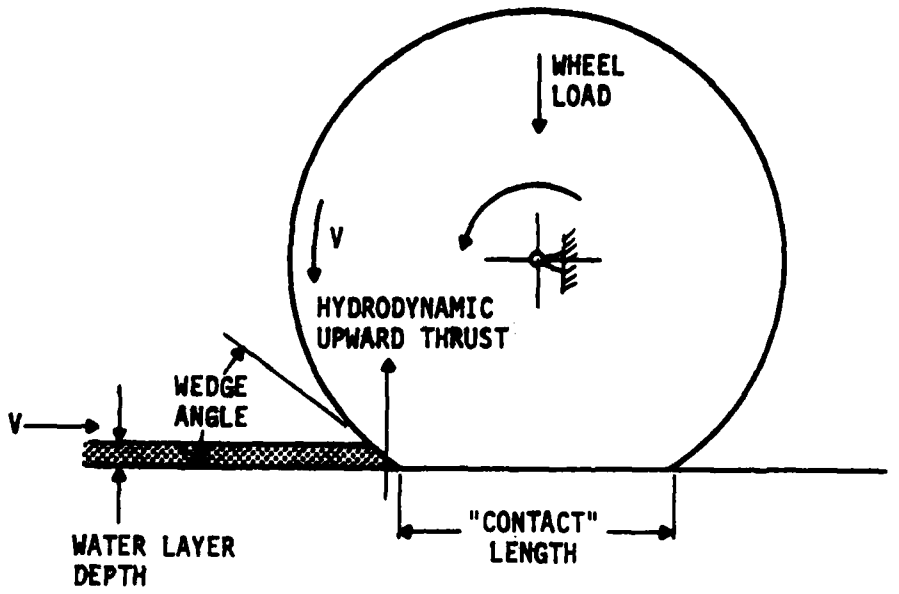

(a) GENERAL

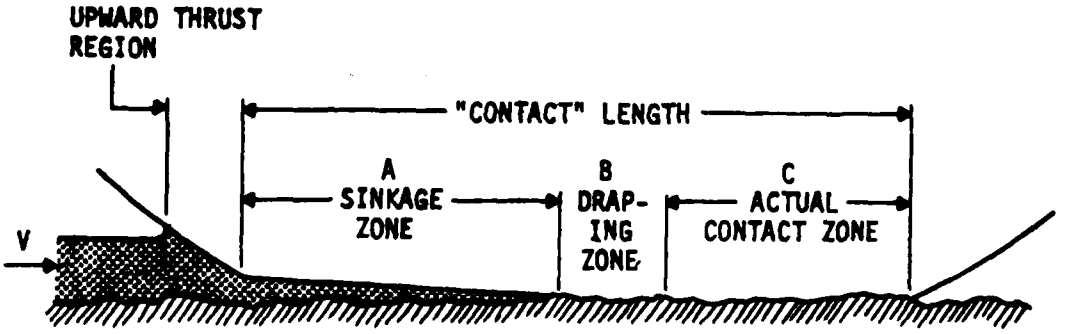

(b) THREE ZONES IN THE CONTACT AREA (ROUGH SURFACE)

FIGURE 5. WET ROLLING BELOW THE HYDROPLANING LIMIT (REF. 2)

	HYDROPLANING		REVERTED RUBBER SKIDDING
	VISCOUS	DYNAMIC	
CAUSES	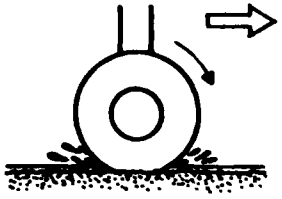	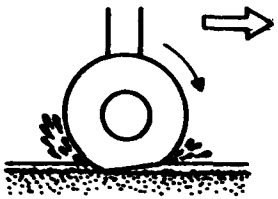	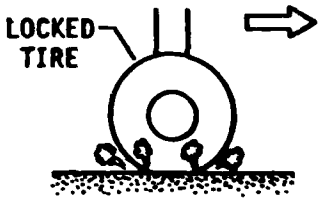
CONTRIBUTING FACTORS	DAMP OR WET PAVEMENT MEDIUM TO HIGH SPEED POOR PAVEMENT TEXTURE WORN TIRE TREAD	FLOODED PAVEMENT HIGH SPEED LOW TIRE PRESSURE WORN TIRE TREAD	WET OR FLOODED PAVEMENT HIGH SPEED POOR PAVEMENT TEXTURE DEFICIENT BRAKE SYSTEM
ALLEVIATING FACTORS	PAVEMENT MICROTEXTURE PAVEMENT GROOVING GOOD TREAD DESIGN	PAVEMENT MACROTEXTURE PAVEMENT GROOVING INCREASED TIRE PRESSURE GOOD TREAD DESIGN	GOOD PAVEMENT TEXTURE PAVEMENT GROOVING IMPROVED ANTISKID

FIGURE 6. PRINCIPAL CAUSES OF WET PAVEMENT TIRE FRICTION LOSSES (REF. 6)

The generally accepted levels of wet friction value (Mu value) and associated hydroplaning potential, according to Burk (Ref. 4), are shown in Table 1. The stopping distance ratio (SDR), which is the ratio of stopping distances of wet and dry pavement measured with the DBV, is also shown.

TABLE 1. HYDROPLANING POTENTIAL (Ref. 4)

Mu (40 mph)	SDR (60 mph)	Aircraft Braking Response	Hydroplaning Response
>50	1.0 - 2.5	Good	No hydroplaning expected
42 - 50	2.5 - 3.2	Fair	Transitional (not well defined)
25 - 41	3.2 - 4.4	Marginal	Potential for hydroplaning
<25	>4.4	Unacceptable	Hydroplaning probability high

EFFECTS OF RUBBER DEPOSITS ON FRICTION LEVELS

From the previous discussion, it becomes quite clear that rubber deposits in runway touchdown zones must have a detrimental affect on wet runway performance from a frictional standpoint.

The friction level as previously stated is dependent on the amount of texture present on the pavement surface. As rubber accumulates on a pavement surface, both the microtexture and macrotexture are progressively reduced. This is not a problem during dry weather operations since the adhesional component is markedly increased resulting in a net increase in frictional coefficient. However, during wet runway operations, the net frictional level is drastically reduced.

Rubber buildup tends to reduce the microtexture initially. Further buildup occludes the macrotexture. Reduction of microtexture in a wet environment prevents the development of adhesional friction which can result in viscous hydroplaning. Occluded macrotexture prevents the removal of bulk water from the tire-pavement contact area, and also prevents the development of the hysteresis frictional component. This lack of macrotexture can cause dynamic hydroplaning.

Various reports (Refs. 1, 4, and 5) indicate that wet friction levels are lower in rubber covered areas as opposed to nonrubber areas. These reports also show that removal of rubber improves the wet friction coefficients to levels comparable to nonrubber-covered areas.

In reporting the results of the National Runway Friction Measurement Program (NRFMP), MacLennan et al. (Ref. 14) found a strong relationship between pavement type, macrotexture, and wet Mu values for pavements with and

---

14. MacLennan, J. R., Wench, N. C., Josephson, P. D., and Erdmann, J. B., **National Runway Friction Measurement Program**, FAA-AAS-80-1, U.S. Department of Transportation, Federal Aviation Administration, Washington, D.C., 1980.

without rubber buildup. Table 2 illustrates these relationships. Note that the average wet Mu value on any pavement type is always greater for nonrubber-covered pavements than rubber-covered pavements. Also, the average texture depth tends to decrease with decreasing Mu value. It is important to note that the texture depths for grooved pavements do not include the influence of the grooving, i.e., all texture measurements were obtained between the grooves. In addition, the texture measurements were all obtained from nonrubber-covered pavement areas.

Experience gained by the authors at NMERI indicate that pavement texture depth is also markedly increased after rubber removal. Tests conducted at a major international airport using grease smear and sand patch volumetric techniques showed up to a 40-percent improvement in texture depth after rubber removal. Measurements included the effects of grooving, i.e., grease and sand were allowed to enter the grooving during performance of these tests.

Figure 7 further illustrates the relationship obtained by MacLennan (Ref. 14) between texture and wet Mu value. The degree of correlation is expressed in terms of the variability of the coefficient "a." It is interesting to note that wet Mu values less than 50 were rarely measured during the NRFMP. Mu values greater than 50 are generally considered acceptable as previously shown in Table 1.

Other conclusions of the NRFMP were that rubber accumulation profoundly affects surface friction, rubber removal improves surface friction, saw-cut grooving improves friction and drainage and reduces the hydroplaning potential, and friction enhancement due to grooving is greater in rubber areas than nonrubber areas. In addition, guidelines were developed for rubber removal frequency for both low- and high-use runways.

In conducting research for the NASA, Horne (Ref. 1) found that high-pressure water blast techniques performed well in removing rubber deposits from concrete runways. Rubber removal was sufficient enough to restore full pavement skid resistance (based on tests with a DBV).

With regard to high-pressure water rubber removal methods at four different airports, Grisel (Ref. 5) found that virtually all rubber deposits were removed from asphaltic runway surfaces by proper water-jet cleaning, and a significant increase in wet surface friction was found in rubber deposit areas after cleaning.

Review of a report on rubber removal processes by Burk (Ref. 4) indicates that, in general, runway frictional values (wet Mu) increase after rubber removal. However, the extent of improvement was not readily relatable to the amount of rubber buildup or amount removed.

TABLE 2. RANKING OF PAVEMENT TYPES BY MEAN WET MU VALUE (REF. 14)

PAVEMENT TYPE	TEXTURE† DEPTH in x 10^{-3}	WET MU VALUE (50 60 70 80)
Asphalt, Porous Friction Course	48.5	R 0
Asphalt, Chip Seal*	24.7	0
Asphalt, Microtexture, Grooved	12.7	R 0
Asphalt, Worn	35.0	R 0
Asphalt, Macrotexture	27.7	R 0
Concrete, Wire Tined, Grooved*	20.9	0
Concrete, Burlap Dragged, Grooved	11.9	R 0
Asphalt, Mixed Texture, Grooved	15.9	R 0
Asphalt, Macrotexture, Grooved	23.3	R 0
Asphalt, New, Grooved	15.3	R 0
Asphalt, Rubberized Chip Seal*	39.9	0
Concrete, Worn, Grooved*	12.8	0
Asphalt, Worn, Grooved*	24.7	0
Concrete, Microtexture, Grooved	11.0	R 0
Asphalt, Slurry Seal*	19.0	0
Concrete, Macrotexture, Grooved*	12.0	0
Concrete, Broomed or Brushed, Grooved	10.5	R 0
Concrete, Wire Tined	22.2	R 0
Concrete, Wire Combed	18.0	R 0
Asphalt, Mixed Texture	19.3	R 0
Concrete, Macrotexture*	16.5	0
Asphalt, Microtexture	14.2	R 0
Concrete, Float Grooved	12.5	R 0
Concrete, Worn*	12.8	0
Concrete, Broomed or Brushed	14.5	R 0
Asphalt, New	12.5	R 0
Concrete, Microtexture	12.4	R 0
Concrete, Burlap Dragged	13.9	R 0

50 60 70 80

0 - Mean value with no rubber
R - Mean value in rubber areas (30 percent rubber accumulation)
* - Insufficient data to analyze in rubber area
† - Texture depth by NASA grease smear test (Ref. 24) in non-rubber areas, the influence of grooving not included for grooved pavements

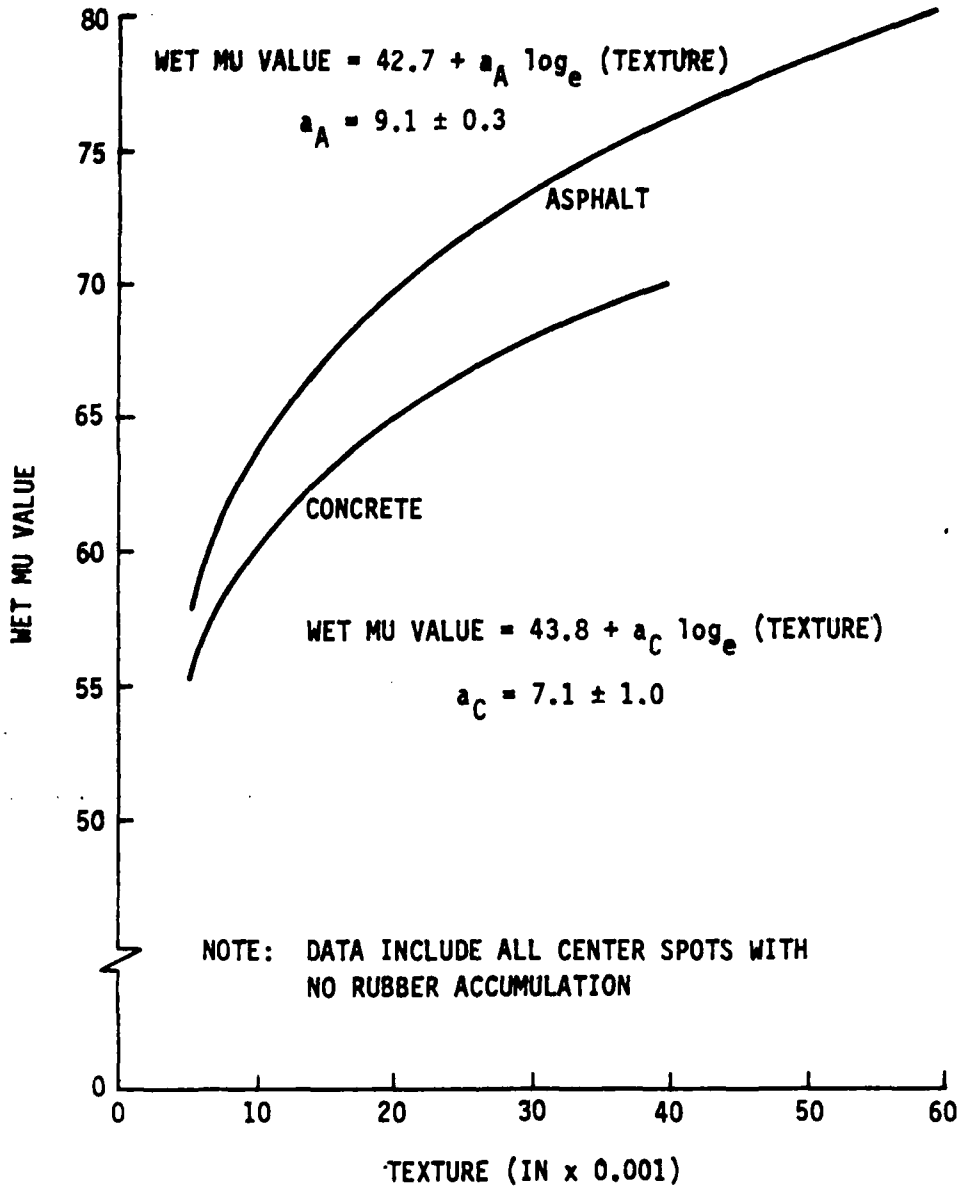

FIGURE 7. RELATIONSHIPS OF WET MU VALUE WITH TEXTURE DEPTH FOR UNGROOVED PAVEMENTS (REF. 14)

III. ROLLING FRICTION MEASUREMENT EQUIPMENT

In the introductory remarks, mention was made of the various types of friction measurement equipment commonly used for evaluating the frictional coefficient of runway (and highway) pavements. Five fairly common devices are in use, namely the M. L. Aviation Mu-Meter, the Diagonally Braked Vehicle (DBV), the Swedish Skiddometer, the Saab Friction meter, and the ASTM Skid Trailer.

Two sliding friction devices used for evaluating small localized pavement areas are the Penn State Drag Tester and the British Pendulum Tester.

According to Kummer and Meyer (Ref. 9), all friction measurement equipment can be grouped into three categories:

1. Steady-state slip devices.
2. Steady-state sliding devices.
3. Nonsteady-state sliding devices.

The first group includes all the types of devices that operate at constant slip in braking, driving, or cornering. Generally, the measured coefficients are up to 35-percent higher than those of the second group. The second group includes those measurement devices which determine the sliding coefficient (locked wheel) at constant velocity. Measurement equipment of the third group are termed energy devices; kinetic or potential energy before a test is transformed in whole or in part into frictional energy.

The Mu-Meter, Swedish Skiddometer, and Saab Friction Meter are all equipment of the first group. The ASTM Skid Trailer is of the second group as is the Penn State Drag Tester. The DBV and British Pendulum Tester can be classified as devices of the third group. The Penn State Drag Tester and British Pendulum Tester will be described later in Section IV as they are sliding friction equipment.

Williams (Ref. 15) categorizes rolling friction measurement equipment as brake-slip or cornering-slip devices. Brake-slip is defined by

$$S_b \approx \frac{\omega - \omega_t}{\omega} \tag{2}$$

where

S_b = slip ratio, braked

ω = angular velocity of a freely rolling or unbraked tire, which corresponds to the vehicle velocity

ω_t = angular velocity of the slipping tire or torqued wheel (braked wheel)

For a free-rolling wheel, the slip ratio is zero; and for a locked wheel, the ratio is unity. Figure 8 illustrates that the maximum braking friction coefficient develops when S_b is approximately 0.15 to 0.20. Thus, the maximum

---

15. Williams, J. H., **Analysis of the Standard USAF Runway Skid Resistance Tests**, AFCEC-TR-75-3, Air Force Civil Engineering Center, Tyndall Air Force Base, Florida, 1975.

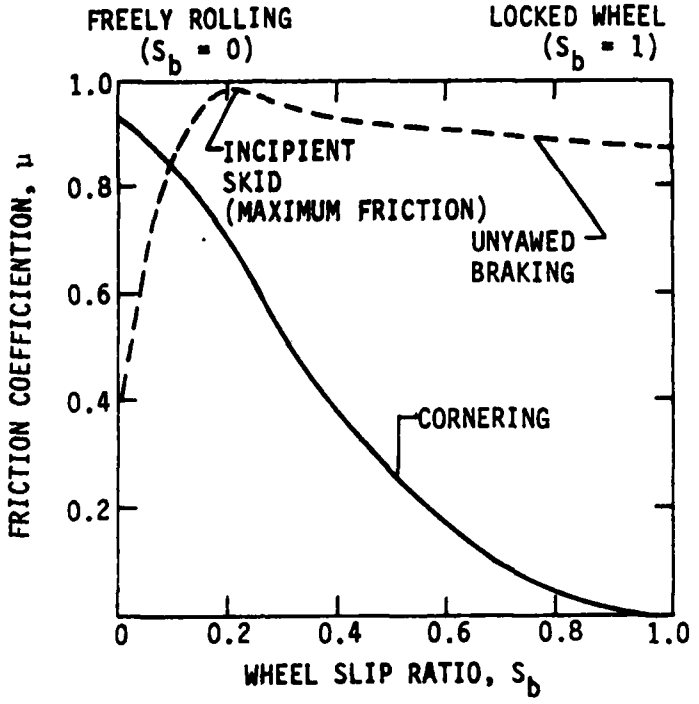

FIGURE 8. BRAKE-SLIP AND CORNERING-SLIP OPERATING MODES, (REF. 15)

braking deceleration for an aircraft occurs when the slip ratio is held in this range (also termed incipient skid) and not when the wheels are locked (which occurs during emergency situations). The Swedish Skiddometer, DBV, Saab Friction Meter, and Highway Skid Trailer (ASTM E-274) all operate on the principle of brake-slip. The Swedish Skiddometer and Saab Friction Meter operate at a constant slip ratio near the incipient skid, while the DBV and ASTM Skid Trailer operate at a slip ratio of unity.

Cornering-slip occurs when a slip angle develops between the direction of motion and the plane of the tire (this is also referred to as toe-in or toe-out). Figure 9 illustrates the forces developed on a tire during cornering-slip. The cornering-slip friction coefficient is

$$\mu_s = \frac{F_c}{F_v} \tag{3}$$

where

F_v = normal wheel load

F_c = cornering-slip force.

For a yawing-unbraked tire, the maximum cornering-slip coefficient is produced at some critical yaw angle (see Fig. 10). The angle of yaw is that angle

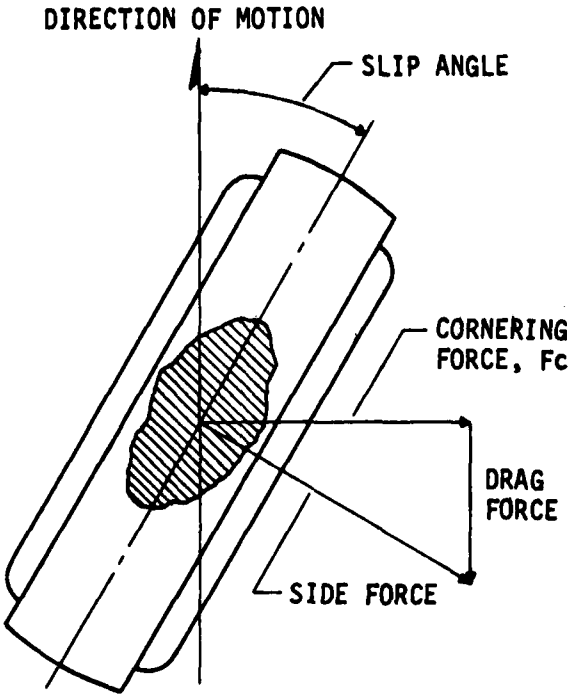

FIGURE 9. TIRE IN CORNERING SLIP MODE (REF. 15)

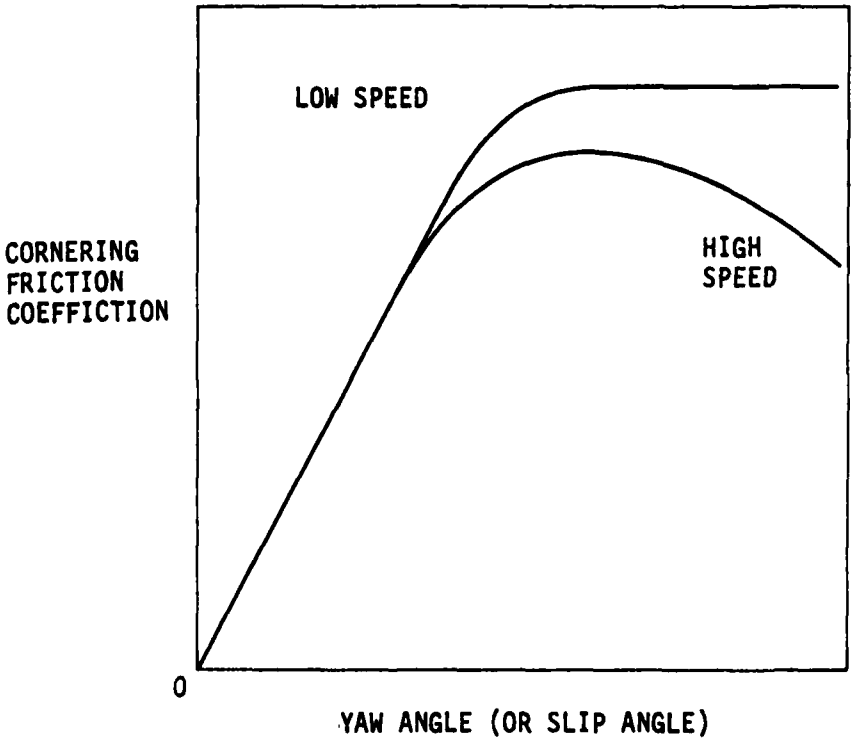

FIGURE 10. UNBRAKED YAWED ROLLING MODE (REF. 15)

between the direction of travel and the plane of the tire. The Mu-Meter operates in this side-cornering mode of operation.

The Mu-Meter is a lightweight, three-wheeled trailer unit which is towed by a standard vehicle (Fig. 11). A remote readout operated from the tow vehicle cab provides distance measurement and average friction value (Mu value). The trailer unit is comprised of a triangular frame on which are mounted two friction-measuring wheels, a rear wheel which drives a recorder, measures distance and stabilizes the unit, a load cell, and a strip chart recorder (Fig. 12). When the Mu-Meter is towed over a test section, the toed-out (approximately 15-deg included angle) smooth-measuring tires tend to move apart. The tires are restrained from this lateral movement by a load cell mounted between the fixed and pivoted side frame members. The load cell transmits this restraining force to the strip chart recorder by hydraulic pressure through a flexible tube. The rear wheel drives the recorder (approximately 1 in per 150 ft). Thus, a continuous analog output of side-force friction (or cornering-slip friction) versus distance is obtained. An integrator provides output to the remote readout of the average friction value over each 450-ft increment (Ref. 16). For further information on the Mu-Meter, refer to Reference 17.

FIGURE 11. MU-METER AND TOW VEHICLE

16. **Standard Test Method for Side Force Friction on Paved Surfaces Using the Mu-Meter**, ASTM Designation E-670-79, Annual Book of ASTM Standards, Vol. 04.03, American Society for Testing and Materials, Philadelphia, Pennsylvania, 1984.

17. **Mu-Meter Instruction and Servicing Manual**, M. L. Aviation Company, Ltd., White Watham Aerodrome, Maidenhead, Berkshire, England, January 1975.

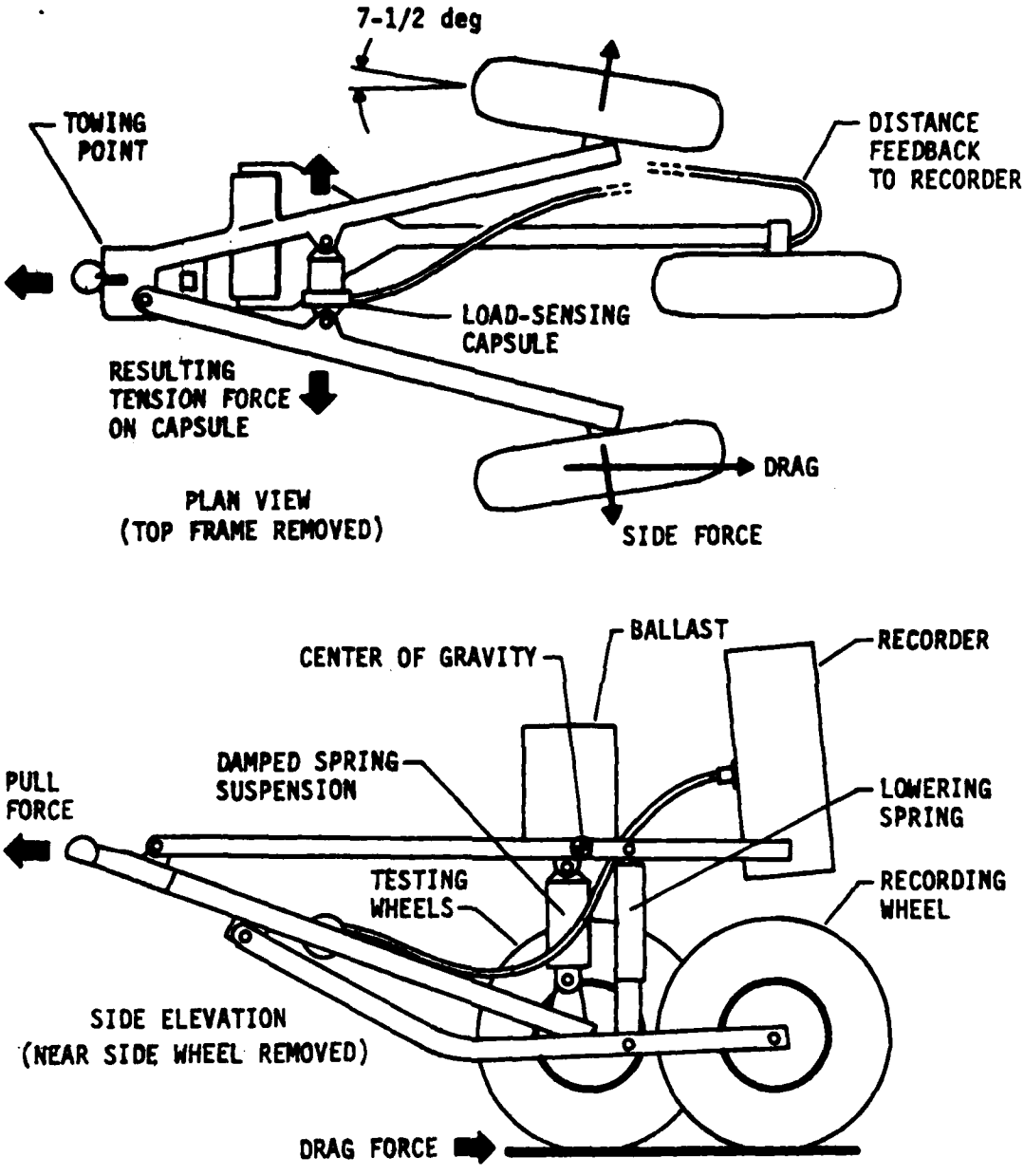

FIGURE 12. DIAGRAMMATIC LAYOUT OF MU-METER

The DBV is generally a standard automobile which has been modified to permit braking of one front wheel and the diagonally opposite rear wheel. The other pair of diagonal wheels are allowed to roll freely (unbraked) permitting directional stability and control during diagonal wheel braking. The tires generally used with the DBV are smooth tires conforming to ASTM E-524 (Ref. 18); these smooth tires ensure repeatability and eliminate the effects of tire-tread design on braking performance. The skid resistance characteristic of a runway obtained with the DBV is the SDR. The SDR is the ratio of wet-pavement stopping distance to dry-pavement stopping distance for a given pavement section. Frictional coefficients can be calculated for both the wet and dry stopping distances.

The Swedish Skiddometer is a three-wheeled trailer which measures and records the brake-slip coefficient at an approximate 12.7-percent brake-slip ratio. The Skiddometer is the instrument currently used by Transport Canada for evaluating runway friction (the Mu-Meter is used as an alternative device).

The Saab Friction Meter is a brake-slip friction coefficient device. It is installed as a fifth wheel in a late model Saab automobile. All data acquisition and recording equipment is self-contained in the automobile.

The ASTM Skid Trailer (Ref. 19) measures skid resistance (frictional level) with a full-scale automotive tire. A braking system locks the test tire on the skid trailer when the trailer is at constant velocity. The resultant friction force is measured and compared to the normal force. The ratio of these values (x 100) is a frictional coefficient termed a skid number.

All of the test procedures for the above five pieces of equipment can be performed on either dry or wet pavements. Generally, wet tests are conducted. Wet tests require the use of a suitable water distribution system to ensure a uniform water depth in front of the test tires.

Ballentine (Ref. 20) found a good correlation between Mu-Meter data and DBV data. The relationship and correlation obtained were comparable to that found in a British study.

Ballentine, (Ref. 20) in conducting research for the Air Force Weapons Laboratory, found that statistically significant differences exist when friction measurements are obtained in the opposite direction of normal travel.

---

18. **Standard Specification for Smooth-Tread Standard Tire for Special-Purpose Pavement Skid-Resistance Tests,** ASTM Designation E-524-82, Annual Book of ASTM Standards, Vol. 04.03, American Society for Testing and Materials, Philadelphia, Pennsylvania, 1984.

19. **Standard Test Method for Skid Resistance of Paved Surfaces Using a Full-Scale Tire,** ASTM Designation E-274-79, Annual Book of ASTM Standards, Vol. 04.03, American Society for Testing and Materials, Philadelphia, Pennsylvania, 1984.

20. Ballentine, G. D., **The Air Force Weapons Laboratory Skid Resistance Research Program, 1969-1974,** AFWL-TR-74-181, Air Force Weapons Laboratory, Kirtland Air Force Base, New Mexico, 1975.

Apparently, many runway pavements are more polished in one direction than the other due to traffic patterns.

Ballentine's (Ref. 20) work suggests that Mu-Meter testing should be conducted in the direction of normal travel. Rubber build-up is always located in the touchdown zone at the end of the runway. Mu-Meter testing must be conducted from the end of the runway for which rubber removal is being evaluated (i.e., direction of travel is the same as the landing aircraft).

IV. SURFACE CHARACTERIZATION TECHNIQUES

The pavement surface characteristic of importance with respect to friction is the surface texture. In a recent state-of-the-art publication, Wambold et al. (Ref. 21) state, "It is now generally agreed that the skid resistance of a pavement is controlled by the surface texture characteristics."

An extensive literature search by Wambold et al. (Ref. 21) revealed 41 commonly or recently used methods of measuring surface texture. These techniques produce a wide variety of texture characteristics including surface tracings, RMS texture depth and slope, average texture depth, mean void width, outflow time, and tire noise generated between tire and pavement.

The measurement techniques reviewed were divided into three categories according to the texture property being measured. The three categories were:

1. Direct profile measurement methods.
2. Direct measurements yielding average texture values.
3. Indirect texture measurement techniques.

These texture measurement techniques are listed in Table 3.

The work of Wambold et al. (Ref. 21) cites the importance of the two components of texture (macro and micro) on surface friction. They found that the most conceptually satisfying model relating friction and texture characteristics is that developed by Leu and Henry (Ref. 22), viz.,

$$SN_V = C_0 \exp (C_1 V) \qquad (4)$$

where SN is the skid number (or friction value), V is the velocity of the equipment performing the friction measurement, and C_0 and C_1 are regression coefficients which define the skid number velocity gradient. This model is consistent with known skid number, texture, and velocity relationships in that the coefficient C_0 (the low-speed skid number) can be correlated with microtexture alone, while coefficient C_1 is dependent on macrotexture alone.

Numerous reports have emphasized the importance of microtexture and macrotexture on the low-speed friction value and the friction-velocity gradient, respectively.

---

21. Wambold, J. C., Henry, J. J., and Hegmon, R. R., **Evaluation of Pavement Surface Texture Significance and Measurement Techniques**, Wear, Vol. 83, No. 2, 1982, pp. 351-368.

22. Leu, M. C., and Henry, J. J., **Prediction of Skid Resistance as a Function of Speed From Pavement Texture Measurements**, Transportation Research Record 666, Transportation Research Board, Washington, D.C., 1978, pp. 7-13.

TABLE 3. TEXTURE MEASUREMENT TECHNIQUES (Ref. 21)

DIRECT PROFILE MEASUREMENT METHODS

Silicone casting and profiling

Macrotexture profile tracing
- Profilograph or profilometer
- Modified versions of the profilograph
- University of New South Wales Unit
- Linear traverse device
- Texturemeter--Rainhart Text-Ur-Meter

Microtexture profile tracing
- Profilograph or profilometer
- Gould Surfanalyzer
- Surfindicator

Stereophoto interpretation mapping

Non-laser light stylus
- Vertically projected narrow light beam
- Zero-slope detector

Laser light stylus
- British TRRL contactless sensor
- Modified British TRRL contactless sensor
- Autech laser dimension gauge models 2DSLT and .5DSLT3

Line-of-light (Goodman) method
- Maryland Vidicon system
- KLD ORWIS
- ENSCO photographic line-of-light system

Shadow interpretation
- Ontario Highway Department system
- Photoestimation

DIRECT MEASUREMENT METHODS PRODUCING AVERAGED TEXTURE VALUES

Sand patch methods
- Simple sand patch
- Modified sand patch
- Vibrating sand patch

Sand track

Grease patch

Putty impression
- Simple putty impression
- Modified putty impression

Schonfeld method (stereophotographic technique)

INDIRECT TEXTURE MEASUREMENT METHODS

Outflow meter
- Static drainage method
- Pressurized drainage method

Tire noise
- Microphone mounted on a moving vehicle (near-field measurement)
- Stationary microphone located by the road-side (far-field measurement)

Ribbed versus blank tire skid test

Light depolarization

British Pendulum Tester

Pennsylvania State University Drag Tester

White light speckle

For example, Smith and Fuller (Ref. 23) have found that texture, speed, and friction value are interrelated. Figure 13 illustrates this relationship. The highway skid number (friction value) is seen to increase with texture for the pavements surveyed. With increasing velocity, the skid number is seen to decrease for a given surface.

Leland et al. (Ref. 24) found similar results for aircraft traveling over a flooded runway at speeds from 25 to 100 knots. Figure 14 illustrates their results.

Gallaway et al. (Ref. 25) ascertained that microtexture measurements were indicative of low-speed frictional values. A coarse and fine profiling device was used in combination to predict the skid number at 20 mi/h. Macrotexture measurements (such as sand patch and silicone putty) were found to predict the decrease in skid number from 20 to 60 mi/h.

Henry and Dahir (Ref. 26) have found that adequate microtexture must be present for adequate skid resistance while adequate macrotexture is required to maintain this skid resistance at high speed. Their study was conducted using a highway skid trailer on bituminous surfaces. The mathematical model used was of the same form as Equation 4.

Figure 15 shows the data obtained by Henry and Dahir (Ref. 26). For example, they found that the most useful measurements of microtexture and macrotexture were the British Pendulum Tester and the sand-patch test, respectively. By using regression equations of the form cited in Equation 4, the low-speed skid number can be estimated by the microtexture measurement and the decrease in skid number with velocity by the macrotexture measurement. In other words, constant C_0 and C_1 of Equation 4 are predicted by microtexture and macrotexture measurements, respectively. Based on profiling measurement techniques with subsequent power spectrum analysis, Henry and Dahir (Ref. 26) ascertained that texture components with wavelengths less than 0.5 mm (0.020 in) can be considered microtexture, while greater wavelengths are associated with macrotexture.

---

23. Smith, L. L., and Fuller, S. L., **Florida Skid Correlation Study of 1967-Skid Testing With Trailers**, ASTM-STP-456, Highway Skid Resistance, American Society for Testing and Materials, Philadelphia, Pennsylvania, 1968, pp. 4-101.

24. Leland, T.J.W., Yager, T. J., and Joyner, U. T., **Effects of Pavement Texture on Wet-Runway Braking Performance**, NASA TN D-4323, National Aeronautics and Space Administration, 1968.

25. Gallaway, B. M., Epps, J. A., and Tomita, H., **Effects of Pavement Surface Characteristics and Textures on Skid Resistance**, Report No. 138-4, Texas Transportation Institute, Texas A&M University, College Station, Texas, 1971.

26. Henry, J. J., and Dahir, S. H., **Effects of Textures and the Aggregates that Produce Them on the Performance of Bituminous Surfaces**, Transportation Research Record 712, Transportation Research Board, Washington, D C., 1979, pp. 44-50.

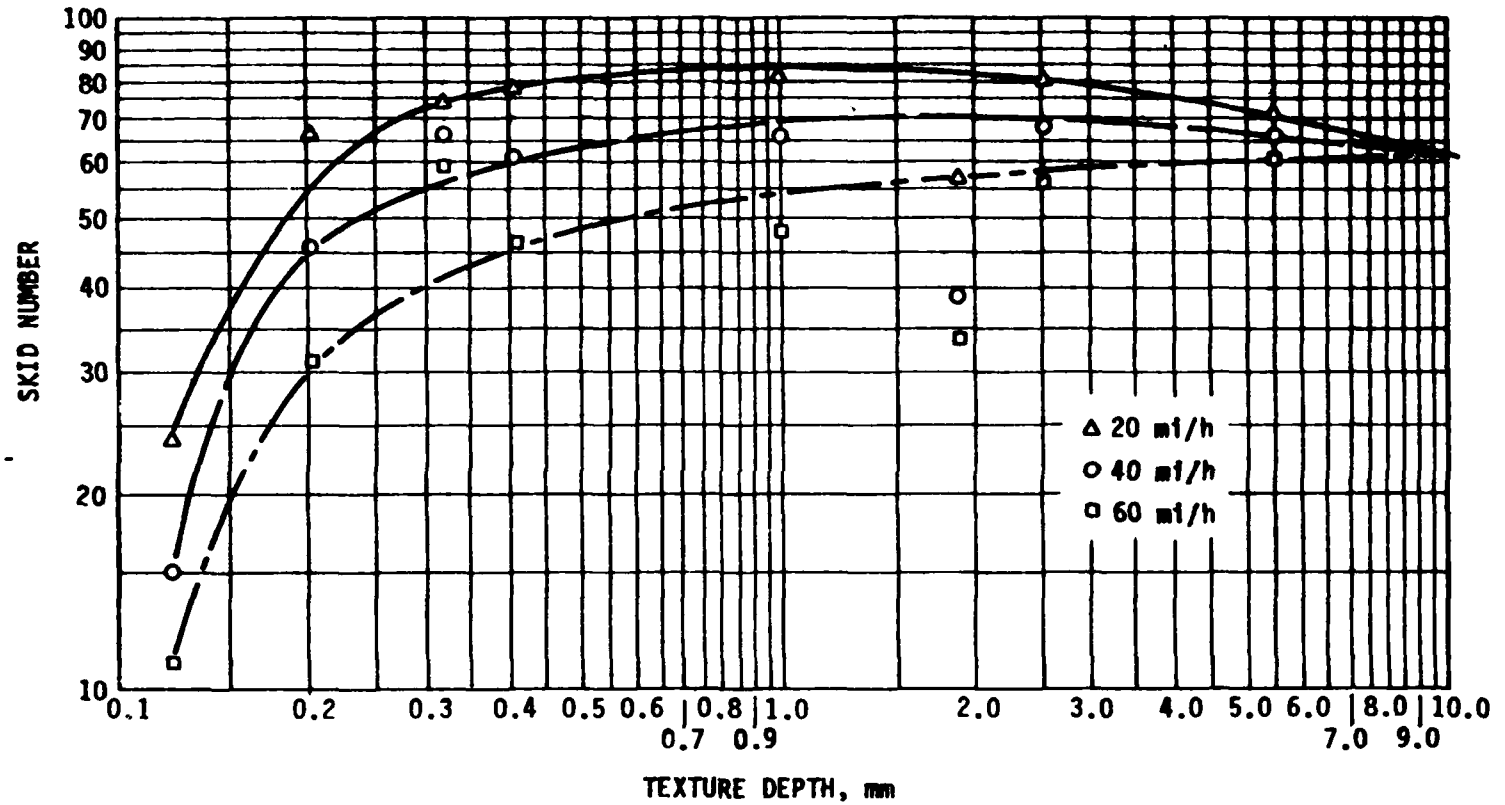

FIGURE 13. SKID NUMBER VERSUS TEXTURE DEPTH--GREASE SMEAR TEST FOR DIFFERENT SURFACES (REF. 23)

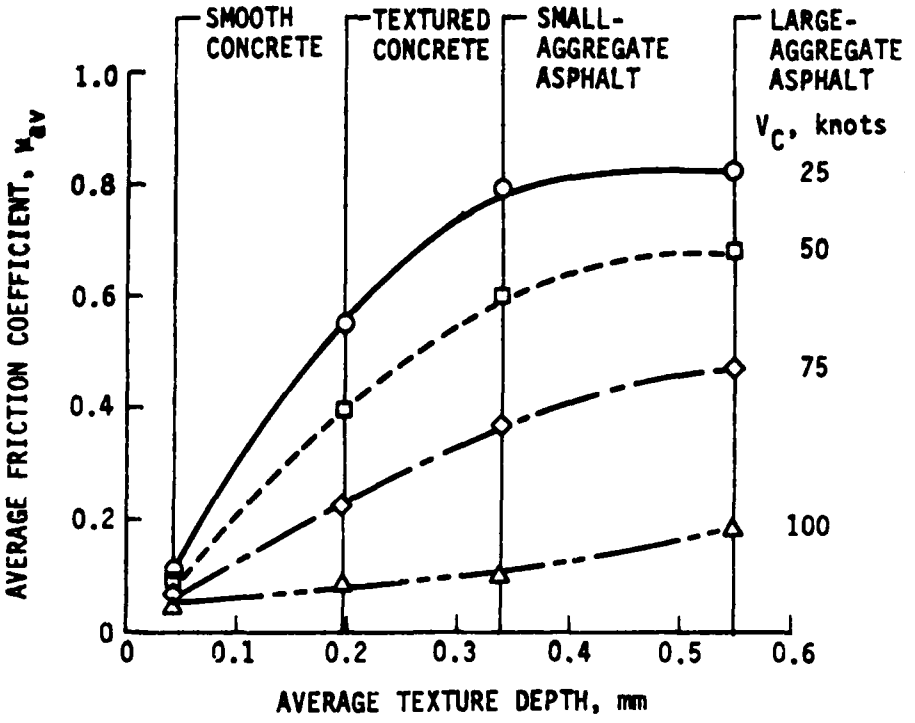

FIGURE 14. EFFECT OF SURFACE TEXTURE ON FRICTION COEFFICIENT--FROM NASA GREASE SMEAR (REF. 24)

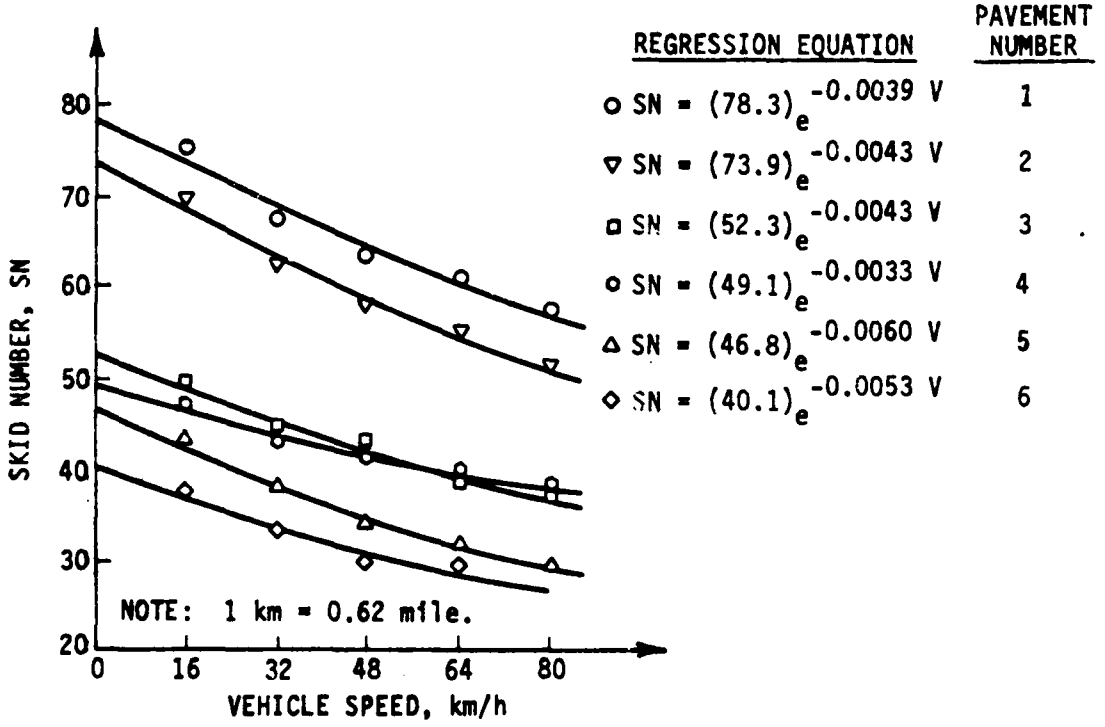

FIGURE 15. SKID NUMBER VERSUS VEHICLE SPEED (REF. 26)

Friction-velocity gradient values are often times ascertained in friction measurement research and evaluation. Olson et al. (Ref. 27) also make use of the percentage gradient which reflects the relative position of the friction velocity curve. Figure 16 illustrates the gradient and percentage gradient and their respective calculation. Most pavement friction researchers are of the opinion that the gradient or percentage gradient is indicative of the macrotexture, conversely, macrotexture can be used to predict the gradient.

Ashkar (Ref. 28) also states that the fine-scale texture (microtexture) of the pavement is the predominant factor determining the skid resistance between tire and pavement at low speeds, while the rate of decrease with speed in the frictional coefficient is dependent on the larger scale texture (macrotexture). Thus, for a wet pavement to have adequate skid resistance at high speed, it is essential that the asperities on its surface be sufficiently large and angular or that the surface have sufficient drainage characteristics.

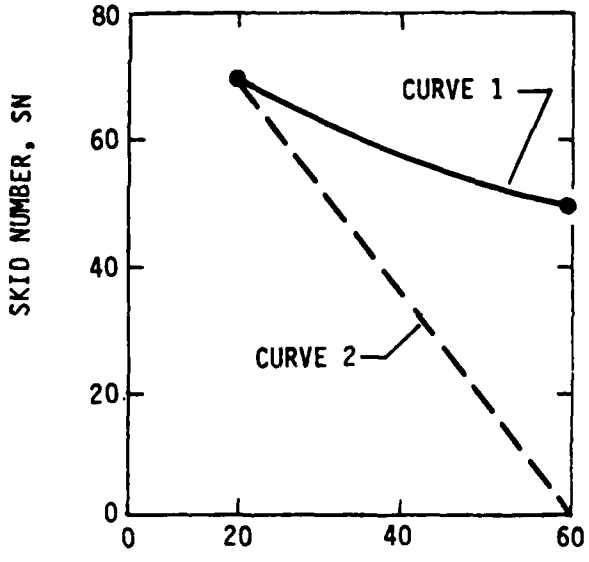

$$\text{GRADIENT (G)} = \frac{SN_{20} - SN_{60}}{40}$$

$$\text{GRADIENT } (G_2) = \frac{SN_{20} - 0}{40}$$

$$\text{PERCENT GRADIENT (PG)} = \frac{G}{G_2} \times 100 = \frac{SN_{20} - SN_{60}}{SN_{20}} \times 100$$

FIGURE 16. GRADIENT AND PERCENTAGE GRADIENT CALCULATIONS (REF. 27)

---

27. Olson, R. M., Johnson, J. H., and Gallaway, B. M., **Vehicle-Pavement Interaction Study**, Report No. 138-7F, Texas Transportation Institute, Texas A&M University, College Station, Texas, 1974.

28. Ashkar, B. H., **Development of a Texture Profile Recorder**, Research Report No. 133-2, Texas Highway Department, 1970.

There are a variety of techniques for appraising pavement texture as outlined by Rose et al. (Ref. 29). They can be generally classified as follows:

1. Volumetric measurements.
2. Profile measurements.
3. Topographic measurements.
4. Contact measurements.
5. Noncontact measurements.
6. Drainage measurements.
7. Dynamic measurements.
8. Miscellaneous.

Each of the measurements listed in Table 3 (Wambold et al., Ref. 21) can be classified according to the techniques listed above.

VOLUMETRIC MEASUREMENTS

This type of measurement yields an average texture depth of the pavement surface. It is predominantly a macrotexture technique since the microtexture has little influence.

In these types of tests, a known volume of test material is uniformly spread on the pavement surface. The test material is applied in such a manner that the surface voids or texture are filled in with just the asperity tips flush with the surface. The area of coverage is ascertained. The ratio of volume to area yields the average texture depth.

Three types of volumetric measurements are commonly made; they are the NASA grease smear, the silicone putty test, and the sand patch test. The sand patch and grease smear procedures use 25 cm^3 and 15 cm^3 of material respectively, while the silicone putty uses 12.87 cm^3.

The NASA grease smear test is described by Leland et al. (Ref. 24). The sand patch test has recently become an ASTM standard (E-965) (Ref. 30). The silicone putty test has been widely used at the Texas Transportation Institute and the Texas Highway Department. The sand patch and silicone putty procedures are detailed in Appendix A.

PROFILE MEASUREMENTS

Ashkar (Ref. 28) cites the development of a texture profile recorder for measuring the macrotexture on highway pavements. This device was designed to magnify the surface texture profile as a stylus is drawn across the pavement

---

29. Rose, J. G., Hutchinson, J. W., and Gallaway, B. M., **Summary and Analysis of the Attributes of Methods of Surface Texture Measurement**, ASTM STP-530, American Society for Testing and Materials, Philadelphia, Pennsylvania, 1973.

30. **Standard Test Method for Measuring Surface Macrotexture Depth Using a Sand Volumetric Technique**, ASTM Designation E-965-83, Annual Book of ASTM Standards, Vol. 04.03, American Society for Testing and Materials, Philadelphia, Pennsylvania, 1984.

surface. The movement of the stylus results in a magnified texture profile scribed on a chart. In addition, the upward vertical excursions are recorded on a counter which represents the cumulative peak heights of the surface texture.

Forster (Ref. 31) studied the microtextural profiles of laboratory-prepared samples using an optical image system. The profiles were characterized by average asperity height, average asperity density, and average asperity shape factor. Correlation with data obtained by the British Pendulum Tester, which measures the friction of a pavement surface due to microtexture, indicates that the asperity shape factor correlates the best. Forster (Ref. 31) also states that the critical wavelength separating micro- and macrotexture is on the order of 0.5 mm (0.020 in). This is in agreement with other studies regarding this critical wavelength.

The Texturemeter, developed at the Texas Transportation Institute (reported by Scrivner and Hudson, Ref. 32), is used to measure macrotexture. This instrument consists of a series of evenly spaced parallel rods mounted in a frame. Each of the rods is spring-loaded and free to move independently of each other. A taut line passes through each rod; one end of the line is fixed, while the other is attached to a dial indicator. When the frame is pressed against a pavement surface, each of the rods deflects in an amount dependent on the texture of the surface. This causes the string to form a zigzag line causing the dial gage to register a reading. The higher the reading, the more texture on the pavement surface. Average peak height of the texture can be calculated from the dial reading.

STEREOPHOTOGRAPHY

Schonfeld (Ref. 33) has developed a photointerpretation method of texture classification. This procedure views the pavement surface as a geometric structure quantified by six parameters, viz., height, width, angularity, distribution, harshness of projections above the matrix, and harshness of the matrix itself. This photointerpretation method makes use of a simple stereophotographic technique. The purpose of the classification method is to correlate pavement texture with test results of skid testing devices. Regression analyses of Schonfeld parameters with skid trailer test results

---

31. Forster, S. W., **Aggregate Microtexture: Profile Measurement and Related Frictional Levels**, FHWA/RD-81/107, U.S. Department of Transportation, Federal Highway Administration, Washington, D.C., 1981.

32. Scrivner, F. H., and Hudson, W. R., **A Modification of the AASHO Read Test Serviceability Index Formula**, Record No. 46, Highway Research Board, Washington, D.C., 1964.

33. Schonfeld, R., **Photo-Interpretation of Pavement Skid Resistance in Practice**, Transportation Research Record 523, Transportation Research Board, Washington, D.C., 1974, pp. 65-75.

yielded correlation coefficients in the range of 0.8 to 0.9. The stereophotographic equipment used is described further in ASTM Standard Test Method E-770 (Ref. 34).

The stereophotographic method is a comprehensive procedure because it appraises the significant characteristics of the asperities that interact with the tire. It relates well with wet skid resistance, but it is somewhat tedious, subjective, and time consuming.

A report by Howerter and Rudd (Ref. 35), for the State of Maryland, showed that automation of the above described Schonfeld (Ref. 33) method was feasible. Electronic photogrammetric techniques were adapted to obtain digital data describing the pavement surface. Algorithms were developed to process these data and classify the surface texture parameters.

Extending the work of Schonfeld (Ref. 33), Holt and Musgrove (Ref. 36) develped a semiautomated system for evaluating the six texture parameters obtained from stereophotography. Making use of a Zeiss Stereocord G-2 system with peripherals, an image-processing system suitable for gathering, processing, and storage of digital data from stereophoto pairs was developed. The system was designed to produce accurate digital profile data, manipulate the data, record, and store data for future manipulation.

Software was developed and algorithms perfected for measuring and evaluating the texture parameters. Profiling routines were developed to scan the photographs in two different directions with subsequent digitizing for future analysis.

Further work is underway by Musgrove and Kazakov at the Ontario Ministry of Transportation and Communications (per personal communication). This work will improve the resolution of the profile measurements by employing more advanced stereo analysis equipment. Also, computer software is under development to perform more advanced data analysis techniques such as power spectrum analysis.

The use of stereophotography was employed by Cechetini (Ref. 37) in a study of rutting effects by studded tires. Profile measurements were obtained

---

34. **Standard Test Method for Classifying Pavement Surface Textures**, ASTM Designation E-770-80, Annual Book of ASTM Standards, Vol. 04.03, American Society for Testing and Materials, Philadelphia, Pennsylvania, 1984.

35. Howerter, E. D., and Rudd, J. T., **Automation of the Schonfeld Method for Highway Surface Texture Classification**, Maryland State Highway Administration, Brooklandville, Maryland, 1975.

36. Holt, F. B., and Musgrove, G. R., **Surface Texture Classification: A Guide to Pavement Skid Resistance**, ASTM STP-763, Pavement Surface Characteristics and Materials, American Society for Testing and Materials, Philadelphia, Pennsylvania, 1982, pp. 31-44.

37. Cechetini, J. A., **The Effects of Studded Tires on Pavement Surfaces in California**, CA-TL-79-04, California Department of Transporatation, Sacramento, California, 1979.

using a stereocomparator. The change in profile over a winter season was indicative of the effects of studded tires.

The NRFMP also conducted stereophotographic measurements; the conclusion gained from these data was that future analysis of stereophotos could provide significant findings on the characteristics of texture which produce desirable friction.

BRITISH PENDULUM TESTER AND PENN STATE DRAG TESTER

The British Pendulum Tester is a dynamic pendulum impact-type tester used to measure the energy loss when a rubber slider edge is propelled over a test surface. The measured value is termed the British Pendulum Number (BPN) which can be converted to a frictional coefficient.

In conducting a test, the pendulum is raised to a locked position (90 deg from surface), when released, the slider attached to the pendulum swings across the surface to be measured. The greater the friction between the slider and test surface, the more the swing through is retarded, and the larger the BPN.

This method has been shown by numerous authors to be representative of the friction component attributed to microtexture. The British Pendulum Tester is described in detail in ASTM E-303 (Ref. 38).

The Penn State Drag Tester is essentially a two-wheeled cart with a rubber slider attached. When pushed over a test surface, the rubber slider resists motion. The force, parallel to the test surface, which acts on the slider registers an output on a dial gage via a hydraulic cylinder. The output is termed a Drag Test Number (DTN) and is easily converted to a frictional coefficient. The development of the drag tester is described by Kummer (Ref. 39). Appendix B of this report contains a description of the drag tester.

In another report, Kummer (Ref. 40) describes the excellent correlation between the Penn State Drag Tester and the British Pendulum Tester. Since the pendulum tester results are indicative of microtexture, then the drag tester results must also be representative of microtexture based on the excellent correlation cited above.

---

38. **Standard Method for Measuring Surface Frictional Properties Using the British Pendulum Tester**, ASTM Designation E-303-83, Annual Book of ASTM Standards, Vol. 04.03, American Society for Testing and Materials, Philadelphia, Pennsylvania, 1984.

39. Kummer, H. W., **The Penn State Drag Tester**, Report No. 7, Joint Road Friction Program, Pennsylvania Department of Highways, Pennsylvania State University, Department of Mechanical Engineering, University Park, Pennsylvania, 1963.

40. Kummer, H. W., **Correlation Tests With the Penn State Drag Tester**, Report No. 9, joint Road Friction Program, Pennsylvania Department of Highways, Pennsulvania State University, Department of Mechanical Engineering, University Park, Pennsylvania, 1964.

CHALK WEAR TEST

A recently suggested method for evaluating the microtexture of a pavement surface is the chalk wear test proposed by Burk (per USAF memorandum, 1979). This wear device consists of a wheeled cart with a swing arm and chalk holder. The chalk holder incorporates a threaded rod to adjust the amount of exposed chalk. The apparatus is machined out of aluminum to reasonable tolerances to ensure a precise normal surcharge on the pavement.

The length of exposed chalk is measured prior to testing. The chalk cart is then pushed across the test surface causing the chalk to wear. The difference in chalk length divided by the length of travel yields a chalk wear coefficient.

After extensive discussions with members of ASTM Committee E-17 (Traveled Surface Characteristics), Burk (per USAF memorandum, 1979) concluded that this test was a viable procedure for evaluating surface microtexture.

The authors have had similar responses at recent E-17 meetings. For example, Mr. Walter Horne (formerly with NASA) was of the opinion that Burk's chalk wear value should be highly influenced by the level of microtexture on the pavement surface (per personal communication, December 1983).

OUTFLOW (DRAINAGE) DEVICE

To evaluate surface texture, Moore (Ref. 12) developed a simple instrument called an outflow meter (Fig. 17). Moore's outflow meter was used to

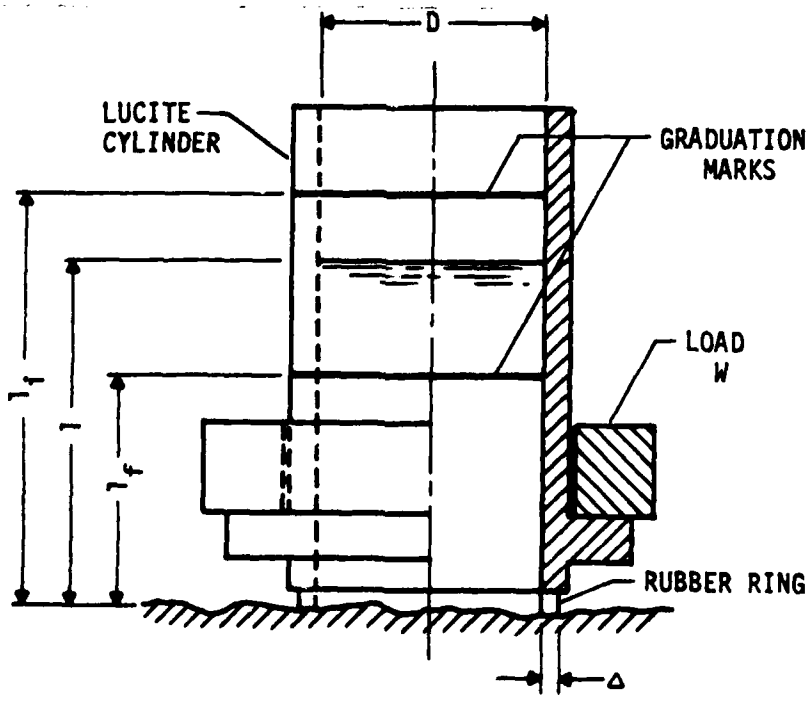

FIGURE 17. THE BASIC OUTFLOW METER (REF. 12)

compare the relative drainage capability of different surfaces. Outflow data were also used to establish the friction-speed gradient for different surfaces.

In the use of the outflow meter, Moore (Ref. 12) developed a mathematical model (based on a hydrodynamic analogy) to account for the affects of both macro- and microtexture on outflow time. Uniformly machined plates (one with a cubed asperity surface and one with a square pyramid asperity surface) were used to evaluate this theory and to calibrate the meter.

Moore (Ref. 12) also describes a profiling device (profilometer) which compared quite well with outflow meter measurements.

NON-CONTACT TECHNIQUES

Various systems for performing high-speed non-contact texture measurements have been developed and evaluated. The following paragraphs describe a few of these.

Her, et al. (Ref. 41) describe a non-contact high-speed method of obtaining texture profile from a vehicle moving at highway speeds. Their system utilizes a light-sectioning technique in which a strobed band of light with high infrared content is projected onto the pavement. A camera with high infrared sensitivity views the band at an angle. The resulting pictures from each strobe are stored in a frame grabber and processed by detecting the shadow along the lead edge of the band to produce a macrotexture profile. Further development and improvements may yield a practical texture profile acquisition system.

Gee et al. (Ref. 42) found that laser depolarization can serve as an unambiguous descriptor of surface textural characteristics. Limited dynamic testing indicated that laser data correlates reasonably well with both skid resistance and conventional coarse texture measurement data. This system offers a noncontact, real time technique of texture measurement.

Harr and Elton (Ref. 43) describe a noncontact, nondestructive method that allows the measurement of pavement texture in addition to loaded and

---

41. Her, I., Henry, J. J., and Wambold, J. C., **Development of a Data Acquisition Method for Noncontact Pavement Macrotexture Measurement**, Presented at the 63rd Annual Meeting of the Transportation Research Board, Washington, D.C., 1984.

42. Gee, S., King, W. L., Jr., and Hegmon, R. R., **Pavement Texture Measurement by Laser, A Feasiblity Study, Surface Texture Versus Skidding: Measurements, Frictional Aspects, and Safety Features of Tire-Pavement Interactions**, STP-583, American Society for Testing and Materials, Philadelphia, Pennsylvania, 1975, pp. 29-40.

43. Harr, M. E., and Elton, D. J., **Non-Contact, Non-Destructive Airport Pavement Profile, Texture, and Deflection Measurements**, DOT/FAA/PM-83/14, U.S. Department of Transportation, Federal Aviation Administration, Washington, D.C., 1983.

unloaded profiles. This technique uses a series of four laser distance measurement gages mounted on the side of a vehicle, three of which are outside the influence of the load wheel, with the fourth being adjacent to the load wheel. The sampling rate is fast enough that the standard deviation of the readings (over a short distance) is indicative of the texture.

Studies at the Pennsylvania Transportation Institute (PTI) by Veres et al. (Ref. 44) indicate that tire noise measurements can be used to distinguish pavements of different macrotexture. A correlation was found to exist between the skid number speed gradient and the near-field tire noise at a frequency band in the vicinity of 1600 Hz. Continued efforts at PTI are being directed at enhancement of decibel output and more sensitive techniques of weighing the noise spectra.

OTHER TEXTURE AND FRICTION MEASUREMENT EFFORTS

Yager and Bühlmann (Ref. 45) evaluated 3 volumetric techniques and 2 outflow meters on 15 different pavement surfaces. The silicone putty test, NASA grease smear test, and sand patch test were the volumetric tests evaluated. In terms of average texture depth, the grease smear results were 58 percent of the sand patch results and 43 percent of the silicone putty results. Silicone putty results were 7 percent higher than the sand patch results.

The outflow devices yielded markedly different outflow times on the same pavement section. This is attributed to the difference in design, specifically with regard to the rubber seal separating the pavement and water reservoir. The different rubber seal design produces significantly different bearing pressures between the seal and pavement.

Comparison of British pendulum test data with volumetric measurements and outflow data was poor. This is attributed to the fact that surface microtexture has a greater influence on British pendulum results than does the surface macrotexture as measured by texture depth or outflow drainage time.

Correlation between the individual volumetric techniques and the individual outflow devices was reasonably good. In general, outflow time increased with decreasing texture depth.

---

44. Veres, R. E., Henry, J. J., and Lawther, J. M., **Use of Tire Noise as a Measure of Pavement Macrotexture, Surface Texture Versus Skidding: Measurements, Frictional Aspects, and Safety Features of Tire-Pavement Interactions**, STP-583, American Society for Testing and Materials, Philadelphia, Pennsylvania, 1975, pp. 18-27.

45. Yager, T. J., and Bühlmann, F., **Macrotexture and Drainage Measurements on a Variety of Concrete and Asphalt Surfaces**, ASTM STP-763, Pavement Surface Characteristics and Materials, American Society for Testing and Materials, Philadelphia, Pennsylvania, 1982, pp. 16-30.

Gallaway and Rose (Ref. 46) evaluated pavement surface macrotexture using the profilograph, texturemeter, sand patch, and silicone putty test methods. They found that all four of these test techniques correlated favorably with each other. Correlation of these test techniques with skid trailer data indicated that the skid number velocity gradient data related the best with these macrotexture test parameters.

Henry and Hegmon (Ref. 47) state that skid resistance on wet pavements always decreases with increasing speed. The rate of this decrease is smaller for coarser textured pavements (higher macrotexture). Thus, the dependence of wet skid resistance on speed is clearly related to the drainage capability of the tire-pavement contact area.

Henry and Hegmon (Ref. 47) evaluated two texture measurement techniques, viz., the outflow meter and the profile tracer (profilograph). The outflow meter measures the drainage capability of a pavement as affected by texture (both micro and macro have an influence) and pavement porosity. The outflow meter, developed by Moore (Ref. 12), has been illustrated in Figure 17. The timed outflow of water is indicative of the pavement texture and porosity. Their profile tracer employed a stylus (1.6-mm-diameter steel with a 20-deg cone and a tip radius of 0.125 mm) with a transducer follower. The output yields a profile of a pavement surface.

The outflow meter data obtained by Henry and Hegmon (Ref. 47) did not yield an acceptable correlation between the skid number speed gradient and timed outflow. Profile parameters (first and second derivatives of profile elevation) derived from profile autocorrelations and spectral densities proved to correlate well with the percent skid number gradient (PSNG) at a 40-mi/h velocity. This relationship is shown in Figure 18 where percent skid number is related to a product of the first and second derivatives of profile elevation.

Hill and Henry (Ref. 48) state that the British Pendulum Number (BPN) obtained from the British Pendulum Tester can be used to predict the skid number at zero speed. In other words, the BPN predicts the intercept value (friction value) of a friction versus velocity curve.

---

46. Gallaway, B. M., and Rose, J. G., **Macro-Texture Friction, Cross Slope, and Wheel Track Depression Measurements on 41 Typical Texas Highway Pavements**, Report No. 138-2, Texas Transportation Institute, Texas A&M University, College Station, Texas, 1970.

47. Henry, J. J., and Hegmon, R. R., **Pavement Texture Measurement and Evaluation, Surface Texture Versus Skidding: Measurements, Frictional Aspects, and Safety Features of Tire-Pavement Interactions**, STP-583, American Society for Testing and Materials, Philadelphia, Pennsylvania, 1975, pp. 3-17.

48. Hill, B. J., and Henry, J. J., **Surface Materials and Properties Related to Seasonal Variations in Skid Resistance**, ASTM STP-763, Pavement Surface Characteristics and Materials, American Society for Testing and Materials, Philadelphia, Pennsylvania, 1982, pp. 45-60.

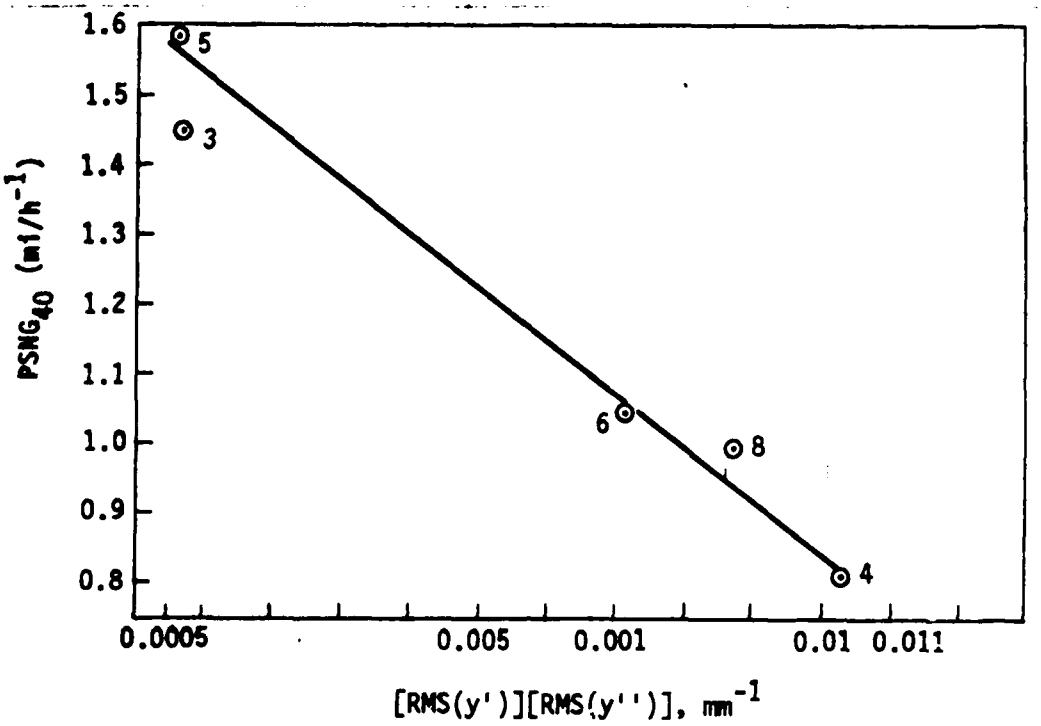

FIGURE 18. PERCENT SKID NUMBER-SPEED GRADIENT VERSUS RMS (y') RMS (y'') (REF. 47)

In conducting studies on the effectiveness of reflective coatings for hangar floors, Hearst (Ref. 49) found that the British Pendulum Tester appeared to be appropriate for measurement of slip resistance.

---

49. Hearst, P. J., **Reflective Coatings for Hangar Floors--Laboratory Studies and Initial Field Test Results**, TM No. 52-84-06, Naval Civil Engineering Laboratory, Port Hueneme, California, 1983.

V. SELECTION OF FIELD TEST TECHNIQUES

The pavement surface characteristic that governs the amount of friction between tire and pavement has been shown to be texture. Pavement texture can be broken into two components, viz., the macrotexture and microtexture. The microtexture controls the low-speed friction characteristics. The macrotexture is influential on the decrease in friction level with speed. Therefore, to define the friction characteristics of a pavement by using a surface measurement technique, both macro- and microtexture must be evaluated.

In evaluating surface texture, a macrotexture test and microtexture test must be used in conjunction. However, single test techniques which can measure the entire pavement spectra (macro- and microtexture components) may be used alone.

In the introductory remarks, it was stated that simple, inexpensive test techniques which are operator insensitive are desirable for measuring rubber build-up on runways. Correlation of these test techniques with Mu-Meter friction data will enable the development of specifications and guidelines for determining when rubber should be removed and when satisfactory completion of rubber removal has been accomplished.

PRELIMINARY SELECTION

In the report by Wambold, Henry and Hegmon (Ref. 21), the statement is made that high-speed measurements of microtexture are difficult to obtain and, in general, the measurement of microtexture must be by a static method. The static methods most commonly used for evaluating microtexture are microtexture profiling equipment, the British Pendulum Tester, and the Penn State Drag Tester.

One of the requirements of the test selection scheme is that the test procedures be simple. Also, the procedures must not require extensive training or presume a prescribed level of training or education.

With this constraint in mind, the noncontact equipment requiring electronic equipment and special sophisticated calibration procedures were eliminated from consideration. These included the various light, laser, tire noise, and shadow techniques. In addition, many of these techniques require interpretive skills unavailable to most field technicians or airport managerial personnel.

The outflow meter was considered for inclusion in a field test matrix. However, as the analysis by Moore (Ref. 12) indicates, the influence of macro- and microtexture on outflow time are both important. This is analogous to the flow of water through a pipe network, whereby the flow rate is governed by the pipe size and roughness of the pipe surface. The separation of the effects of macro- and microtexture on outflow data is not an easy task from a mathematical standpoint. Therefore, the outflow measurement equipment was eliminated from further consideration.

The volumetric techniques are considered a good descriptor of macrotexture. Good correlations between macrotexture and friction-speed gradient have

been obtained as cited previously. The profiling techniques and Texturemeter were also considered for macrotexture determination.

During preliminary review of the various techniques, the only combined macro/microtexture method felt worthy of further consideration was the stereophotographic technique of Schonfeld (Ref. 33). The excellent correlations obtained between Schonfeld texture parameters and friction values warranted further consideration of this system.

Field evaluation of microtexture using the chalk wear test was considered based on the input gained by Burk and the authors in conversations with ASTM E-17 committee members.

The preliminary selection process described above generated the following macrotexture, microtexture, and combined macro/micro test techniques for further consideration:

1. Macrotexture
   - Volumetric Techniques
     - Sand Patch
     - Silicone Putty
     - Grease Smear
   - Profiling Techniques

2. Microtexture
   - Profiling Techniques
   - British Pendulum Tester
   - Penn State Drag Tester
   - Chalk Wear Test

3. Combined Macro/Micro
   - Stereophotography

A field test scheme incorporating all nine of the above test methods was felt to be too time consuming. Based on further review of the literature and conversations with various experts in the pavement friction evaluation community the profiling techniques and British Pendulum Tester were eliminated.

The profiling devices in general are mechanical devices that require some amount of time to set up and operate. In addition, depending upon the profiling device selected, electronic hardware and calibration procedures may be required.

The British Pendulum Tester is also known to be quite time consuming to set up and operate. Other information indicates that the setup procedures can be susceptible to operator error. The cost of the British Pendulum Tester is thought to be excessive. The British Pendulum Tester and Penn State Drag Tester both measure microtexture in a similar fashion and are known to correlate with each other. Therefore, the British Pendulum Tester was eliminated in favor of the Penn State Drag Tester.

Based on the excellent recommendations found in the literature, the stereophotographic technique was retained for inclusion in future field evaluations. The cost of obtaining commercially available camera equipment and

fabricating a stereo camera box is relatively inexpensive (such a design is shown in Appendix C). The real cost would be found in analyzing the photographs. However, if reasonable data could be obtained using this technique, then such a procedure could be justified.

For example, if stereophotographic methods were incorporated into a USAF or FAA specification, the cost of analyses could be markedly reduced. Stereophotographs could be obtained by airport or airbase personnel and then evaluated at a central processing center. This processing center might be a government contractor with photogrammetric capabilities or an organization with similar capabilities within the FAA or USAF.

LABORATORY COMPARISON OF VOLUMETRIC TECHNIQUES

The literature review, along with queries to various individuals familiar with the three volumetric techniques, did not indicate which of the three volumetric test procedures would be superior for routine field testing. All three of these procedures are known to correlate extremely well with each other as discussed in Section IV.

In order to select a volumetric technique for inclusion in the field test program, a limited laboratory experiment was conducted to compare the three test procedures.

The laboratory experiment was of a completely randomized statistical design. The dependent variable (or measured variable) was the average texture depth. The independent variables were the three test procedures (grease smear, sand patch, and silicone putty), the effects of three operators (technicians), and the effects of two different texture surfaces. The test matrix described is illustrated in Figure 19. Three replications of each procedure on each test surface was conducted by each technician.

A fourth independent variable was the affect of repeating the test matrix described above at a later date. The second laboratory series was altered slightly from the first laboratory series in that the volumes of grease and sand used were reduced from 15 cm^3 and 25 cm^3 to 10 cm^3 and 15 cm^3, respectively.

Texture Surface	TD-20			TD-40		
Operator	1	2	3	1	2	3
NASA grease smear	---	---	---	---	---	---
	---	---	---	---	---	---
	---	---	---	---	---	---
ASTM E965 sand patch	---	---	---	---	---	---
	---	---	---	---	---	---
	---	---	---	---	---	---
Silicone putty	---	---	---	---	---	---
	---	---	---	---	---	---
	---	---	---	---	---	---

FIGURE 19. TEST MATRIX--LABORATORY COMPARISON OF VOLUMETRIC TEXTURE TECHNIQUES

The texture surfaces were machined on aluminum plates to yield a uniform texture depth. The machined surfaces were of a truncated pyramid design (Fig. 20). One texture plate was machined to yield an average texture depth of 0.5 mm (0.020 in), while the other plate had average depth of 1.0 mm (0.040 in). Figure 21 shows a closeup of the 1-mm plate (TD-40).

Typical laboratory results of the sand patch, silicone putty, and grease smear tests are shown in Figure 21. The texture depths obtained throughout the experiment (both laboratory series one and two) are shown in matrix form in Table 4.

Table 4 also shows the mean ($\bar{x}$) and standard deviation (s) of the individual procedures for a given textured surface. A review of Table 4 shows that the average values for the grease smear and sand patch are virtually identical for a given test plate. However, the silicone putty results are generally on the order of 0.009 in greater than the sand patch and grease smear.

Before performing an Analysis of Variance (ANOVA), the variances from laboratory series one and two were determined to be homogeneous by use of the Burr-Foster Q-Test (see Anderson and McLean, Ref. 50, for description of the Q-Test and the ANOVA). Since homogeneity was confirmed, transformation of the data was not required.

The ANOVA was then conducted, the results of which are shown in Table 5. This table shows the four independent variables as well as all the possible interaction terms. The critical F values were obtained from standard F-distribution statistical tables for a significance level of 1 percent. The calculated F values are the ratio of the mean square for a given source type to the mean square of the error.

When the calculated F value is greater than the critical F value, a significant difference exists between one or more variables within that source. For example, the texture test plate variable yields an F value of 3322.1 versus a critical F value of 7.03. This indicates that the texture plates are significantly different when texture measurements are conducted on these textured plates. Table 4 shows that all three texture measurement techniques are able to significantly distinguish between a textured surface of 1 mm and a surface of 0.5 mm. Also, the operators conducting these test procedures were able to obtain significant differences between test plates.

Significant differences were found to exist between test procedures. As discussed earlier, the silicone putty results were always greater than the sand patch or grease smear, the two of which were virtually identical. Performance of a Newman-Keuls test (see Anderson and McLean, Ref. 50) verified that the silicone putty test is significantly different than the other two test procedures. The sand patch and grease smear tests are not significantly different based on the Newman-Keuls analysis.

Table 5 shows that the interaction term of technician and procedure (T x P) is significant. Extensive training of all three technicians was

---

50. Anderson, V. L., and McLean, R. A., **Design of Experiments, A Realistic Approach**, Marcel Dekker, Inc., New York, New York, 1974.

TABLE-DIMENSIONS, in

TEXTURE PLATE	B	N	S	L (±0.020 in)
TD-40	0.077	33	0.231	7.623
TD-20	0.039	108	0.117	12.636

(TOLERANCES: ±0.001 in)

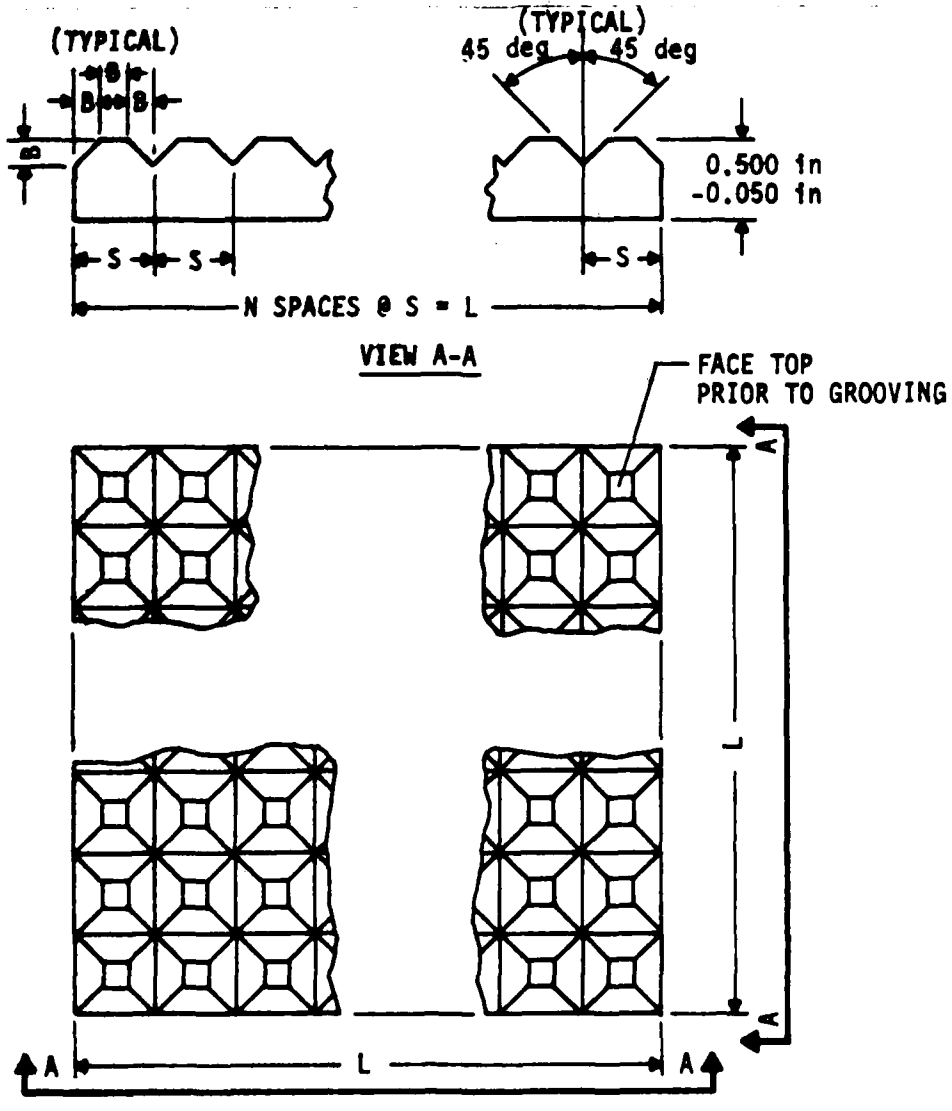

FIGURE 20. TEXTURE PLATES

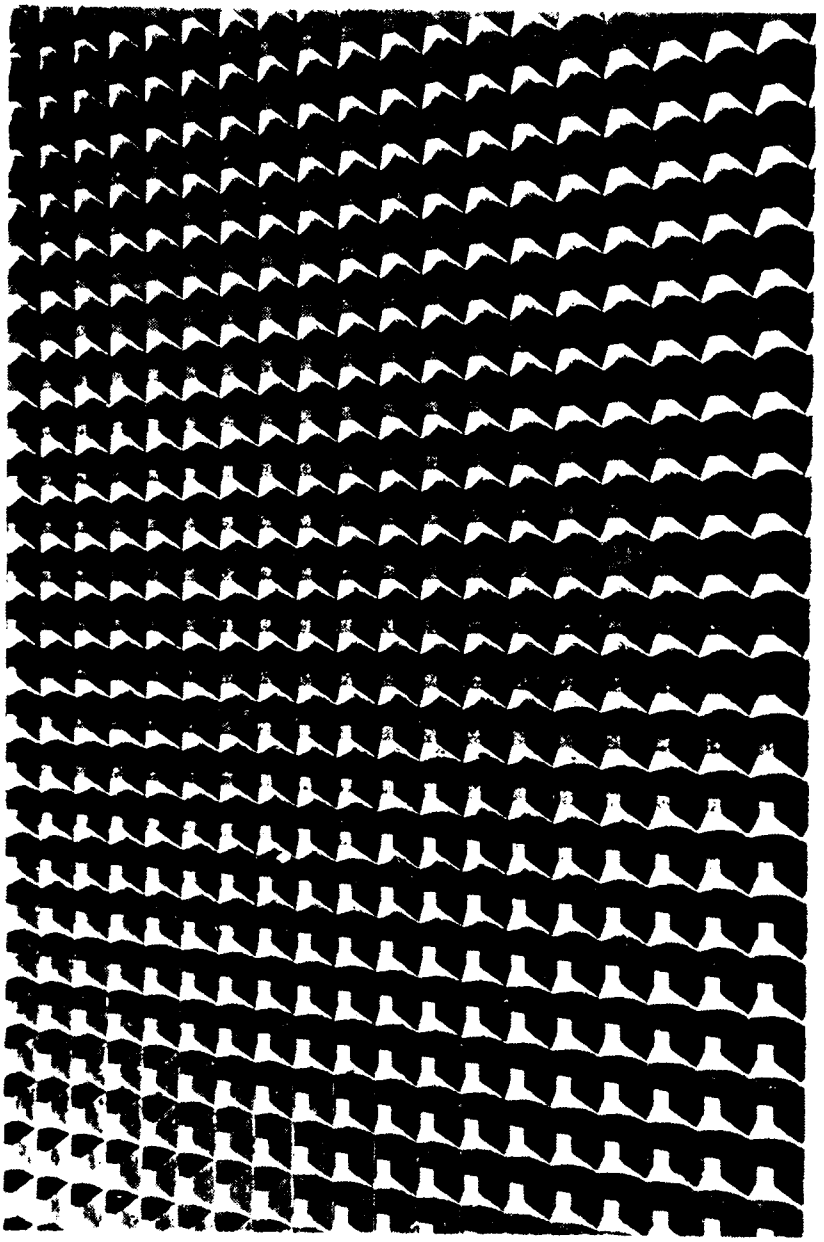

FIGURE 21. TEXTURE PLATE TD-40 (CLOSEUP)

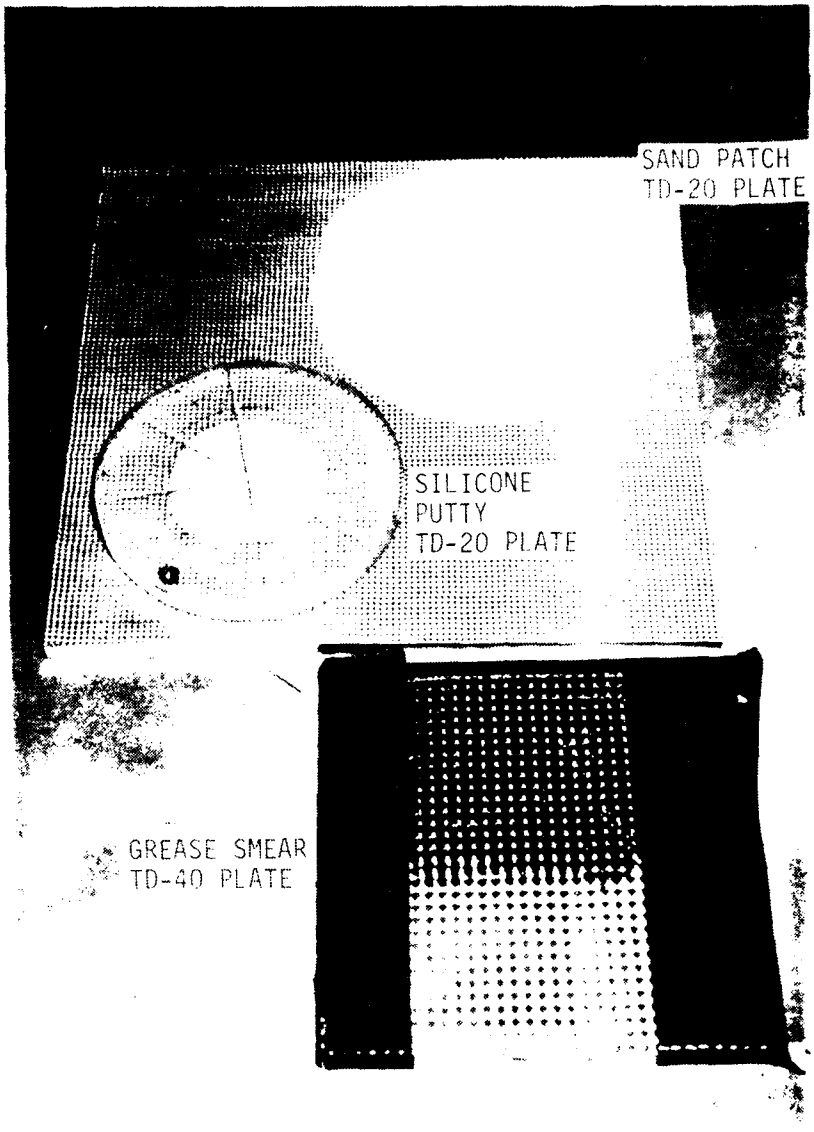

FIGURE 22. TYPICAL RESULTS OF LABORATORY COMPARISON OF VOLUMETRIC TEXTURE TECHNIQUES

TABLE 4. LABORATORY RESULTS FROM COMPARISON OF VOLUMETRIC TEXTURE TECHNIQUES

	LAB SERIES 1 TEXTURE DEPTH, in							LAB SERIES 2 TEXTURE DEPTH, in				
Texture Plate	TD-20			TD-40				TD-20		TD-40		
Operator	1	2	3	1	2	3	1	2	3	1	2	3
Grease Smear	0.0184	0.0213	0.0181	0.0407	0.0387	0.0460	0.0182	0.0200	0.0206	0.0367	0.0399	0.0451
	0.0197	0.0194	0.0208	0.0422	0.0393	0.0452	0.0180	0.0180	0.0208	0.0386	0.0371	0.0401
	0.0174	0.0208	0.0210	0.0380	0.0406	0.0441	0.0195	0.0206	0.0222	0.0420	0.0384	0.0436
Mean	$\bar{x}$ = 0.0197			$\bar{x}$ = 0.0416				$\bar{x}$ = 0.0198		$\bar{x}$ = 0.0402		
Std. Dev.	s = 0.0014			s = 0.0029				s = 0.0015		s = 0.0029		
Sand Patch	0.0196	0.0189	0.0220	0.0413	0.0396	0.0422	0.0223	0.0239	0.0176	0.0399	0.0420	0.0369
	0.0204	0.0179	0.0220	0.0401	0.0365	0.0406	0.0225	0.0195	0.0192	0.0382	0.0404	0.0372
	0.0187	0.0199	0.0176	0.0409	0.0390	0.0398	0.0181	0.0169	0.0188	0.0395	0.0389	0.0347
Mean	$\bar{x}$ = 0.0197			$\bar{x}$ = 0.0400				$\bar{x}$ = 0.0199		$\bar{x}$ = 0.0386		
Std. Dev.	s = 0.0016			s = 0.0016				s = 0.0024		s = 0.0022		
Silicone Putty	0.0306	0.0275	0.0285	0.0511	0.0492	0.0516	0.0332	0.0300	0.0263	0.0499	0.0490	0.0509
	0.0277	0.0261	0.0307	0.0514	0.0522	0.0550	0.0280	0.0259	0.0280	0.0484	0.0488	0.0512
	0.0282	[a]0.0284	0.0281	0.0466	0.0464	0.0497	0.0239	0.0265	0.0270	0.0479	0.0479	0.0486
Mean	$\bar{x}$ = 0.0284			$\bar{x}$ = 0.0504				$\bar{x}$ = 0.0276		$\bar{x}$ = 0.0492		
Std. Dev.	s = 0.0015			s = 0.0027				s = 0.0027		s = 0.0012		

[a]Average of eight other values in cell TD-20 x Silicone Putty x Lab Series I.

TABLE 5. ANOVA OF VOLUMETRIC TEXTURE TECHNIQUE EXPERIMENT

Source	df	SS	MS	$F_{crit}^{(\alpha = 0.01)}$	F
Lab Series (LS)	1	0.00001511	0.00001511	7.03	4.29
Test Plate (TP)	1	0.01171042	0.01171042	7.03	[a]3322.1
Technician (T)	2	0.00003206	0.00001603	4.94	4.55
Procedure (P)	2	0.00194380	0.00097190	4.94	[a]275.7
LS x TP	1	0.00000948	0.00000948	7.03	2.69
LS x T	2	0.00001936	0.00000968	4.94	2.75
LS x P	2	0.00000076	0.00000038	4.94	0.11 (<1)
TP x T	2	0.00001461	0.00000731	4.94	2.07
TP x P	2	0.00002328	0.00001164	4.94	3.30
T x P	4	0.00006040	0.00001510	3.45	[a]4.28
LS x TP x T	2	0.00000472	0.00000236	4.94	0.67 (<1)
LS x TP x P	2	0.00000208	0.00000104	4.94	0.30 (<1)
LS x T x P	4	0.00002318	0.00000580	3.45	1.64
TP x T x P	4	0.00002556	0.00000639	3.45	1.81
LS x TP x T x P	4	0.00000655	0.00000164	3.45	0.46 (<1)
Error	72	0.00025380	0.00000353		1
Total	107				

[a]Significant @ $\alpha = 0.01$

NOTES: df = degrees of freedom
SS = Sum of Squares
MS = Mean Square = SS/df
F = MS Source/MS Error

conducted prior to performing this experiment. However, it appears that technician technique in conducting the three test procedures is an important factor in accurate testing. This point emphasizes the importance of using uniform standardized procedures when performing volumetric texture measurements. The use of controlled surfaces as used in this experiment could prove beneficial in training personnel to use these types of procedures.

The presumed reason for the difference between the silicone putty test results and those obtained by either the grease smear or sand patch tests is as follows. Inevitably, when performing the grease smear or sand patch, the grease and sand is forced to a level below the tips of the asperities (in this case, the flat top of the truncated pyramids). This is caused by the squeegee used in the grease smear or the rubber disc used in performing the sand patch.

In performance of the silicone putty tests, a 1/16-in layer of putty remains above the asperity tips due to the recess in the plexiglass plate used in performing this test. While this 1/16-in layer is accounted for in calculating the average texture depth, it does ensure that the entire texture depth is accounted for since the putty completely fills in all surface voids to a point even with the tops of all the asperities.

Strict tolerances and quality control were maintained in machining the texture plates. However, certain rounding effects of the edges can result. Deburring of the many machined edges could possibly lead to rounding of edges producing a net increase in texture depth.

To evaluate the effects of rounding during machining, the average thickness of the plates was ascertained. This was accomplished by determining the specific gravity of the aluminum texture plates and calculating the thickness of each plate based on weight-volume relationships. This average thickness was then subtracted from an average value of the maximum thickness for each plate yielding an average texture depth. This process yielded an average texture depth for the TD-20 plate of 0.025 in and 0.046 in for the TD-40 plate.

Based on the above discussion, it is clear that the silicone putty tests, in general, overpredicted the texture of the plates, while the grease smear and sand patch procedures underpredicted the texture depth.

Since the grease smear and sand patch results were comparable, the grease smear test was eliminated from the preliminary field test plan. It was felt that the grease smear was a messy procedure and too time consuming to perform.

Both the sand patch procedure and silicone putty procedures were selected for future field evaluation. Both are simple and quick to perform and both are inexpensive to procure and maintain.

FINAL SELECTION

The procedures selected for use in developing criteria and specifications for rubber removal are listed in Table 6.

TABLE 6. SELECTED FIELD PROCEDURES

Macrotexture	Sand Patch Volumetric Technique (ASTM E-965) Silicone Putty Volumetric Procedure
Microtexture	Penn State Drag Tester Chalk Wear Test
Combined Micro/Macro	Stereophotography

Equipment and procedural aspects of the selected procedures are detailed in Appendixes A, B, and C.

VI. DESIGN OF FIELD EXPERIMENT

The following proposed field test plan is suggested for developing criteria and specifications for rubber removal from airport runways.

The plan is based on the theoretical concepts and available experimental data that suggest wet pavement friction can be predicted by the measurement of pavement surface texture.

In order to validate this theory, a field test plan was designed which will statistically show the pavement macro- and/or microtexture measurements indicative of wet pavement friction levels as obtained with a Mu-Meter.

These tests are to be conducted immediately before and after rubber removal in the pavement areas where rubber build-up is of concern. In addition, measurements in nonrubber pavement control areas along the centerline and edge of the runway will also be evaluated. Measurements in these areas will aid in determining the possible effects of wear due to traffic and weathering.

Figure 23 illustrates three distinct friction curves obtainable during field testing. Since rubber deposits reduce the macro- and microtexture, the friction curve obtained before rubber removal would yield lower intercept values and higher friction gradients. After rubber removal is conducted, the curve would move vertically upward to position two yielding a greater intercept value and lower friction gradient as both micro- and macrotexture have been improved.

Removal of rubber is not always 100-percent efficient. Therefore, the after-rubber removal curve may not be the maximum obtainable for the specific pavement evaluated. The effects of polish due to traffic and weathering may also prevent the development of the full friction capability of the evaluated pavement. Rubber removal processes may also tend to polish the surface. The control areas to be measured during field testing are indicative of the theoretical maximum friction capability of the pavement surface.

Based on these concepts, a field test matrix as shown in Figure 24 has been developed. All tests are to be performed in duplicate in each of three separate and distinct test sections, viz., a centerline rubber-covered area, a centerline nonrubber area, and a runway pavement edge nonrubber area. All three test sections are to be of the same pavement type; they should all be uniform in terms of their surface characteristics. Measurements will be conducted on the centerline rubber area both before and after rubber removal.

Each test section is approximately 480 ft in length with three distinct test locations placed evenly throughout. These three test locations are located so that all the candidate test procedures can be compared with Mu-Meter test data at precisely known points. Figure 25 shows a typical runway layout with the designated test sections and test locations.

In order to develop friction-speed gradients, Mu-Meter testing is performed at 20, 40, and 60 mph. In addition, both wet and dry Mu-meter tests are performed. An unpublished data report by Burk (inter-Air Force correspondence) suggests that macrotexture dictates the difference between dry and wet Mu values.

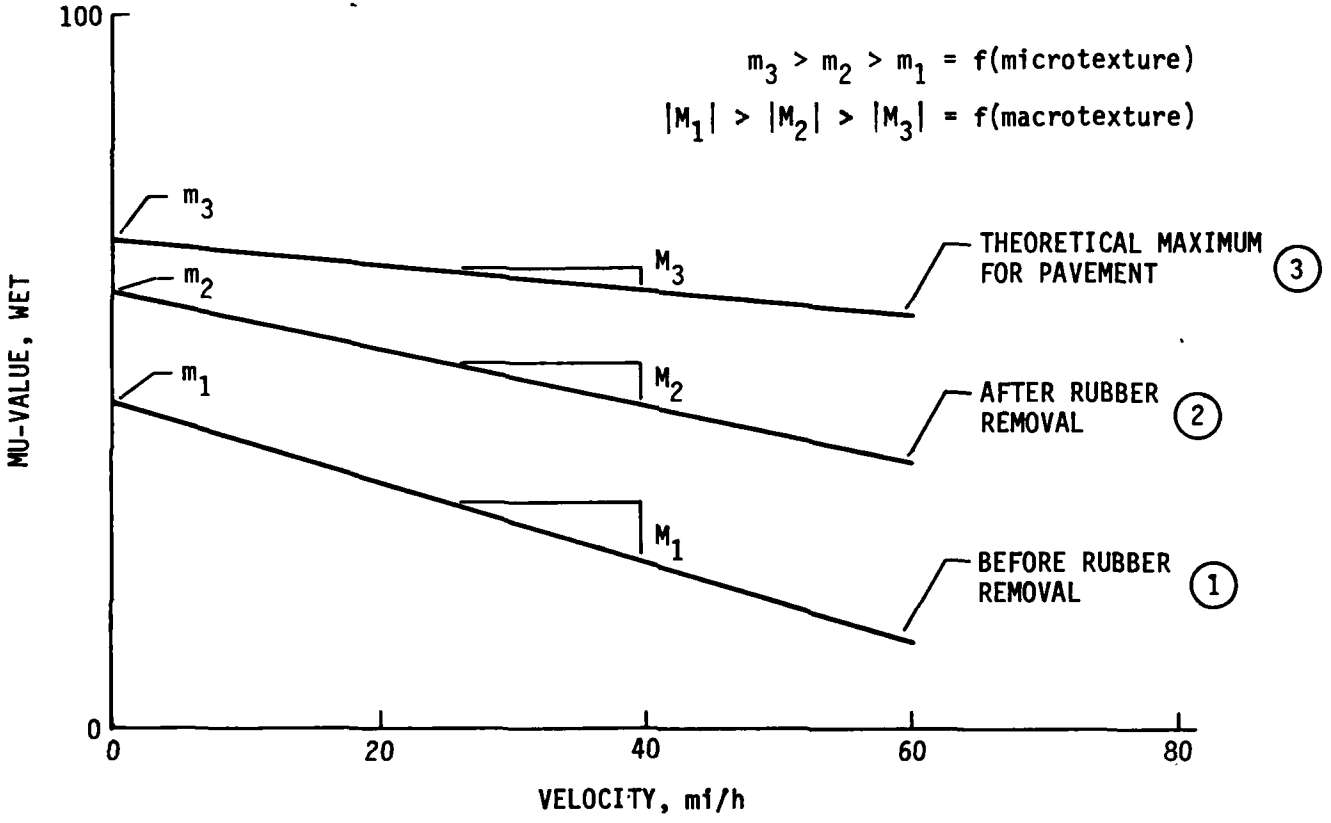

FIGURE 23. THEORETICAL FRICTION CURVES

TEST SECTION			Test Location	TEST PROCEDURES																							
				Mu-Meter (Mu values and temperatures)												Candidate Procedures											
				20 mi/h				40 mi/h				60 mi/h				Sand Patch, $x10^{-4}$ in	Sili-cone Putty, $x10^{-4}$ in	Penn State Drag Test (Drag test number and temperature)						Chalk Test		Stereo Photography
																		Dry			Wet			Chalk $x10^{-4}$	Wear, in	
				Dry	Temp.	Wet	Temp.	Dry	Temp.	Wet	Temp.	Dry	Temp.	Wet	Temp.			Long.	Trans.	Temp.	Long.	Trans.	Temp.	Long.	Trans.	
	Rubber Area	Before Rubber Removal	1																							
			2																							
			3																							
		After Rubber Removal	1																							
			2																							
			3																							
	Nonrubber Area		1																							
			2																							
			3																							
	Pavement Edge Nonrubber Area		1																							
			2																							
			3																							

Notes: "Temp." is pavement temperature in degrees Fahrenheit.
Two repetitions per cell (four for stereophotography)
"Long." is longitudinal direction of runway.
"Trans." is transverse direction on runway.

FIGURE 24. FIELD EVALUATION TEST MATRIX

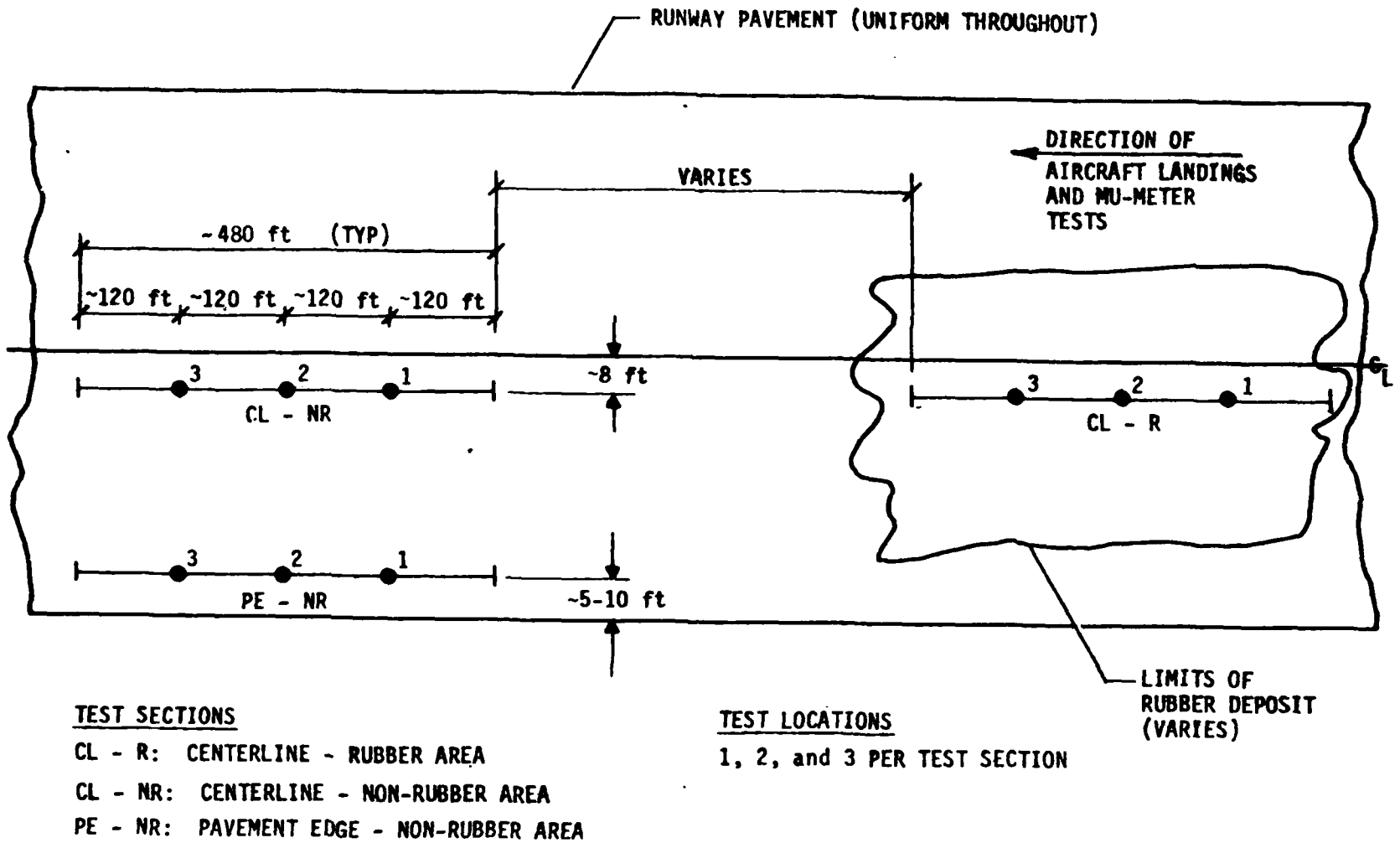

TEST SECTIONS

CL - R: CENTERLINE - RUBBER AREA

CL - NR: CENTERLINE - NON-RUBBER AREA

PE - NR: PAVEMENT EDGE - NON-RUBBER AREA

TEST LOCATIONS

1, 2, and 3 PER TEST SECTION

FIGURE 25. TYPICAL TEST SECTION LAYOUT

The Mu-Meter provides an analog output of friction over a given test section. Therefore, a point-for-point comparison can be made between Mu-Meter data and the candidate test procedure data for a given test location within a specified test section. In addition, average Mu-Meter values can be obtained within a given test section; these average data can be compared to average texture measurements within that test section.

The candidate test procedures are the silicone putty, sand patch, Penn State Drag Tester, chalk wear tester, and stereophotography. The drag tester is conducted both on dry and wet pavement. In addition, both longitudinal and transverse measurements are obtained, the longitudinal in the direction of travel. The chalk wear test is also performed in longitudinal and transverse directions, again, the longitudinal in the direction of travel. Stereophotographs are obtained at four locations in the vicinity of each test location.

The statistical approach described above should provide meaningful relationships between Mu-Meter data and texture data. Since replicative measurements are to be obtained, ANOVA procedures can be used to ascertain significance of relationships. General linear models can also be evaluated.

Plans currently provide for the performance of the proposed field test at a minimum of 12 air facilities (commercial and military) within the continental United States. In addition, evaluation will be conducted on a wide spectrum of pavement surfaces such as Portland Cement Concrete (PCC), asphaltic concrete (AC), and Porous Friction Surfaces (PFS). The PCC and AC surfaces may be of the grooved or ungrooved variety. Other surface types will also be considered for inclusion in this field test program.

VII. MU-METER WATER NOZZLE DEVELOPMENT

Wet testing of runway friction has been a subject of dispute for sometime. Methods for wetting pavement prior to friction testing have included:

1. The use of a water truck equipped with spray bars to douse the runway prior to testing. (The USAF simulated a 0.5-in/hr to 0.8-in/hr rainfall intensity before testing.)

2. The use of a self-watering vehicle using brushes to apply water to the runway. (The M. L. Aviation Corporation supplied brushes with their Mu-Meters and suggested a 0.013-in film thickness and the 1979 National Runway Friction Measurement Program used brushes delivering a 0.04-in water film thickness.)

3. The use of a self-watering vehicle using nozzles to apply water to the runway. (The ASTM E-670 Mu-Meter Standard requires a suitable nozzle capable of delivering a 0.02-in water film thickness.)

While each of these methods has its own merits and faults, a consistent method of wetting the pavement is not yet available. Compounding this problem, tire pavement friction is dependent upon water film thickness; therefore, establishment of a standard is necessary for comparison of results.

The use of a water truck to wet the runway is currently used by the USAF. Although this method does wet the runway, inherent problems exist. First, a water truck equipped with spray bars can only give a crude approximation of a required water film. Second, during the waiting period used to ascertain the friction recovery rates, the water is allowed to drain from the runway. Thus, the actual water film thickness is thinner than during an actual rainfall condition, and any possible ponding on the runway surface affects the friction test results.

A self-watering test vehicle equipped with brushes to distribute the water was an improvement over the water truck method. Test results were more consistent and testing costs were reduced. The use of this method enabled the amount of water applied directly in front of the test tires to be regulated. The procedure more closely approximated the water film thickness of a rainfall and eliminated the possible problems of dry pavement patches and ponding of water that exist with truck distribution methods. However, two major problems still existed:

1. The cross section of the water film was not consistent at the test tire. This inconsistent flow occurred because water flow through the center of the brush is more concentrated than at the outer edges of the brush.

2. Turbulent water flow across the pavement did not simulate rainfall conditions. This turbulent flow was caused by the water striking the pavement at high velocities relative to the pavement (see Fig. 26).

Further developments on the pavement watering system employed a nozzle to distribute the water in front of the test tires. The design of this nozzle should meet two conditions:

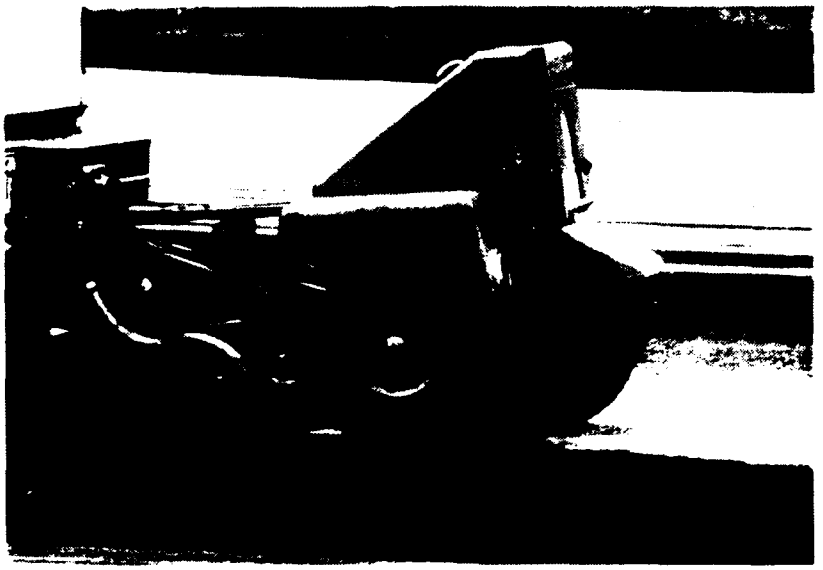

NOTE TURBULENT WATER PRECEDING TIRE

FIGURE 26. MU-METER SELF-WATERING SYSTEM USING BRUSHES

1. The water film thickness should be of a depth simulating worst probable rainfall conditions.

2. The water should strike the pavement at a zero relative velocity and settle in front of the test tire in a laminar fashion without splash or rebound.

A water film thickness of 1 mm (0.04 in) was suggested by the National Runway Friction Measurement Program (NRFMP). This film thickness was based on a hydrological analysis as described in Appendix H of the NRFMP. This film thickness was considered the worst probable case of rainfall on a runway. Using a film thickness of 0.04 in and a total wetted width of 9 in (total for two Mu-Meter tires), flow rates at various test speeds were computed. Flow rates for 20-, 40-, and 60-mi/h test speeds were calculated as 33, 65, and 100 gal/min, respectively (see Appendix E for detailed computations).

To ensure zero velocity of the water relative to the pavement, the flow exiting the nozzles must be at the same speed as the test vehicle. This exit velocity can only be achieved when the apparent opening size of the nozzle is the same as the wetted cross-sectional area of the pavement. Thus, both the nozzle and the wetted pavement cross section should be 0.04 x 4.5 in (per test tire).

Since the pumping system used in the NRFMP test vehicle would not produce pressures required to operate a nozzle of the previously mentioned configuration, an analysis of the required system was conducted. This analysis, outlined in Appendix E, yielded a pump requirement of 255 ft of head operating at

100 gal/min. Attempts were made to locate a pump with an appropriate power drive to satisfy these conditions. All of the manufacturers contacted were unable to supply such a pump that could be mounted in the test vehicle at a reasonable cost. All the pumps considered were either too heavy or too large for the test vehicle.

Since the previously mentioned pumping system could not be installed in the test vehicle, and the existing pump system used during the NRFMP was inadequate for test speeds above 40 mi/h (see Appendix E), a larger system was designed and installed. Modifications to the original pump system included the following:

1. Installing a higher capacity pump.
2. Installing a larger pump motor.
3. Installing a 6.5-kW generator.
4. Installing a larger diameter plumbing system.

Once this revised pumping system was installed, a selection of nozzles to distribute the water was initiated. Since, as mentioned earlier, a system capable of spraying water out of the nozzle at the same speed as the test vehicle proved to be impractical, a pseudo-water depth was used. The pseudo-water depth is developed by pumping a specified flow rate through an enlarged nozzle opening (0.125 x 4.5 in) equaling the known flow rate required to produce the desired water cross section (0.04 x 4.5 in for each test tire) at the specified test speeds. This enlarged opening produces a water depth greater than the desired water depth (0.04 in), traveling at a velocity relative to the pavement other than zero. Using the improved pumping system and the concept of a pseudo-depth, three nozzle configurations were evaluated.

The first water nozzle evaluated was designed by the FAA (see Appendix D for nozzle details). This nozzle was a prototype designed by the FAA for use on existing Mu-Meter test vehicles. Since the NRFMP pump system could not generate the high pressures required by the 0.04- x 4.5-in nozzle opening, a nozzle opening of 0.125 x 4.5 in (three times the theoretical size) was selected by the FAA in designing this nozzle. These enlarged nozzle dimensions permitted the 65-gal/min flow required at the 40-mi/h test speed.

Photographs were taken of this nozzle at 65-gal/min flow rates as shown in Figures 27 and 28. Figure 27 was taken at a fast shutter speed (1/1000 s) and Figure 28 was taken at a slow shutter speed (1/4 s) for comparison. The 1/1000 s shutter speed produces a stop-action photograph while the 1/4 s shutter speed produces a blurred image of the nozzle flow pattern. The latter enhances the image of the flow pattern by smoothing the streamlines. As shown in these photographs, the FAA nozzle produced crossover with corresponding splash. Due to its nonuniform cross section, this nozzle design was deemed inappropriate.

An alternate nozzle evaluated was a modified ASTM E-274 locked-wheel skid trailer nozzle. (See Reference 19 for description of E-274 nozzle). As the required spray width for the Mu-Meter nozzle was 4 1/2 in, the skid trailer nozzle was modified by narrowing its flow pattern from an 8-in width to a 4 1/2-in width with all other dimensions remaining the same (see Appendix D for details). This nozzle used a hole pattern of two sizes; a top row of 12

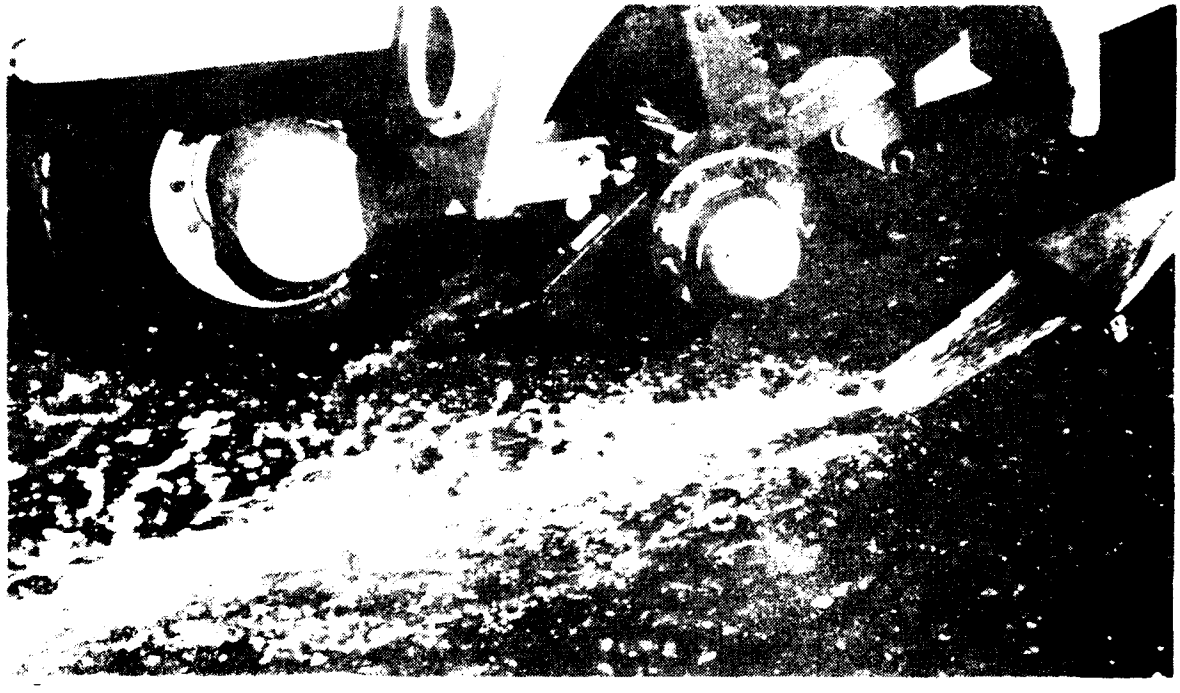

FIGURE 27. FAA PROTOTYPE WATER NOZZLE (SHUTTER SPEED 1/1000 s)

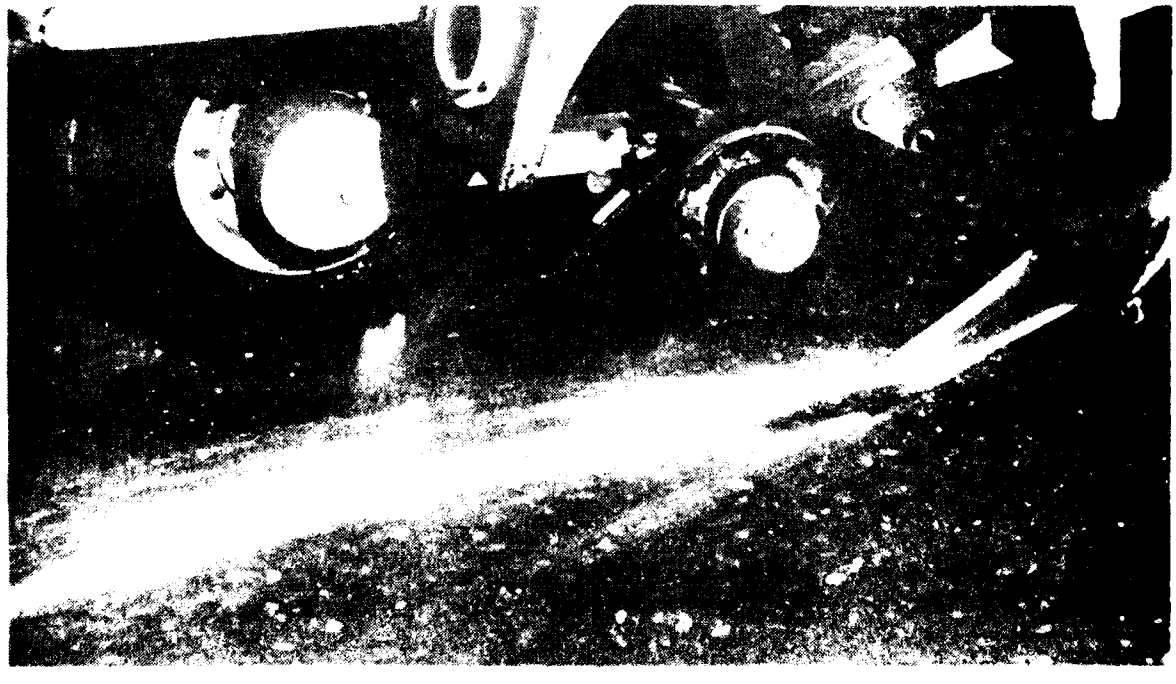

FIGURE 28. FAA PROTOTYPE WATER NOZZLE (SHUTTER SPEED 1/4 s)

holes 1/8-in in diameter and a bottom row of 13 No. C (0.242 in) holes. This hole pattern produced two different exit speeds at the nozzle tip and a slower overall exit velocity for the 65-gal/min flow rate (3.75-mi/h exit velocity versus 12.80-mi/h exit velocity for the FAA nozzle). Photographs of this nozzle design are shown in Figures 29 and 30, and were taken at shutter speeds of 1/1000 s and 1/4 s, respectively. Although this nozzle produced a more uniform flow cross section, the varied and slower exit velocities eliminated this nozzle for use.

The final nozzle evaluated was a modified FAA nozzle developed by NMERI at the University of New Mexico. This nozzle used the same exit opening as the FAA nozzle, 0.125 x 4.5 in, but incorporated a longer exit duct. The crossover flow of the original FAA nozzle was due to an underdeveloped flow pattern arising from the sudden transition at the nozzle exit. An increase in the length of the exit duct from 1/2 to 3 in was used to develop a stable, fully turbulent flow suitable for the required flow pattern. Photographs of this nozzle design, using a 65-gal/min flow rate and shutter speeds of 1/1000 s and 1/4 s, verify this result (Figs. 31 and 32, respectively). Therefore, with its uniform cross section and reasonably high exit velocity, the UNM nozzle was a noticeable improvement over the other two nozzles evaluated.

Based on this evaluation, the UNM nozzle was selected for use in wet friction testing by NMERI. This nozzle was able to correct the problem of uneven water film cross section and reduced the affects of high water stream velocities relative to the pavement. The development of an accurate 1-mm water film thickness was not obtained due to the design constraints of available pump equipment. However, the establishment of a standard pseudo-water film thickness should prove to be a reasonable, cost effective method of simulating rainfall conditions necessary for comparison of wet friction test results.

Appendix D presents details of the evaluated nozzles as well as a nozzle design deemed suitable for standardization (Model GSL). Model GSL incorporates better fabrication technique and materials selection. The flow characteristics of the GSL nozzle are the same as the UNM design.

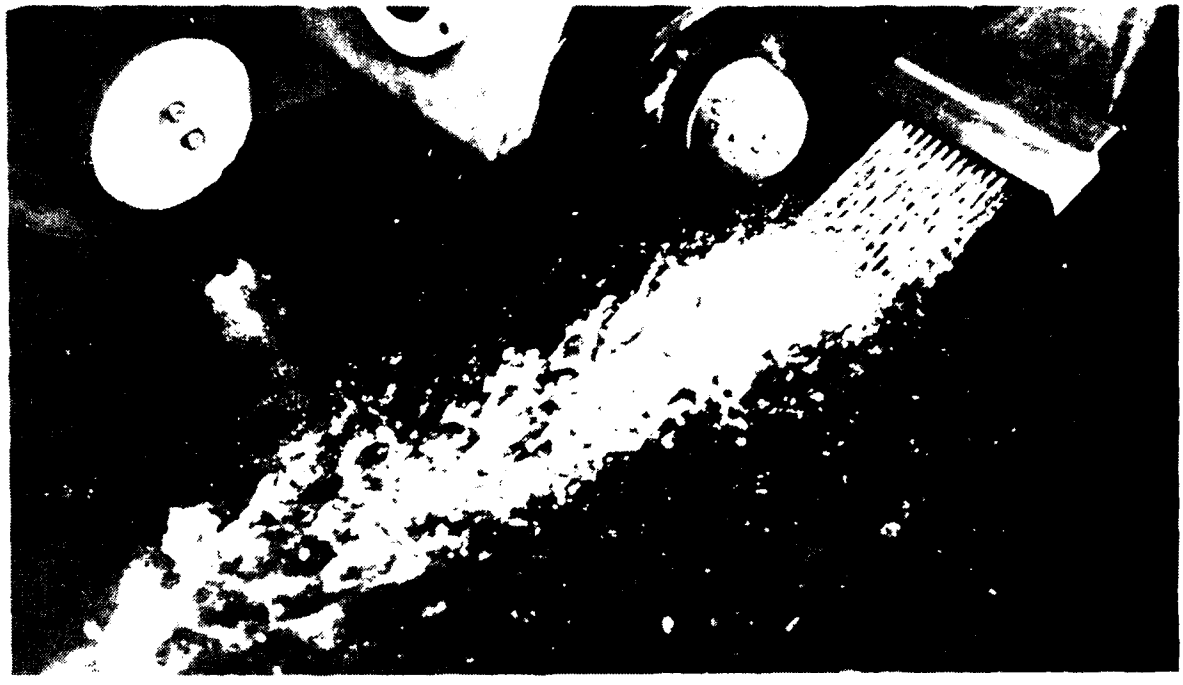

FIGURE 29. MODIFIED E-274 WATER NOZZLE (SHUTTER SPEED 1/1000 s)

FIGURE 30. MODIFIED E-274 WATER NOZZLE (SHUTTER SPEED 1/4 s)

FIGURE 31. UNM WATER NOZZLE DESIGN (SHUTTER SPEED 1/1000 s)

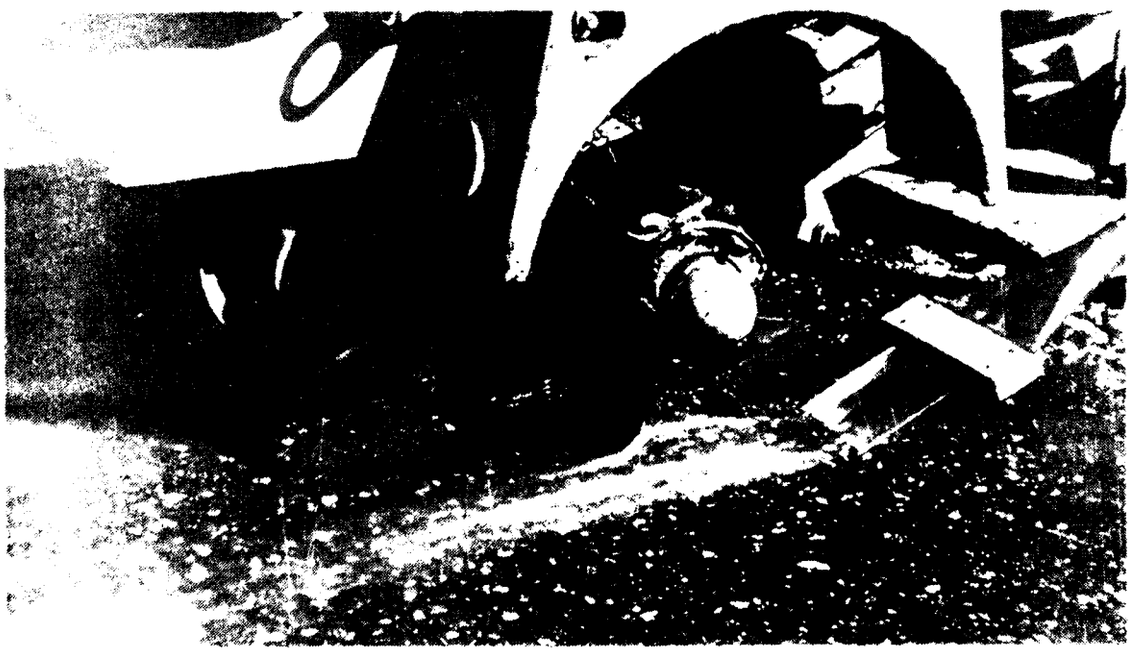

FIGURE 32. UNM WATER NOZZLE DESIGN (SHUTTER SPEED 1/4 s)

APPENDIX A
MACROTEXTURE DEPTH DETERMINATION BY VOLUMETRIC TECHNIQUE

*This description was obtained from the 1984 Annual Book of ASTM Standards, Section 4 Construction, Volume 04.03 Road and Paving Materials; Traveled Surface Characteristics pp. 803-806. Reprinted with permission from ASTM, 1916 Race Street, Philadephia, PA 19103.

Designation: E 965 - 83

Standard Test Method for MEASURING SURFACE MACROTEXTURE DEPTH USING A SAND VOLUMETRIC TECHNIQUE[1]

This standard is issued under the fixed designation E 965; the number immediately following the designation indicates the year of original adoption or, in the case of revision, the year of last revision. A number in parentheses indicates the year of last reapproval. A superscript epsilon (ε) indicates an editorial change since the last revision or reapproval.

1. Scope

1.1 This test method describes a procedure for determining the average depth of pavement surface macrotexture (1)[2] by careful application of a known volume of sand on the surface and subsequent measurement of the total area covered. The technique is designed to provide an average depth value of only the pavement macrotexture and is considered insensitive to pavement microtexture characteristics.

1.2 The results obtained using this procedure to determine average pavement macrotexture depths do not necessarily agree or correlate directly with those obtained by other pavement macrotexture measuring methods (1 through 6).

1.3 *This standard may involve hazardous materials, operations, and equipment. This standard does not purport to address all of the safety problems associated with its use. It is the responsibility of whoever uses this standard to consult and establish appropriate safety and health practices and determine the applicability of regulatory limitations prior to use.*

2. Applicable Documents

2.1 *ASTM Standards:*

C 778 Specification for Standard Sand[3]

E 178 Recommended Practice for Dealing with Outlying Observations[4]

3. Summary of Test Method

3.1 The standard materials and test apparatus consist of a quantity of uniform sand, a container of known volume, a suitable wind screen or shield, brushes for cleaning the surface, a flat disk for spreading the sand on the surface, and a ruler or other measuring device for determining the area covered by the sand patch. A standard laboratory balance is also recommended for further ensuring consistently equal sand amounts for each measurement sample.

3.2 The test procedure involves spreading a known volume of sand on a clean and dry pavement surface, measuring the area covered, and subsequently calculating the average depth between the bottom of the pavement surface voids and the tops of surface aggregate particles. This measurement of pavement surface texture depth reflects primarily the surface macrotexture characteristics (1, 5).

NOTE 1—In spreading the sand specified in this test method, the surface voids are completely filled flush to the tips of the surrounding aggregate particles. This test method is not considered suitable for use on grooved surfaces or pavements with large (≥1.0 in. (25 mm)) surface voids.

4. Significance and Use

4.1 This test method is suitable for field tests to determine the average macrotexture depth of a pavement surface. The knowledge of pavement macrotexture depth serves as an additional tool in characterizing the pavement surface texture. When used in conjunction with other physical

---

[1] This test method is under the jurisdiction of ASTM Committee E-17 on Traveled Surface Characteristics and is the direct responsibility of Subcommittee E17.23 on Surface Characteristics Related to Tire-Pavement Friction.

Current edition approved Sept. 30, 1983. Published December 1983.

[2] The boldface numbers in parentheses refer to the list of references at the end of this standard.

[3] *Annual Book of ASTM Standards*, Vol 04.01.

[4] *Annual Book of ASTM Standards*, Vol 14.02.

tests, the macrotexture depth values derived from this test method may be used to determine the pavement skid resistance capability and the suitability of paving materials or finishing techniques. Improvements in pavement finishing practices and maintenance schedules may result from use of this test method.

4.2 The texture depth measurements produced using this test method are influenced primarily by surface macrotexture characteristics and not significantly affected by surface microtexture. Pavement aggregate particle shape, size, and distribution are surface texture features not addressed in this procedure. This test method is not meant to provide a complete assessment of pavement surface texture characteristics.

4.3 The pavement surface macrotexture depth values measured by this test method, with the equipment and procedures stated herein, do not necessarily agree or correlate directly with other techniques of surface texture measurements. This test method is also suitable for research and development purposes, where direct comparisons between pavement surfaces are to be made within the same test program.

NOTE 2—The pavement surface to be measured using this test method must be dry and free of any construction residue, surface debris, and loose aggregate particles which would be displaced or removed during normal environmental and traffic conditions.

5. Materials and Apparatus

5.1 The essential elements of the apparatus, shown in Fig. 1, consist of the following material and equipment:

5.1.1 *Sand*—A natural silica sand from Ottawa, IL conforming to Specification C 778 shall be used. The clean, dry sand shall be graded to pass a No. 50 sieve and retained on a No. 100 sieve.

5.1.2 *Sand Sample Container*—A metal or plastic cylinder closed at one end and containing a predetermined internal volume of at least 1.5 cubic in. (25 000 mm^3) shall be used to determine the volume of sand spread.

5.1.3 *Sand Spreader Tool*—A flat, hard disk approximately 1 in. (25 mm) thick and 2.5 to 3.0 in. (60 to 75 mm) in diameter shall be used to spread the sand. The bottom surface or face of the disc shall be covered with a hard rubber material and a suitable handle may be attached to the top surface of the disc.

NOTE 3—An ice hockey puck is considered suitable for use as the hard rubber material in this test method.

5.1.4 *Brushes*—A stiff wire brush and a soft bristle brush shall be used to clean thoroughly the pavement surface prior to application of the sand sample.

5.1.5 *Wind Screen*—A small, portable screen or shield shall be mounted on the pavement surface for protection of the sand sample from the wind during spreading and obtaining measurements.

5.1.6 *Scale*—A standard scale 12 in. (305-mm) or greater in length and having 0.1-in. (2.5-mm) or 1-mm (0.04-in.) divisions should be used.

5.2 Use of a standard laboratory-type balance, sensitive to 0.1 g, is recommended with this test method to provide additional control and to ensure that the amount of sand used for each surface macrotexture depth measurement is equal in both mass and volume.

6. Procedure

6.1 *Test Surface*—Inspect the pavement surface to be measured and select a dry, homogeneous area that contains no unique, localized features such as cracks and joints. Thoroughly clean the surface using the stiff wire brush first and subsequently the soft bristle brush to remove any residue, debris, or loosely bonded aggregate particles from the surface. Position the portable wind screen around the surface test area.

6.2 *Sand Sample*—Fill the cylinder of known volume with dry sand and gently tap the base of the cylinder several times on a rigid surface. Add more sand to fill the cylinder to the top, and level with a straightedge. If a laboratory balance is available, determine the mass of sand in the cylinder and use this mass of sand sample for each measurement.

6.3 *Test Measurement*—Pour the measured volume or weight of sand onto the cleaned test surface within the area protected by the wind screen. Carefully spread the sand into a circular patch with the disk tool, rubber-covered side down, filling the surface voids flush with the aggregate particle tips. Measure and record the diameter of the sand patch at a minimum of four equally spaced locations around the sample circumference. Compute and record the average diameter of the sand patch.

NOTE 4—For very smooth pavement surfaces where the patch diameters are greater than 12 in. (305 mm), it is recommended that half the normal volume of sand be used.

6.4 *Number of Test Measurements*—The same operator should perform at least four, randomly-spaced measurements of average macrotexture depth on a given test pavement surface type. The arithmetic average of the individual macrotexture depth values shall be considered to be the average macrotexture depth of the test pavement surface.

7. Calculations

7.1 *Cylinder Volume*—Calculate the internal volume of the sand sample cylinder as follows:

$$V = \frac{\pi d^2 h}{4}$$

where:

V = internal cylinder volume, in.^{3} (mm^3),
d = internal cylinder diameter, in. (mm), and
h = cylinder height, in. (mm).

7.2 *Average Surface Macrotexture Depth*—Calculate the average surface macrotexture depth using the following equation:

$$MATX_d = \frac{4V}{\pi D^2}$$

where:

$MATX_d$ = average surface macrotexture depth, inches (mm),
V = sand sample volume, in.^{3} (mm^3), and
D = average sand patch diameter, in. (mm).

8. Faulty Tests

8.1 Tests that are manifestly faulty or that give average surface macrotexture depth values differing by more than 0.005 in. (0.13 mm) from the average of all tests on the same pavement surface shall be treated in accordance with Recommended Practice E 178.

9. Report

9.1 The report for each pavement test surface shall contain data on the following items:

9.1.1 Location and identification of test pavement surface,

9.1.2 Date,

9.1.3 Volume of sand used for each test measurement, in.^{3} (mm^3),

9.1.4 Number of test measurements,

9.1.5 Average sand patch diameter, in. (mm), for each test,

9.1.6 Average surface macrotexture depth, in. (mm), for each test, and

9.1.7 Average macrotexture depth, in. (mm), for total pavement test surface.

10. Precision and Bias

10.1 Analysis of sand patch data collected during extensively controlled tests (6) produced estimates of the repeatability (method precision) and reproducibility (applied precision) of the sand patch method, as well as sampling errors that can be expected in measuring the average texture depths of a pavement section by the method. The sand patch precision estimates are expressed as a percentage, such as the ratio of the standard deviation of the texture measurements to the mean texture depth times 100.

10.2 The standard deviation of the repeated measurements by the same operator on the same surface can be as low as 3.3 % of the average texture depth.

10.3 The standard deviation of the repeated measurements by different operators on the surface can be as low as 4.7 % of the average texture depth.

NOTE 5—The standard deviation of the site-to-site measurements may be as large as 27 % of the average texture depth. Here site defines a randomly selected location within a nominally homogeneous pavement section. This means that a sizeable number of measurement observations would be necessary to estimate the average texture depth reliably for a given pavement type, despite the fact that the method is highly repeatable and not subject to large operational influences.

REFERENCES

(1) Yager, T. J. and Buhlmann, F., "Macrotexture and Drainage Measurements on a Variety of Concrete and Asphalt Surfaces," *Pavement Surface Characteristics and Materials*, ASTM STP 763, ASTM, 1982.

(2) American Concrete Paving Association, "Guideline for Texturing of Portland Cement Concrete Highway Pavements," *Technical Bulletin No. 19*, March 1975.

(3) Hegmon, R. R. and Mizoguchi, M., "Pavement Texture Measurement by the Sand Patch and Outflow Meter Methods," *Automotive Safety Research Program, Report No. S40, Study No. 67-11*, Pennsylvania State University, January 1970.

(4) Dahir, S. H. and Lentz, H. J., "Laboratory Evaluation of Pavement Surface Texture Characteristics in Relation to Skid Resistance," *Federal Highway Administration Report No. FHWA-RD-75-*

60, June 1972.
(5) Rose, J. G. et al., "Summary and Analysis of the Attributes of Methods of Surface Texture Measurements," ASTM STP 53, ASTM, June 1972.
(6) Chamberlin, W. P. and Amsler, D. E., "Measuring Surface Texture of Concrete Pavements by the Sand-Patch Method," *Federal Highway Administration Report No. FHWA-NY-78-RR62*, July 1978.

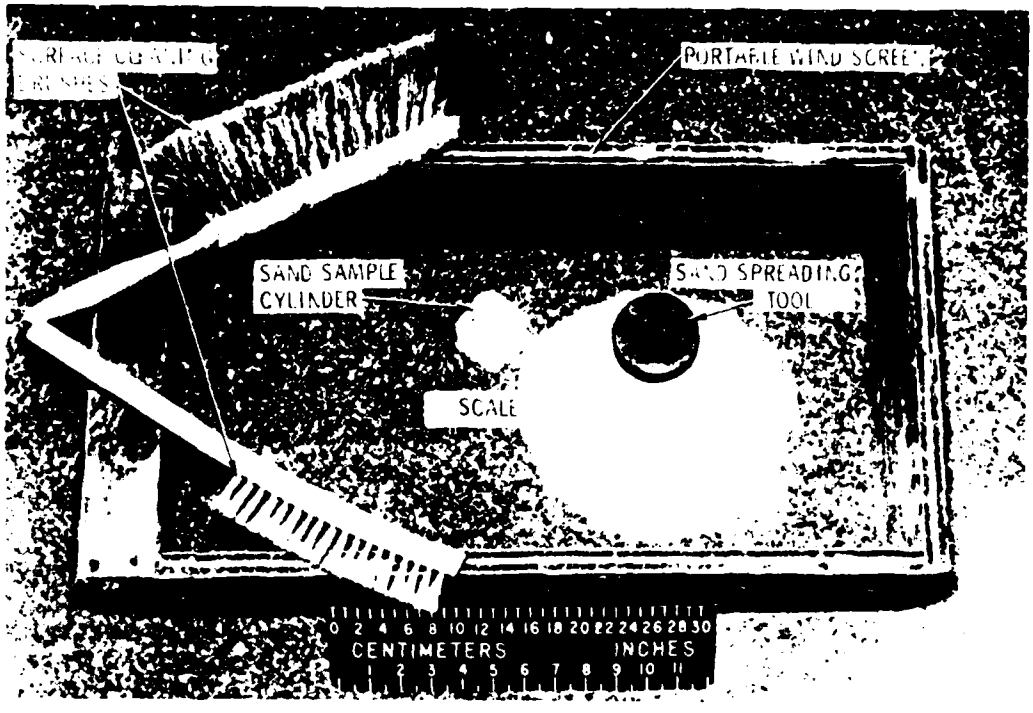

FIG. 1 Apparatus for Measuring Surface Macrotexture Depth

TEST METHOD FOR MEASURING SURFACE MACROTEXTURE DEPTH USING A SILICONE PUTTY VOLUMETRIC TECHNIQUE

SUMMARY OF TEST METHOD

A known volume of silicone putty is formed into an approximate sphere and placed on the pavement surface. A 6-in plate with a 4-in-diameter by 1/16-in-deep recess is centered over the putty and pressed down in firm contact with the surface. The average diameter of the resulting flat-topped circle of putty is recorded. The volume of putty is selected so that on a smooth, flat surface with no texture, the silicone putty will completely fill the recess giving a 4-in-diameter flat-topped circle. A decrease in diameter of the deformed putty is related to an increase in texture depth thus giving a rapid and simple index of pavement macrotexture.

The friction between a tire and the pavement surface required for various vehicle maneuvers on a wet pavement, particularly in braking, depends in part on the thickness of the water film between the contact surfaces. This thickness, in turn, is controlled by the water drainage characteristics of the pavement as well as tire tread design and condition. Pavement drainage is influenced strongly by its surface macrotexture, one measure of which is the so-called texture depth. Additionally, an important contribution to friction at the tire-pavement interface is the energy losses due to hysteresis, which occur as a result of cyclic deformation of the tread rubber; these are also influenced by the macrotexture.

The texture depth determined by this method is a number representing the ratio of the volume of the putty used to the resultant measured circular area covered. Accordingly, it is only an indirect measure of pavement macrotexture wavelength and amplitude, and gives no information on shape, distribution or other factors which may influence pavement surface drainage or losses due to hysteresis. Additionally, it is assumed that the putty completely fills all voids under the measured circular area.

It is well known that in a given nominally uniform section of pavement, surface macrotexture may vary significantly from spot to spot. On the other hand, the area covered by the putty in this test is only a small fraction of the total pavement surface to be evaluated. Accordingly, appropriate selection of test locations will be a significant factor in achieving the objective of this test procedure. In a given section of pavement, putty depth measurement must be made at a sufficient number of locations which appear to be most representative of the texture of the pavement section to be evaluated.

MATERIALS

The following materials are required to conduct this test.

1. A filled high-viscosity polysiloxane polymer, known as silicone putty.* Approximately 14.35 g of this material will be required to completely fill the recess in the test plate on a flat surface. It is usually possible to completely remove the putty from most pavement surface after a test is completed, and reuse this material in subsequent tests. However, it has proven to be advantageous to provide a number of pre-weighed putty specimens

*Dow Corning 3179 Dilatant Compound has been found to be acceptable.

at the test site, transported in the covered 3 oz containers described in 9 below. Therefore, used putty is generally discarded.

2. Dilute solution of dioctyl sodium sulfosuccinate for use as a wetting and parting agent between the pavement surface and silicone putty test specimen. This solution can be made by mixing 5 ml of 75 percent aqueous Aerosol OT solution with 5 gal (19 L) of distilled water.

EQUIPMENT REQUIRED (See Figure A-1)

1. A 6-in-diameter x 1/2-in thick circular plate machined from flat acrylic plastic sheet stock with a centrally machined 4-in-diameter x 1/16-in deep recess on one side, as shown in Figure A-2.

2. A 50-lb (22.7 kg) weight with convenient handle.

3. One whiskbroom.

4. One stiff bristle general utility scrubbing brush.

5. A 250 ml polyethylene "squeeze" washing or dispensing bottle fitted with a delivery tip drawn to give a fine directed stream of dewetting agent. A spray bottle is also acceptable.

6. A synthetically produced, wear resistant, cellulose, polyurethane, or other type of polymer foam sponge suitable for quick removal of excess dewetting agent from the pavement surface.

7. A machinist scale capable of measuring putty diameter to 0.01 in.

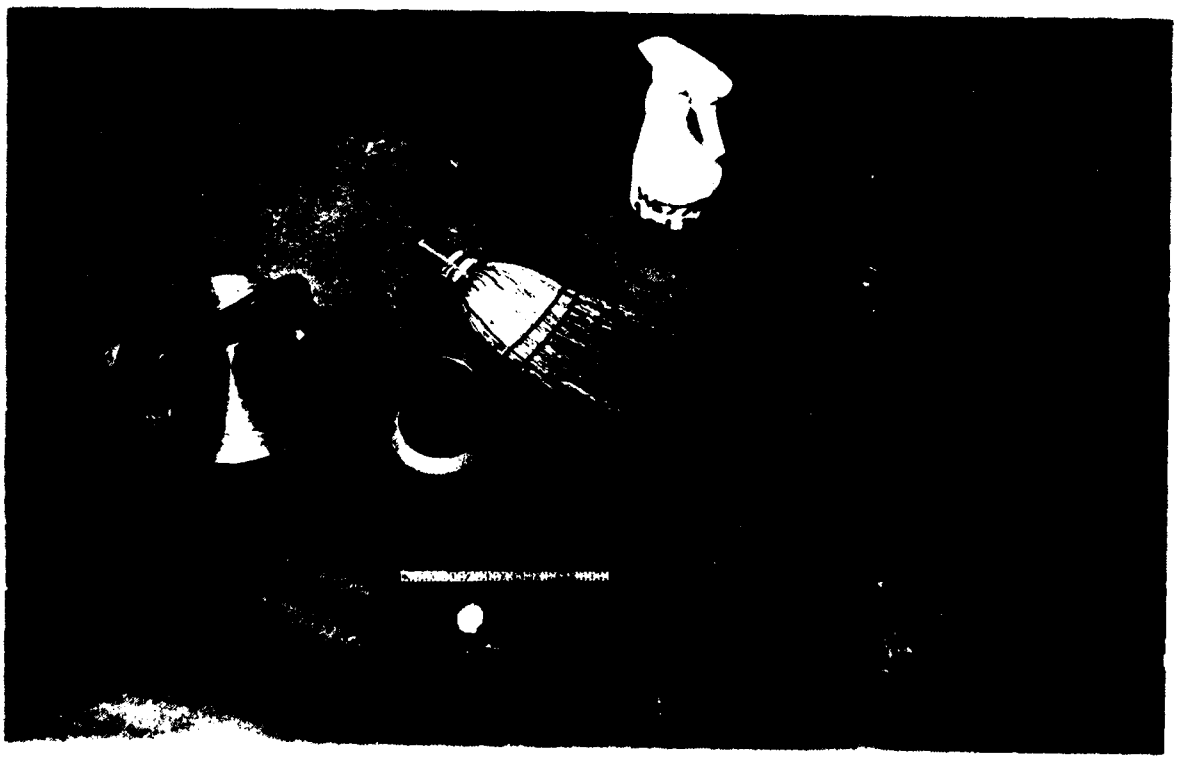

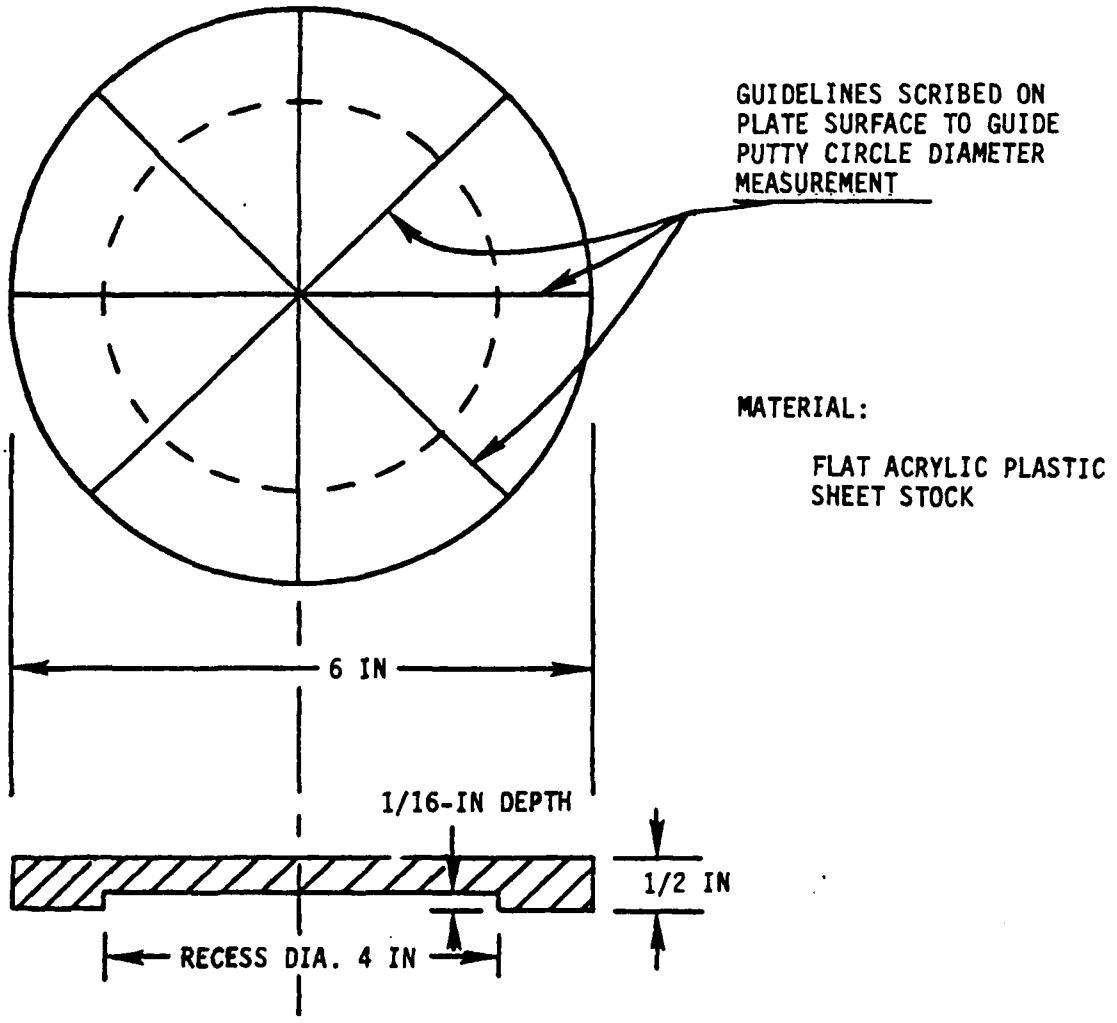

FIGURE A-2. TEST PLATE FOR SILICONE PUTTY TEXTURE DEPTH MEASUREMENTS

8. A metal pry bar for separation of the circular plate from the pavement at the end of the test.

9. Three oz seamless tin plate containers with fitted lid (such as used in ASTM D6).

PROCEDURE

At the locations selected for texture depth measurements, proceed as follows:

1. Remove all loose stones other debris, and contaminants by vigorous application of the whiskbroom.

2. Remove remaining sand and dust from the surface by carefully dry brushing with the scrubbing brush. In rubber build-up areas, minimal brushing is generally required.

3. Wet a section at least as large as the test plate with a spray of dilute Aerosol OT solution from a squeeze bottle.

4. Remove excess Aerosol OT solution by dopping or wiping the surface with the sponge.

5. Form silicone putty into an approximate sphere and place on the pavement surface.

6. Center the recess of the test plate over the putty and press the plate down in firm contact with the road surface. Use of the 50 lb weight to exert pressure for approximately 1 to 2 min will usually ensure that the edges of the test plate are in contact with the pavement surface.

7. Make four diameter measurements at an angular spacing of 45 deg with a machinist scale to the nearest 0.01 in (0.25 mm). The average of these readings is taken as the diameter of the pressed-down circle of putty.

8. Remove the test plate from the pavement surface, using a pry bar if necessary. At the same time the putty also should be removed from the surface. In most instances, complete removal of the putty can be achieved by lightly pressing the putty ball against the few fragments which may try to cling to the surface. Discard used putty.

CALIBRATION

Before the apparatus is used for field measurements, the following laboratory procedure should be conducted to determine the weight of putty to be used during each test.

1. Separate putty obtained from supplier into six lots of approximately equal size.

2. Randomly select three samples of approximately 30 g mass from each lot.

3. Roll each sample into a ball attempting to remove all excess air that may be occluded in the sample (the presence of air will distort specific gravity measurements).

4. Weigh each sample to the nearest 0.01 g and record.

5. Next, weigh each sample in a 500 ml beaker of distilled water at a normal laboratory temperature (68°F). Tare out beaker and water prior to weighing. Use a fine copper wire or monofilament line to support the sample. Ensure that the putty sample is supported solely by the line, is completely submerged, and does not touch the bottom or the sides of the beaker. Record this submerged weight to the nearest 0.01 g.

6. Divide dry weight by submerged weight and record to nearest 0.001. This is the specific gravity of the silicone putty. The variability within lots and from lot to lot should be minimal. The variability should be less than 0.010.

7. Multiply the average specific gravity (g/cm^3) by the volume of the plate recess (12.87 cm^3). This yields the weight in grams of the sample for field test use.

CALCULATION OF TEXTURE DEPTH

Texture depth is calculated from the putty diameter by the following equation:

$$T_p = \frac{1}{D^2} - 0.0625 \qquad \text{(A-1)}$$

where

T_p = texture depth, in

D = average putty circle diameter, in

or,

$$T_p = \frac{(2.54)^3}{D^3} - 0.1588 \qquad \text{(A-2)}$$

where

T_p = texture depth, cm

D = average putty circle diameter, cm

The average putty diameter is the sum of the four diameter measurements divided by four.

APPENDIX B
MICROTEXTURE PROCEDURES

PENN STATE DRAG TESTER

TEST FUNCTION

The tester measures the drag force developed between a rubber-heeled shoe and a wetted surface at low sliding speeds. Since the former is, in general, proportional to the skid resistance of automotive tires, the tester permits the relative rating of pavements as to their danger to skidding.

PRINCIPLE OF OPERATION

The tester is pushed by the operator at a brisk and uniform pace over the wetted pavement. The drag force acting on the rubber shoe is converted into a proportional hydraulic signal and displayed by an indicator.

By design the slider load is practically independent of the drag force and the handle motion by the operator, so that the displayed quantity is directly proportional to the sliding coefficient. The quantity is referred to as Drag Tester Number (DTN) and its relation to the sliding coefficient is now derived.

By definition,

$$f = \frac{F}{L} \tag{B-1}$$

where

f = sliding coefficient
F = drag force acting on slider
L = effective slider load

Also:

$$F = Ap \tag{B-2}$$

where

A = effective diaphragm area
p = pressure generated in transducer

and

$$p = C(DTN) \tag{B-3}$$

where

C = constant of indicator (lb/in^2/dial unit)
DTN = dial reading, Drag Tester Number

Combining (3) + (2)

$$F = AC(DTN) \tag{B-4}$$

also

$$L = L_0 - \frac{b}{a} F \tag{B-5}$$

where

L_0 = static slider load

b = pivot-ground height = 1/2 in

a = pivot-slider distance = 12 in

combining (4) and (5)

$$L = L_0 - \left(\frac{b}{a}\right) AC(DTN) \tag{B-6}$$

Inserting (4) and (6) in (1)

$$f = \frac{AC\ (DTN)}{L_0 - \left(\frac{b}{a}\right) AC(DTN)} \tag{B-7}$$

where

tester constants

(AC), lb/dial unit = 0.10

L_0, lb = 6.00

$$\frac{b}{a} = \frac{1}{24}$$

Hence Equation (7) becomes

$$f = \frac{DTN}{60 - \left(\frac{1}{24}\right)(DTN)} \tag{B-8}$$

Or solving for (DTN)

$$(DTN) = \frac{60\ f}{1 + \left(\frac{1}{24}\right) f} \tag{B-9}$$

While equations (B-8) and (B-9) can be used to convert the dial readings to sliding coefficients and vice versa, the data obtained with the tester shall aways be presented as Drag Tester Numbers (DTN) so as to prevent misinterpretation of the significance of the measurements.

TESTER DESCRIPTION

The tester consists of two subassemblies, as shown in Figure B-1.

Subassembly A--This assembly consists of the housing which contains the slider support and guide mechanism, the hydraulic transducer, the fluid compensating chamber, the hose fittings and connection, and the damping valve and indicator.

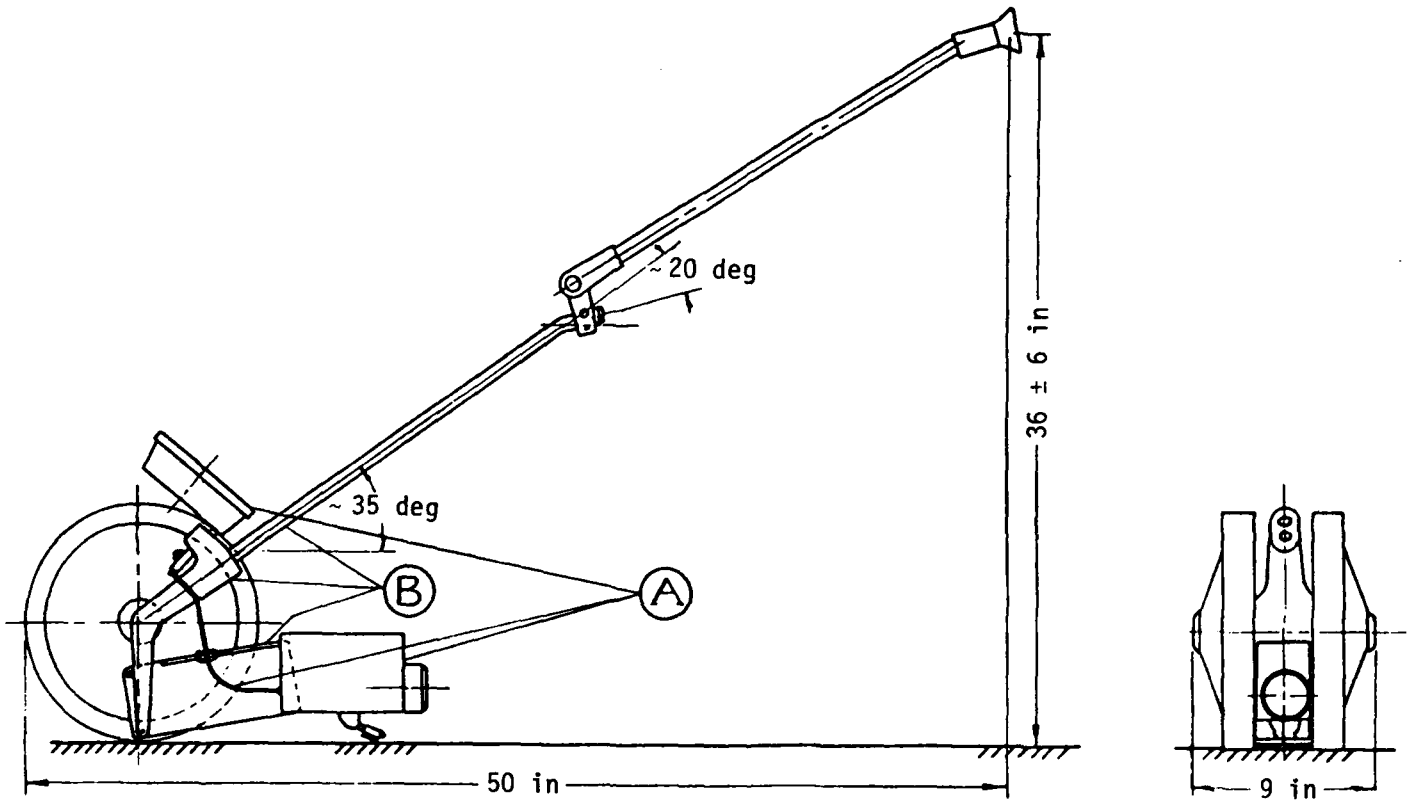

FIGURE B-1. PENN STATE DRAG TESTER (OVERALL VIEW)

Subassembly B--This assembly consists of the two side panels connecting the housing to the chassis, the chassis, two ten-in wheels, and the adjustable handle.

The parts of the subassemblies are shown in Figure B-2 and are identified and described below with respect to their function.

Subassembly A--The housing (1) contains two resiliently mounted antifriction ball bushings (2), (only one shown), which support the hardened main shaft (3). The connector (5) is clamped to the latter by set screws (4) and holds at its lower end the slider shaft (6), recoil spring (7), and rubber-heeled slider (8). Attached to the upper end of the connector is a ball bushing (9) which glides on the hardened auxiliary shaft (10), and thus, prevents lateral movement of (5), (6), and (8).

Connected to the end of the main shaft (3), is the transducer piston (11) and a rolling diaphragm (12), which is held against the latter by a retainer (13) and screw (14). The transducer cap (15) is pressed against the flange of the diaphragm and housing by three socket screws (16), (only one shown), thus, forming a sealed chamber for the working fluid. The transducer cap contains a bore connecting the chamber to a fluid passage in the housing and the fluid is carried to the indicator (21) via the nipple (17), the transparent plastic hose (18), elbow (19), and the damping needle valve (20).

In addition, the housing contains a compensating chamber (see cut A-A, Fig. B-2) which communicates through a vertical bore with the fluid passage. The upper end of this bore is closed by a set screw (22), which permits venting of all fluid spaces within the housing. The compensating chamber contains a compensator piston (23) sealed against the cylinder bore by O-rings (24), and an adjusting screw (25). The latter is retained by the end plug (26) and the snap ring (27). Counterclockwise rotation of the adjusting screw causes the piston to move to the right and thus permits compensation for fluid lost by leakage.

The compensator can also be used for correcting temperature originated expansion of the fluid, or for setting the pressure in the hydraulic system to a predetermined value to decrease the time constant of the hydraulic system.

The moving components inside the housing are completely protected against entry of dust and moisture by plugs (28), (29), and a seal (30). The seal is supported by a grommet (31) on the slider shaft (6).

Subassembly B--The two side panels (32), (only one shown), are connected by six flat head screws (33), (only one shown), to the housing (1) and via a pivot (34) to the chassis (35). Attached to the latter are two treadless rubber wheels (36), (only one shown). The operator may move the handle and the chassis freely within the limits set by contact of the chassis with the side panels and the eccentric spacer (38). Movement within these limits does not affect the load on the slider. One side panel contains an opening protected by a rubber grommet (31) for the passage of the transparent plastic hose (18).

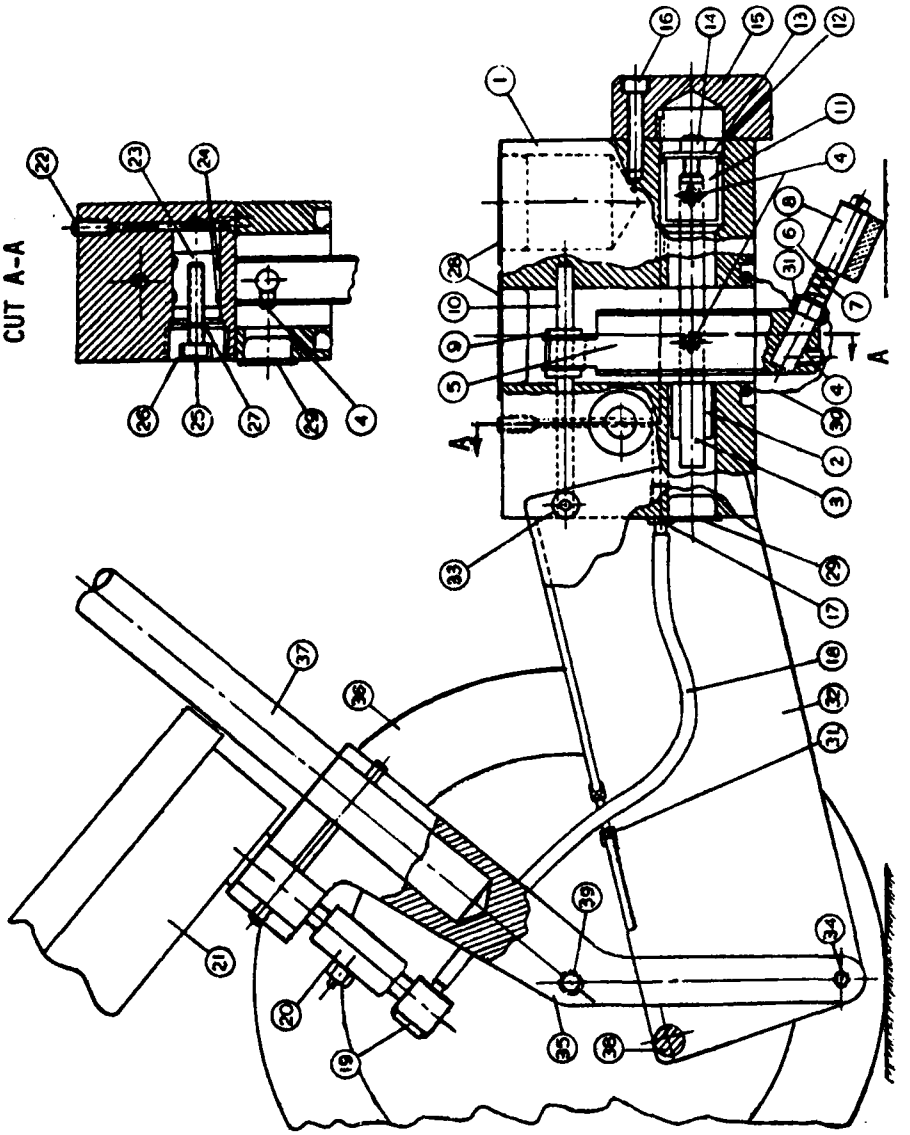

FIGURE B-2. PENN STATE DRAG TESTER (ASSEMBLY DRAWING)

TEST PROCEDURE

1. Check rubber shoe for wear. Replace when the edge is worn by more than 3/16 in as measured with a rule laid flat across the slider width.

2. Adjust the handle to most comfortable position (see Fig. B-3).

3. Prepressurize the hydraulic system until the indicator pointer is displaced by 10 dial units. Counterclockwise rotation of the knurled knob on the left side of the housing produces a pressure increase.

4. Thoroughly flush pavement surface with clean water to remove grit and dust. A commercially available garden sprayer works well.

5. Keep handle within stops provided, and walk in direction of travel at a uniform brisk pace (about 3 mi/h). Do not run.

6. Test pavement section for a distance of approximately 15 ft, monitor gage reading, and keep average in mind.

7. Lift off rubber shoe by raising handle and roll tester for a distance of about 10-15 ft for second test.

8. Depending on pavement homogeneity, repeat steps 6 and 7 and average all readings.

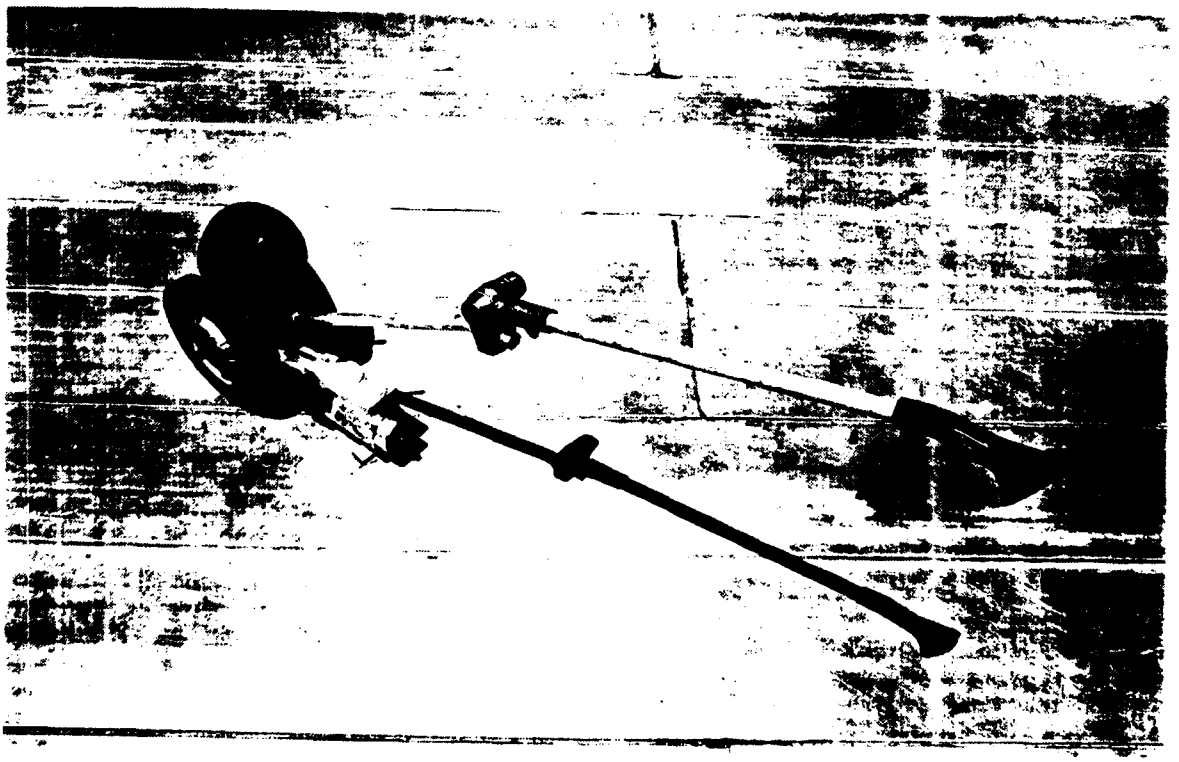

FIGURE B-3. PENN STATE DRAG TESTER

9. Report data as Drag Tester Number (DTN).

10. Record other pertinent data such as surface temperature; if temperature is different from 76 ± 6°F, make correction by adding/ subtracting three dial units per 10°F increase/decrease. Applicable range of correction factor is 76 ± 15°F.

MAINTENANCE

The tester, being a fully enclosed and hydraulically operating device, should require no maintenance other than occasional cleaning of the housing, rubber boot, and indicator with a wet cloth. When the rubber boot becomes damaged, it must be replaced immediately to prevent dust from entering the guide mechanism.

If a full counterclockwise rotation of the knurled compensator screw does not produce a prepressurization of 10 dial units, the tester has lost fluid. If the leak appears to be in the transducer, the instrument should be returned to the manufacturer for repair. Otherwise, the fluid can be replenished by adding clean brake fluid meeting SAE 70RI standards through the filler plug (22), while turning the knurled compensator screw clockwise (Fig. B-2).

In the event the complete hydraulic system is drained by failure of the hose, or for any other reason, it will be necessary to refill the system and bleed all air from the circuit. This can best be accomplished by using the following procedure:

1. Place the gage (21) face down and allow the air to escape when filling the gage.

2. Remove the needle valve (20) and connection (19).

3. Fill hose (18).

4. Bleed the air from the system.

In order to bleed air from the hydraulic system, a small hex socket head cap screw has been installed on the top of the bourdon tube in the indicator (21) and is accessible through the rubber grommet on the indicator case. A suggested procedure for bleeding the air from the hydraulic system requires the following:

1. Remove the hex socket cap screw from the bourdon tube and maintain the access at the highest point to allow air to escape.

2. After a full flow of fluid has been obtained, reinstall the cap screw and replace the grommet cover.

3. After complete filling of the components is accomplished, reinstall the needle valve (20) and connection (19).

4. Continue to fill the system with fluid.

5. When the system is full, slip the filled hose (18) on to the connection (19).

The complete hydraulic system must be free of any air entrapment or false readings will be obtained.

CALIBRATION CHECK

Unless damaged, the calibration of the tester will not change over the years. The tester is calibrated at the factory prior to shipment, and the results are entered on the enclosed calibration certificate. The calibration may be checked as follows:

1. Prepressurize the hydraulic system to 10 dial units.

2. Remove the rubber shoe and, with the tester housing in a vertical position, attach a 3-lb weight to the slider shaft (use a thin wire or fishline, threaded through the hole in the slider shaft).

3. Slightly pluck the wire or fishline and tap the indicator. The reading must agree with the data given under "Field Check" in the calibration certificate, and must be within the given tolerances.

If the reading obtained is outside the recommended tolerance the tester may be damaged and should be returned to the manufacturer. If the tester has not been in recent use, it is advisable to subject it to several test cycles prior to checking the calibration.

CALIBRATION PROCEDURE (INDICATOR)

1. Remove the slider and secure the housing in a horizontal position on calibration stand. The calibration stand is a suitable one-piece jig that that can be used to:

    1. Chock the wheels to hold the drag tester in place.
    2. Support the main body of the drag tester ensuring that no load is applied to the slider.
    3. Align the pulley both horizontally and laterally with the slider.
    4. Level the tester and the stand as a unit.

If a stand is not available, the top of a sturdy table may be used. The slider shaft (6) must clear surface (Fig. B-2).

2. Depressurize the hydraulic system completely. This may be done either by turning the compensator adjusting screw (25) clockwise or by bleeding system through the set screw (22). Remove the indicator cover and position the pointer to indicate approximately two units on dial (for initial calibration only) (Fig. B-2).

3. Fasten a pulley, supported by antifriction bearings, on the calibration stand (or table top). Thread a length of fishline (15-lb tensional strength) through the pin hole of the slider shaft. Pass the line over the pulley and fasten a tray of known weight to the free end of the line. Check that the fishline between the slider and pulley is horizontal and laterally aligned with the housing.

4. Place weights on the tray in increments of 1 lb up to 6 lb and record corresponding dial readings. Slightly pluck the fishline several times to shake out Coulomb friction in the pulley and tester ball bushings and tap the indicator before taking readings.

5. Plot dial readings against pull of fishline (weight of tray plus weights). The resulting curve is a straight line which does not necessarily pass through the origin of the coordinate system (Fig. B-4).

6. In case the curve obtained by step 5 does not pass through the origin draw a parallel curve through the origin. Read from curve dial reading corresponding to 6-lb pull.

7. Apply 6-lb pull by placing appropriate weights on tray and adjust pointer to indicate dial reading found by step 6. Repeat steps 4 and 5: the resulting curve must now go through origin.

8. From corrected graph determine pull which produces a dial reading of 60. The force thus found is equal to the required slider load.

A parts list and calibration certificate for the Penn State Drag Tester are shown in Figures B-5 and B-6.

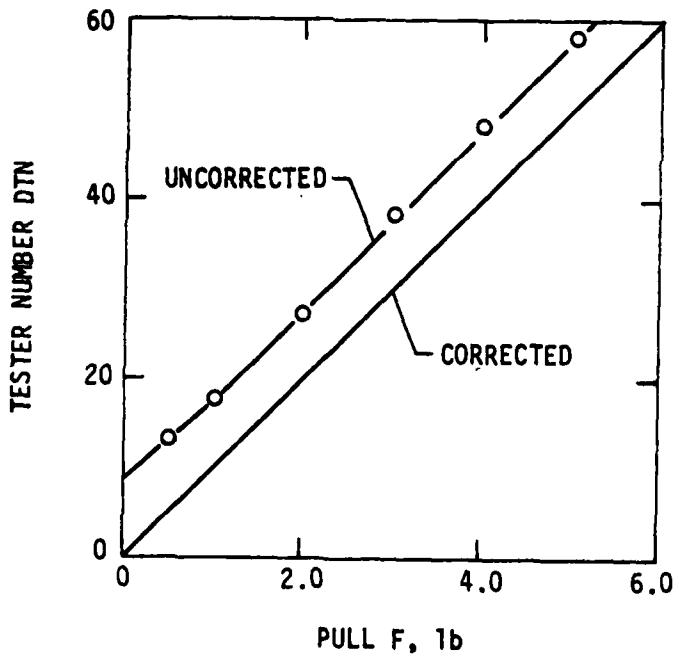

FIGURE B-4. CALIBRATION OF HYDRAULIC SYSTEM

PARTS LIST FOR PENN STATE DRAG TESTER

Part No.	Part	No. Required
	Subassembly (A)	
1	Housing	1
2	Ball bushing, 2 resilient mount	2
3	Main shaft	1
4	Set screw	5
5	Connector	1
6	Slider shaft	1
7	Recoil spring	1
8	Slider	5
9	Ball bushing	1
10	Auxiliary shaft	1
11	Transducer piston	1
12	Diaphragm	1
13	Retainer	1
14	Socket screw	1
15	Transducer cap	1
16	Socket screw	4
17	Nipple	1
18	Plastic hose	1
19	Nipple	1
20	Needle valve	1
21	Indicator	1
22	Set screw	1
23	Compensator piston	1
24	O'ring	2
25	Socket screw	1
26	End plug	1
27	Snap ring	1
28	Plug	2
29	Plug	2
30	Seal	1
31	Grommet	1
32	Side panel	2
33	First head screw	8
34	Bearing, pivot	2
35	Chassis	1
36	Wheel	1
37	Handle assembly	1
38	Stop	1
39	Shoulder screw	2

NOTE: Bleed screw has been added to tip of bourdon tube in pressure gage to assist in bledding air from hydraulic system.

FIGURE B-5. PARTS LIST FOR PENN STATE DRAG TESTER

PENN STATE DRAG TESTER
CALIBRATION CERTIFICATE

TESTER NO._____

CALIBRATED BY _____ DATE_____

A. Calibration of hydraulic system with housing horizontal prepressurization dial units = _____

Drag Force F	Indicator Display[1] DTN	
	Up	Down
0	....	....
1	....	....
2	....	....
3	....	....
4	....	....
5	....	....
6	....	....

B. Slider load (casting within provided stops)

L_o = ... lb

C. Field Check (housing vertical, rubber shoe removed and weight attached to slider shaft through thin wire or fishline).

Weight lb	Indicator Display DTN
3	..... ± .....

[1]Obtained after slightly plucking fishline and tapping indicator.

It should be noted that the reading obtained from attaching a three-pound weight to the shaft under (c) is higher than that obtained for a three-pound pull under (A). This is due to the weight contribution of the guide mechanism when the housing is in a vertical position.

NOTE: Unit must be prepressurized to 10 DTN for operation. All above calibration was made with this same prepressurization.

FIGURE B-6. CALIBRATION CERTIFICATE

CHALK WEAR TESTER

TEST FUNCTION

The tester measures the wear of a piece of chalk per unit length while traveling at low sliding speeds on a pavement. Since microtexture plays an important role in pavement friction, the tester ranks pavements by abrasion due to pavement microtexture.

While the tester can be used on any surface with a hardness greater than the chalk, pavements with low microtexture due to polish may be difficult to test.

PRINCIPLE OF OPERATION

The tester is pushed by the operator at a slow and uniform pace over a clean dry pavement. The normal load on the chalk produces contact pressures and corresponding shear forces that wear the bottom edge of the chalk. To ensure consistent results of wear, a commercially available railroad chalk is used in all tests.

TESTER DESCRIPTION

The tester consists of eight parts:

1. Cart: This furnishes both a convenient handle and an axle to which the tester can be attached. (Harper fold-a-truck, Model No. FT-80EN).

2. Axle weight: This two-piece arrangement attaches the chalk tester to the cart axle and provides a hinged connection to the rest of the unit.

3. Vertical hinge: This eliminates any lateral force on the chalk.

4. Connecting bracket: Connects hinge with alignment bars.

5. Alignment bars: These two bars and the chalk guide form a triangular truss which provides vertical stability of the unit. Connecting the alignment bars to the connecting bracket with a limited rotational fitting also eliminates any torsional bias of the test.

6. Chalk guide: This holds the chalk in place during testing. The chalk is held in place by a friction fit.

7. Extruder screw: This pushes the chalk out of the chalk guide enabling the operator to reset the height of the chalk.

8. Balancing counterweight: This weight is used to balance the axle weight at the cart axle. This ensures proper weight distribution upon the chalk.

(Balancing is accomplished with only one alignment bar attached to the connecting bracket. The unconnected end of this alignment bar is unsupported during balancing.)

The tester is illustrated in Figure B-7. Detailed fabrication drawings are shown in Figures B-8 and B-9.

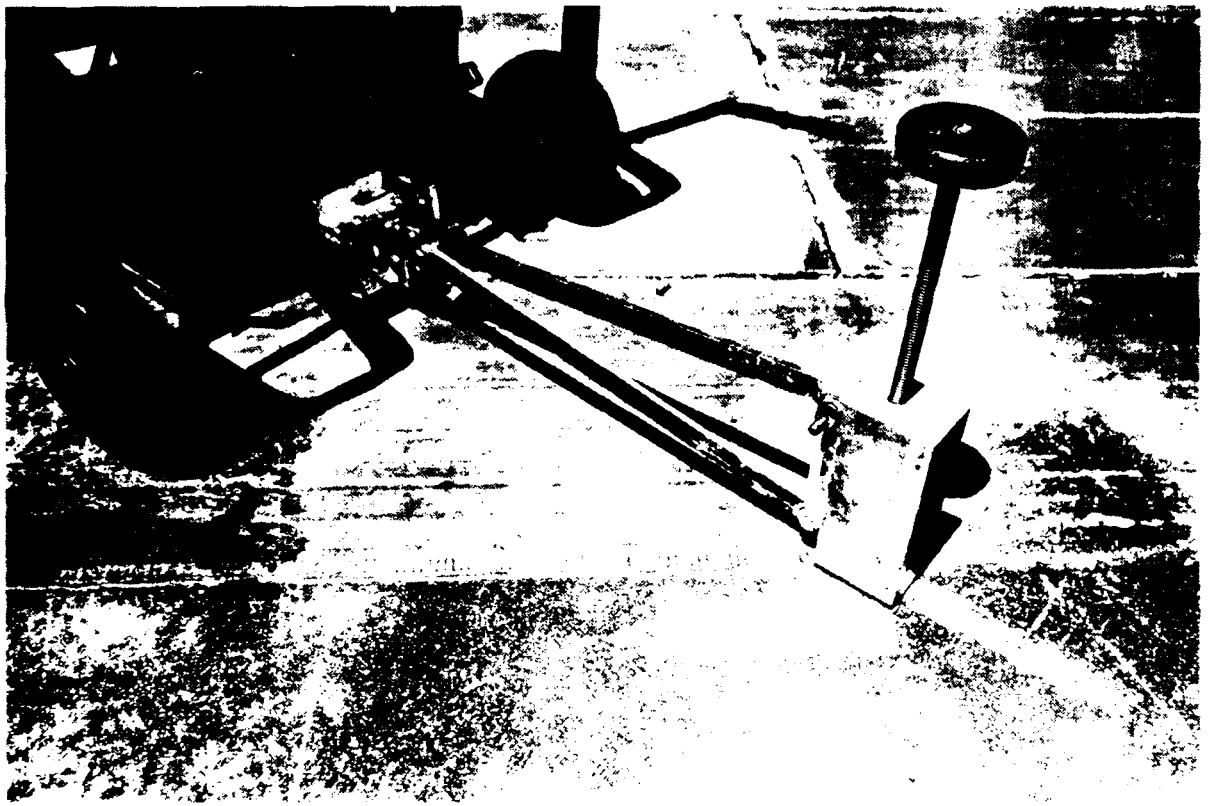

FIGURE B-7. CHALK WEAR TESTER

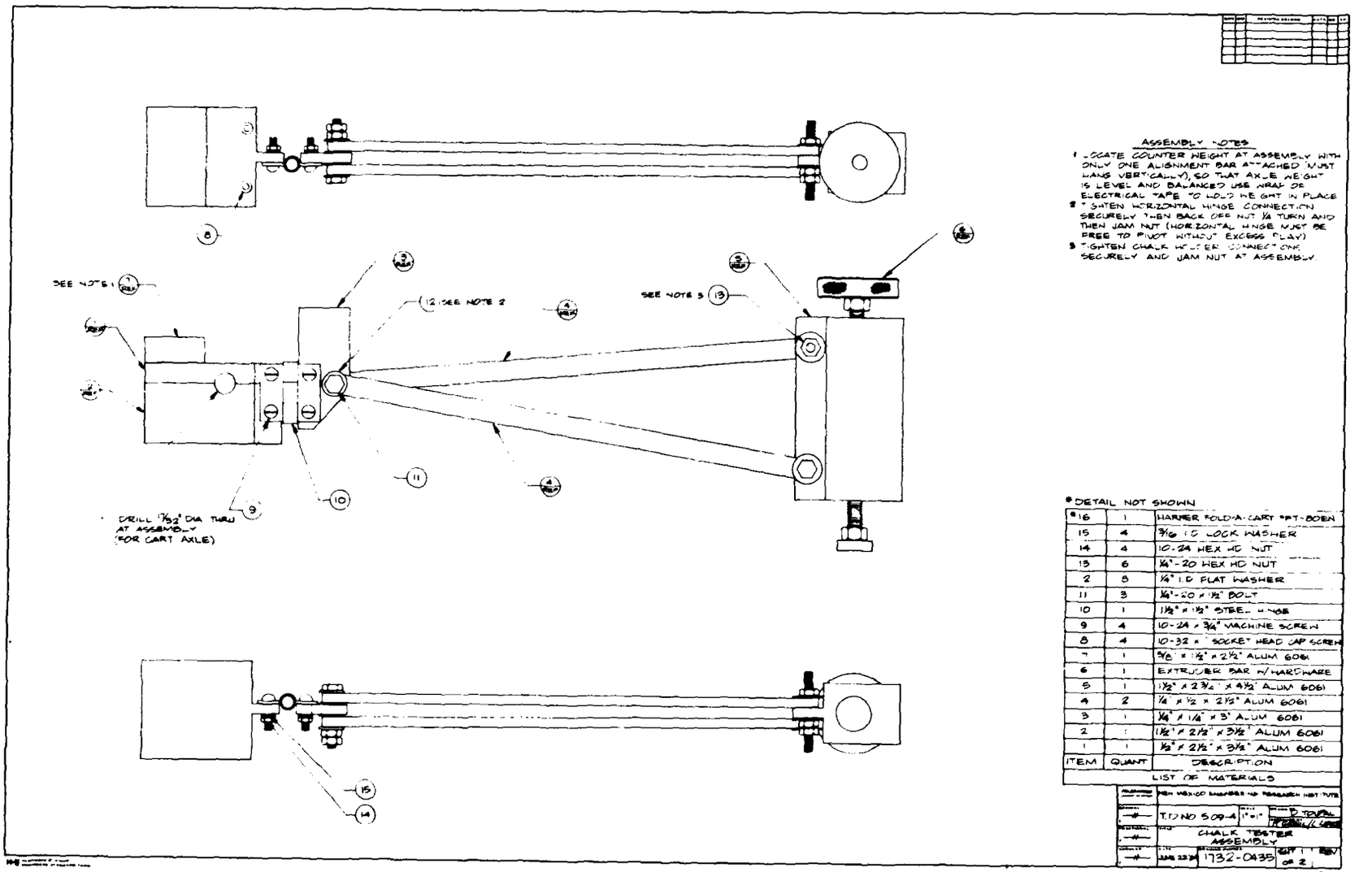

FIGURE B-8. CHALK WEAR TESTER ASSEMBLY

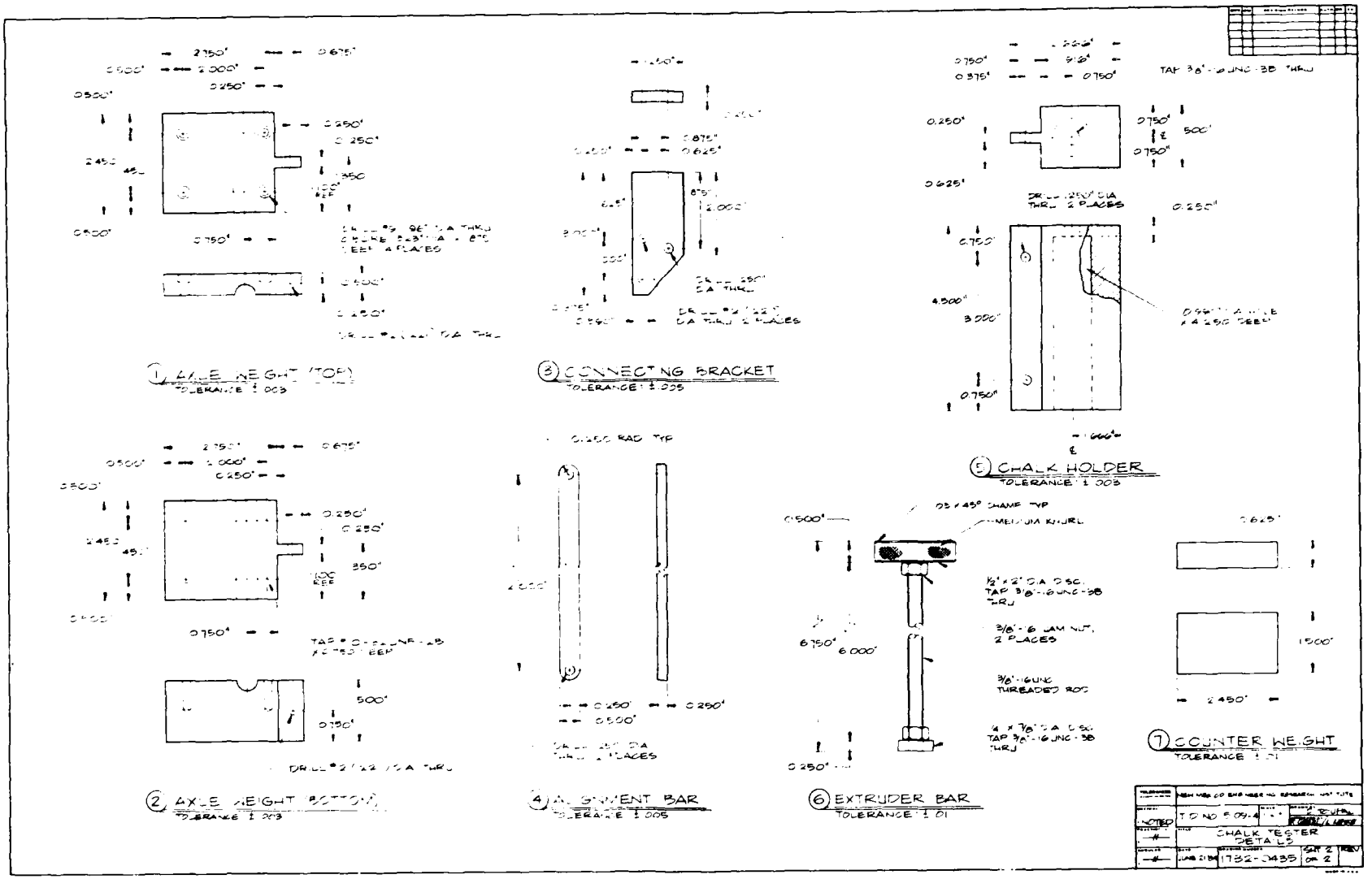

FIGURE B-9. CHALK WEAR TESTER DETAILS

AD-A153 262 RUNWAY RUBBER REMOVAL SPECIFICATION DEVELOPMENT: FIELD EVALUATION PROCEDU.. (U) AIR FORCE ENGINEERING AND SERVICES CENTER TYNDALL AFB FL ENGI.. 2/2

UNCLASSIFIED R G MCKEEN ET AL. JUL 84 AFESC/ESL-TR-84-40 F/G 1/5 NL

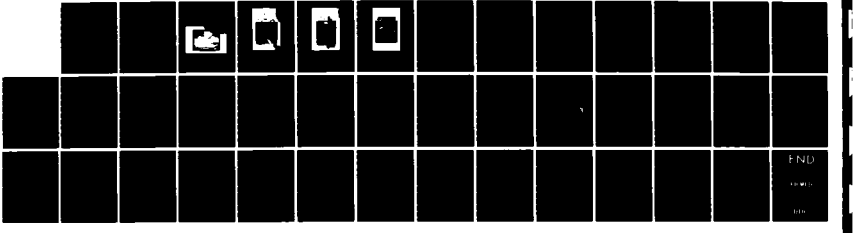

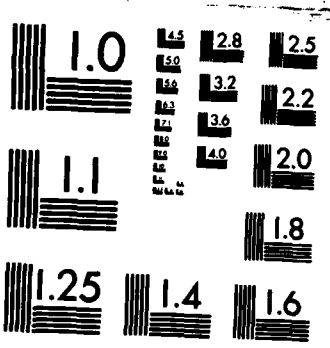

TEST PROCEDURE

1. Check the chalk for wear. Replace the chalk when it is eroded beyond half of its original length. This will be evident since the chalk is tapered and will fall from its holder at this time. (The tapered end of the chalk is inserted into the chalk guide.)

2. Extrude approximately 1/2 in of chalk from tester.

3. Measure chalk length* at four places 90-deg offset from each other to the nearest 1/100 in (R_1).

4. Inspect the surface and ensure that it is clean and dry. When testing always test in direction of travel.

5. Gently place the chalk on the ground where the test is to start.

6. Tilt the cart back and check that the front axle weight is level and that the chalk guide is normal to the ground.

7. Keep handle at a comfortable height and be careful that axle weight is level and chalk guide is normal to the ground. Walk slowly forward at a uniform pace (about 1 mi/h).

8. Test a section of at least 10 ft when practical.

9. Measure the length of test section (length of chalk mark) to nearest 1 in (L_W).

10. Measure the chalk length* at four places 90-deg offset to the nearest 1/100 in (R_2).

11. Calculate chalk wear per unit length of test surface.

$$W = \frac{\frac{\Sigma R_1 - \Sigma R_2}{4}}{L_W}$$

12. When replacing chalk use, No. 888 enamel-coated white railroad chalk produced by the American Crayon Company. A parts list for the chalk tester is shown in Figure B-10.

PARTS LIST

1 ea.	Cart, Harper fold-a-truck, Model No. FT-80EN
1 ea.	Balancing counterweight
1 ea.	Axle weight
1 ea.	Hinge
1 ea.	Connecting bracket
2 ea.	Alignment bars
1 ea.	Chalk holder
1 ea.	Extruder screw
	Enamel-coated white railroad chalk produced by the American Crayon Company No. 888.

FIGURE B-10. PARTS LIST CHALK WEAR TESTER

*Measurements made with reference to bottom of chalk guide.

APPENDIX C
STEREOPHOTOGRAPHY

This appendix contains photographs and detailed fabrication drawings of a stereocamera system suitable for obtaining stereophotographs of a pavement surface. This design is similar to that proposed by Holt and Musgrove (Ref. 36) at the Ontario Ministry of Transportation and Communications.

All camera and flash settings are listed in Figure C-4. The camera and flash specifications are provided on the fabrication drawings (Fig. C-5 through C-8).* The flash unit is triggered off of the left camera. The dual cable release activates the right camera first followed by the left camera at which point the flash is triggered. The shutter release of both cameras is accomplished within 1/2 s by a firm fluid stroke on the cable release.

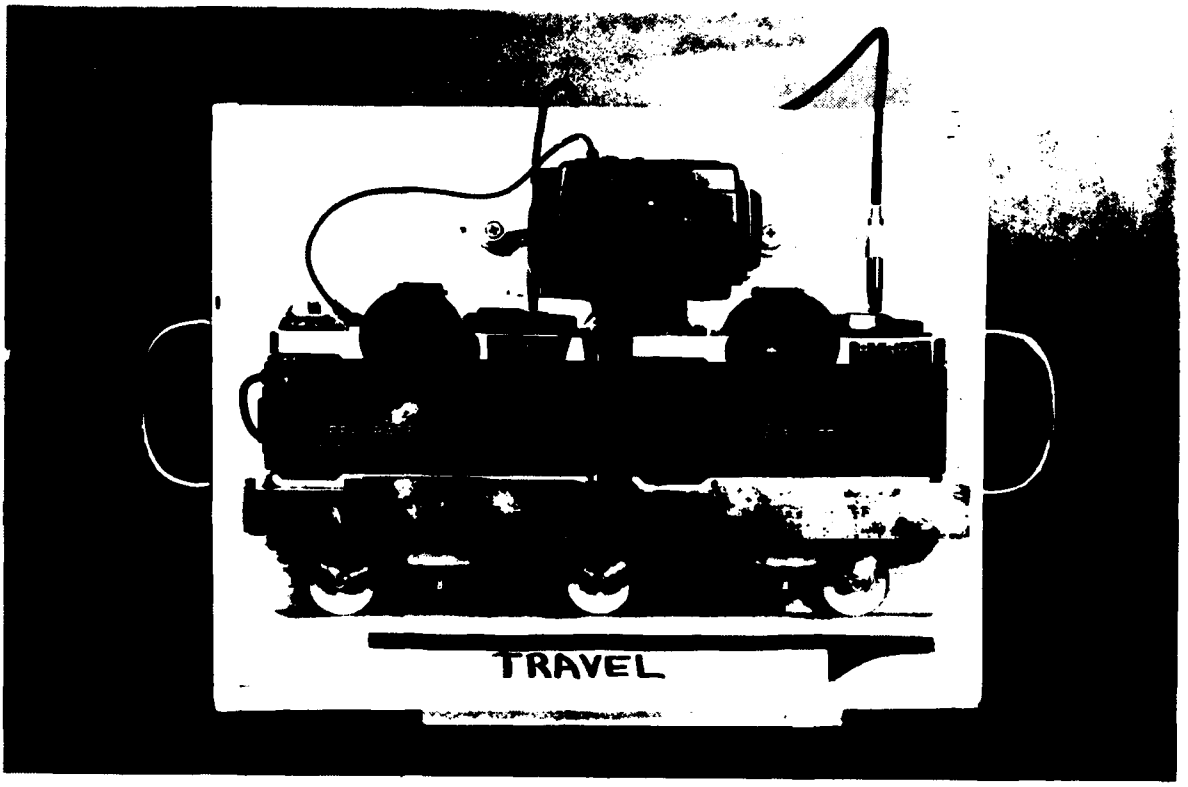

FIGURE C-1. TOP VIEW OF STEREOCAMERA SYSTEM

*Full-sized prints are available from NMERI upon request.

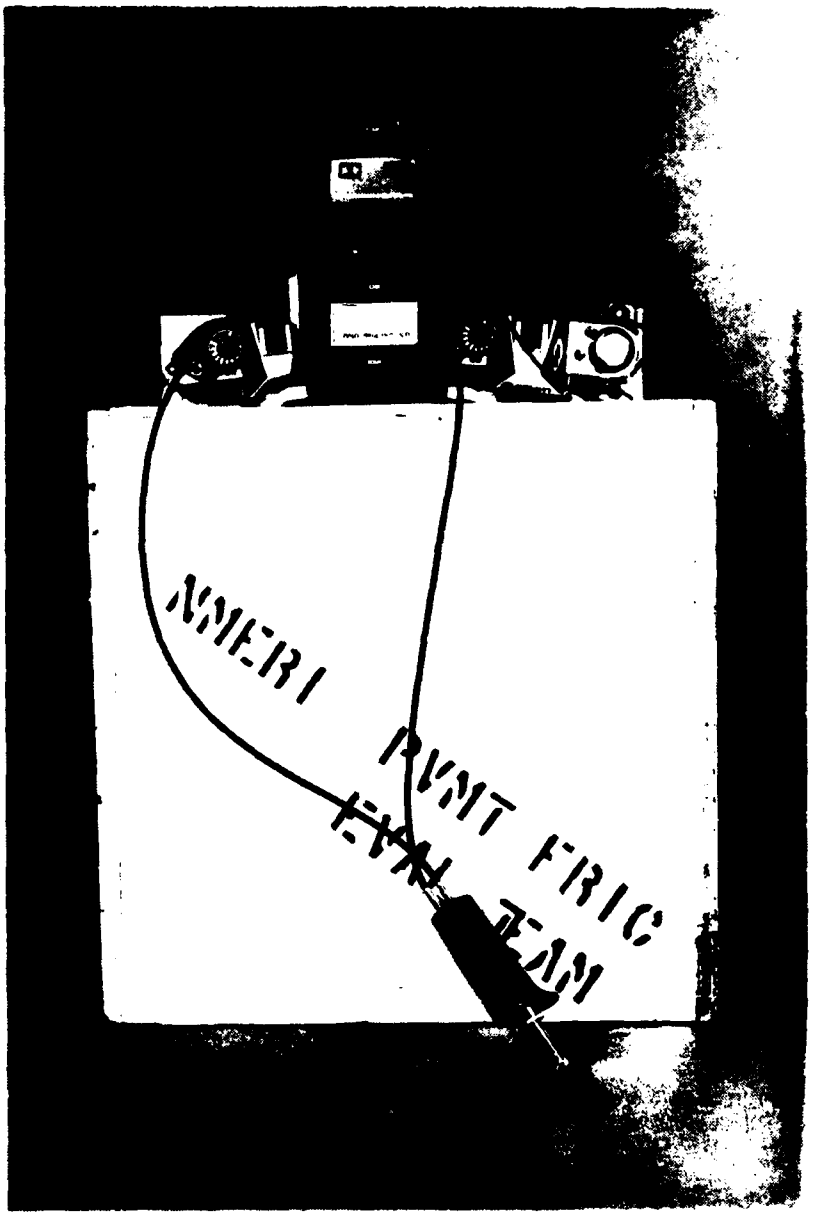

FIGURE C-2. FRONT VIEW OF STEREOCAMERA SYSTEM

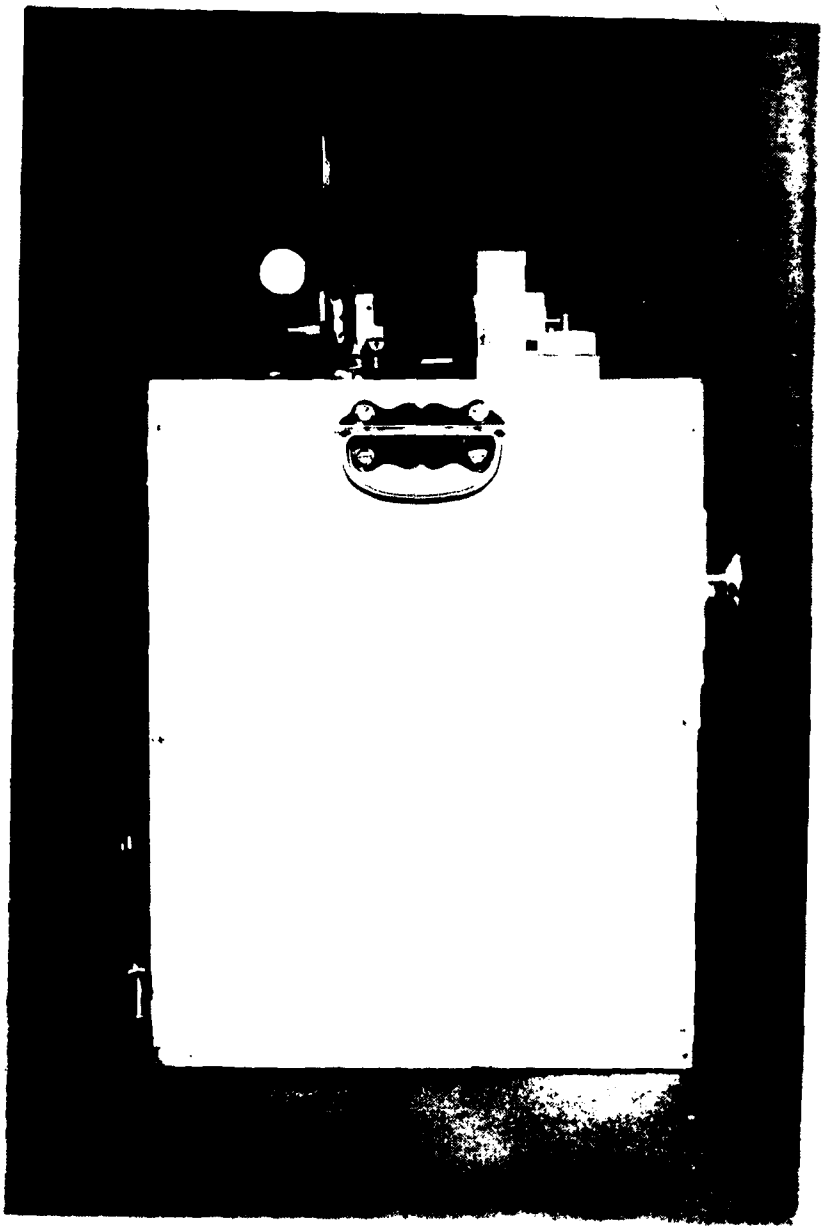

FIGURE C-3. SIDE VIEW OF STEREOCAMERA SYSTEM

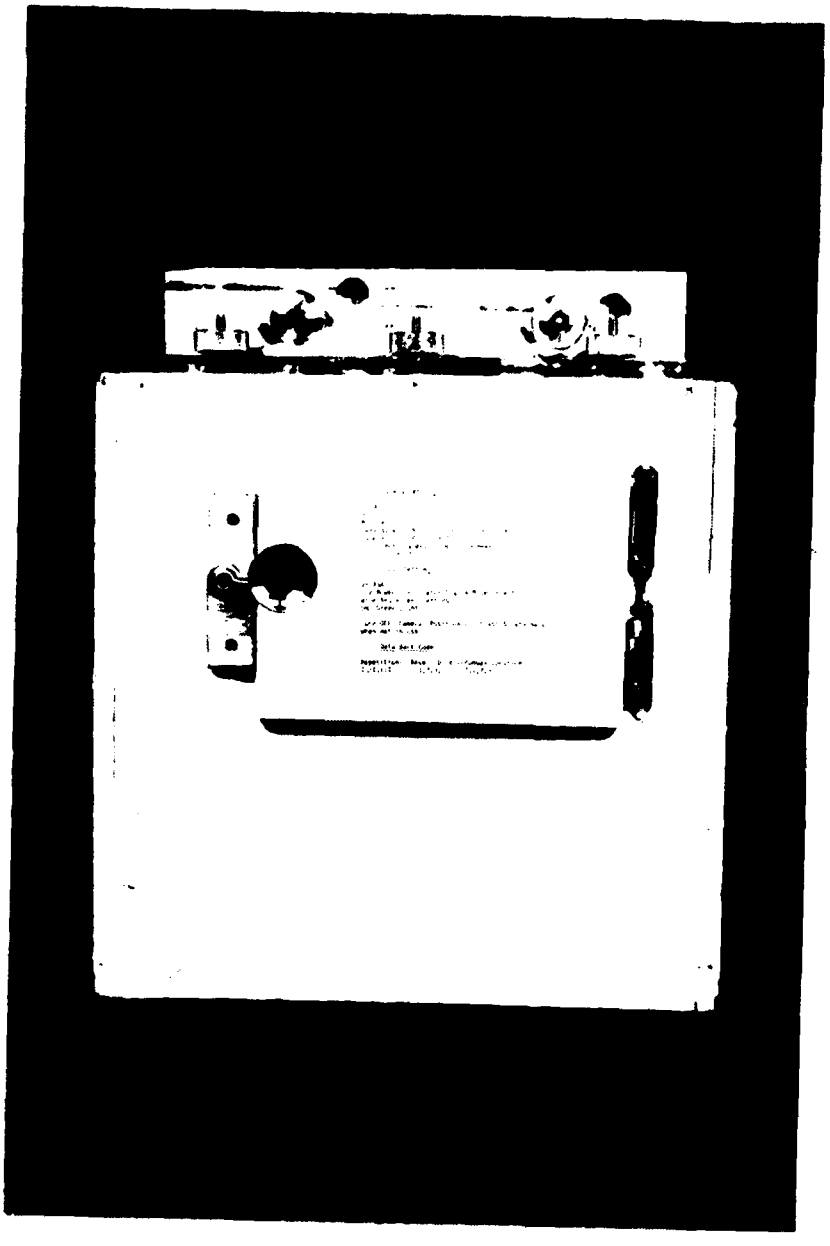

FIGURE C-4. REAR VIEW OF STEREOCAMERA SYSTEM

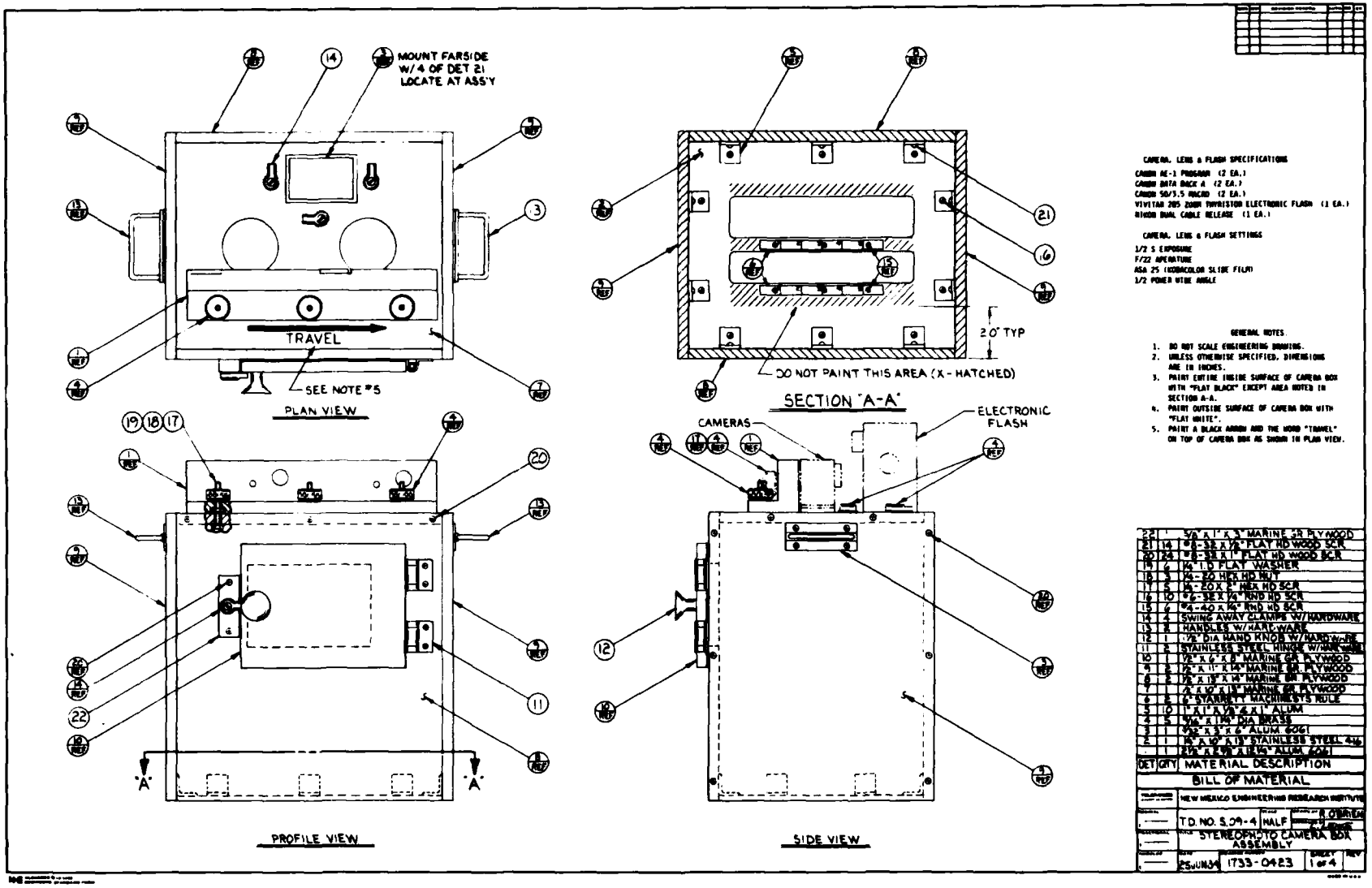

FIGURE C-5. STEREOPHOTO CAMERA BOX--ASSEMBLY

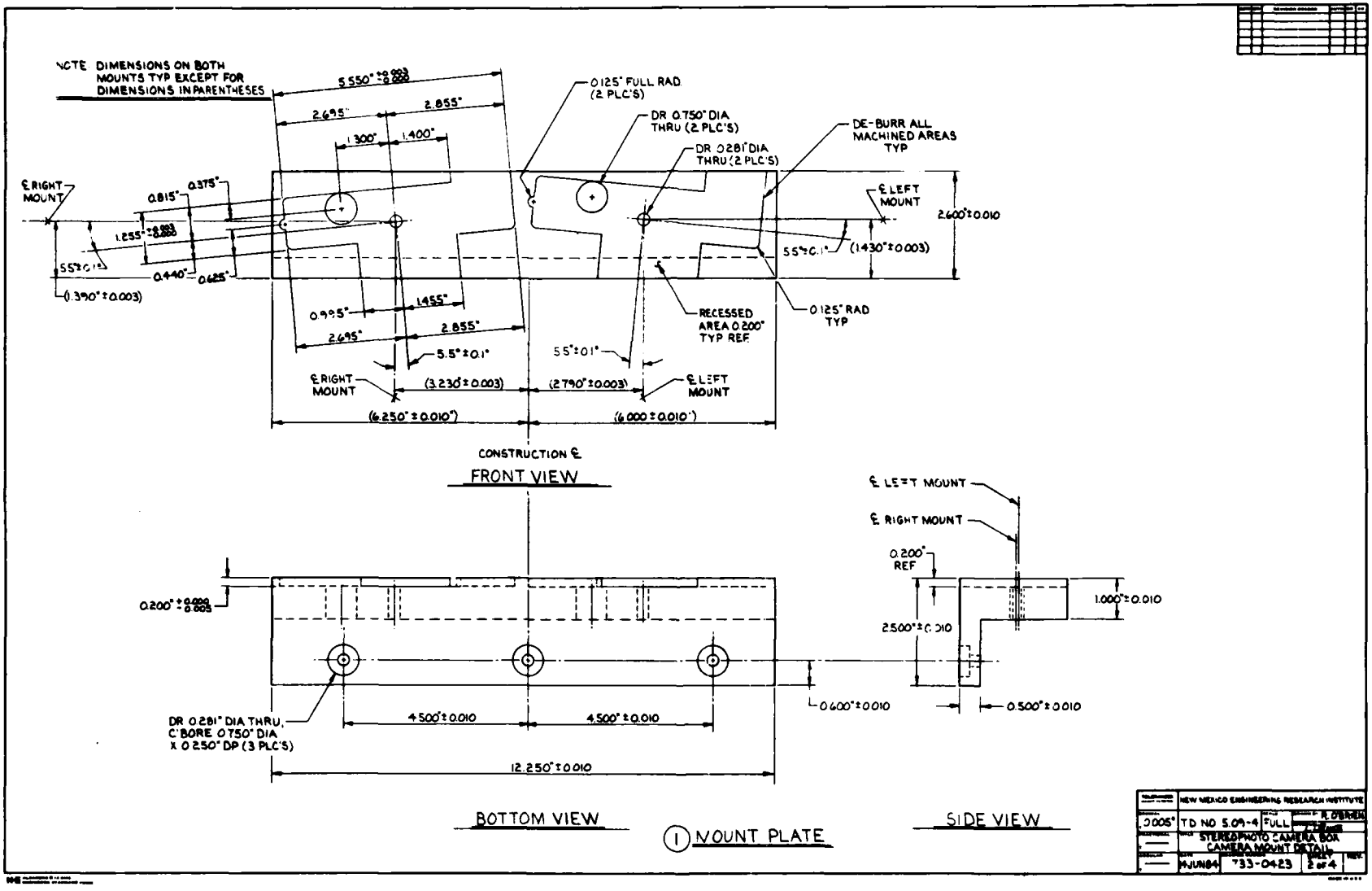

FIGURE C-6. STEREOPHOTO CAMERA BOX--CAMERA MOUNT DETAILS

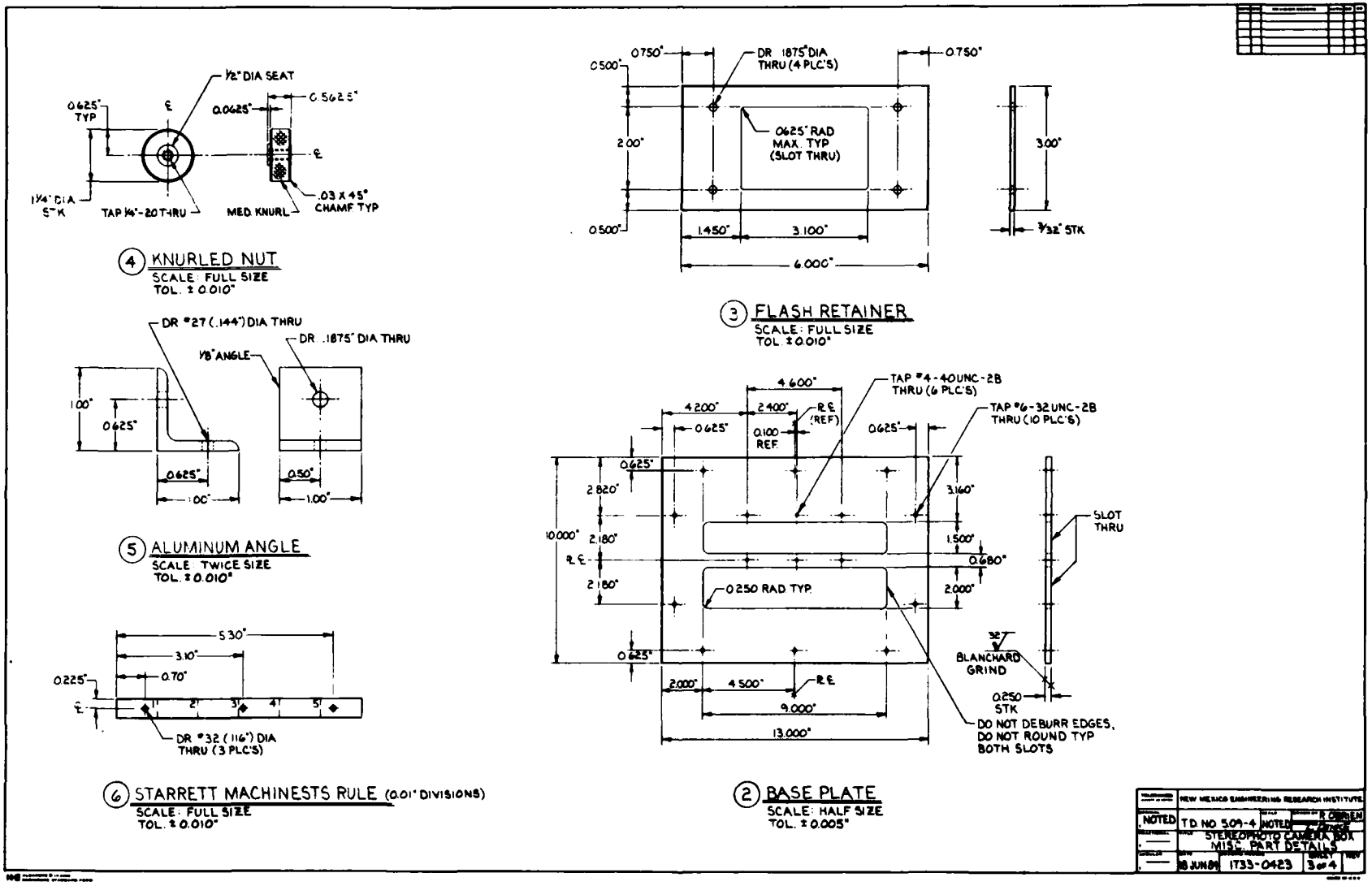

FIGURE C-7. STEREOPHOTO CAMERA BOX--MISCELLANEOUS PART DETAILS

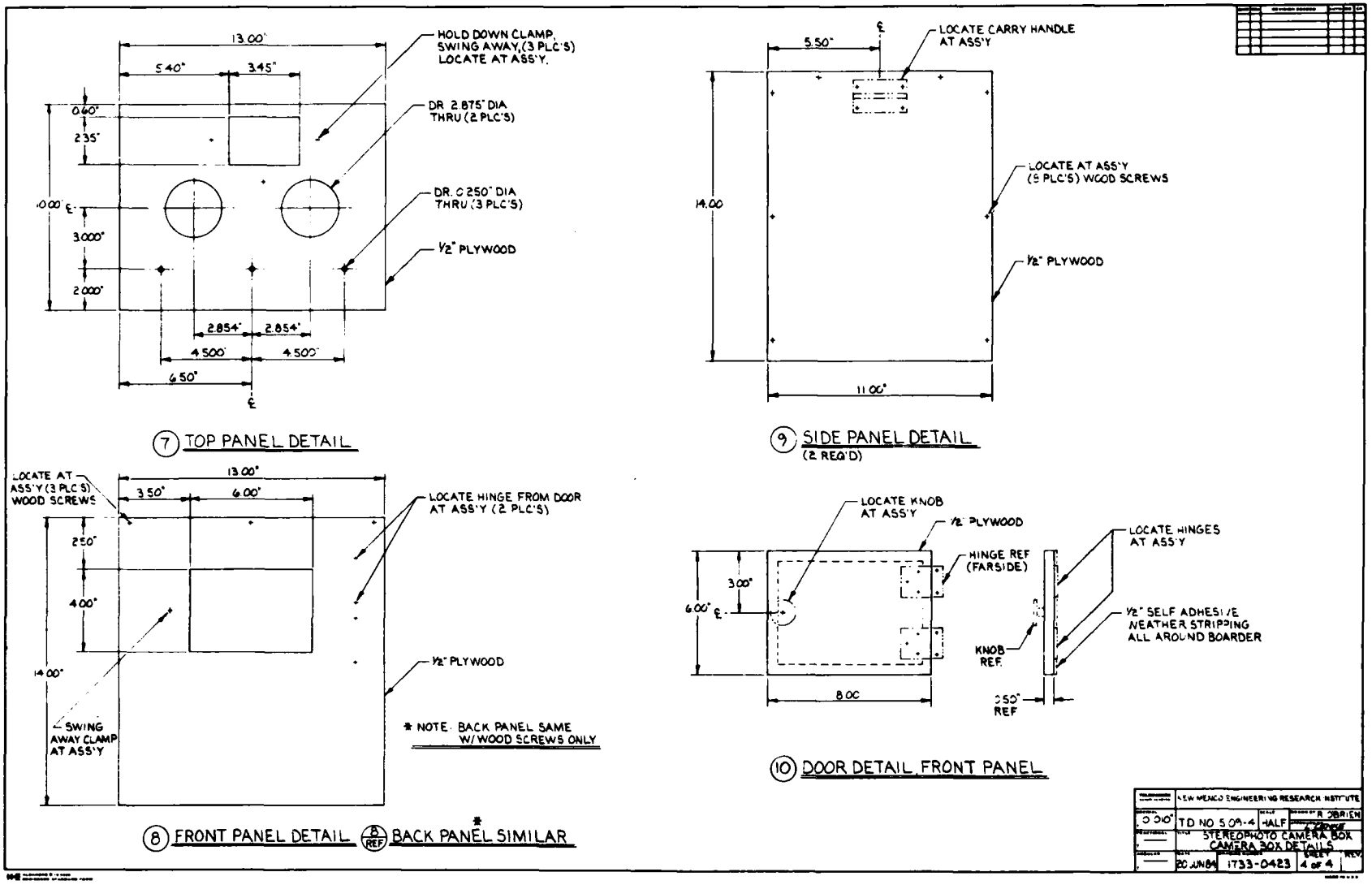

FIGURE C-8. STEREOPHOTO CAMERA BOX--CAMERA BOX DETAILS

APPENDIX D
MU-METER WATER NOZZLE DESIGNS EVALUATED

This appendix contains detailed fabrication drawings of the three nozzle designs fabricated and evaluated at NMERI. Figures D-1 and D-2 detail the UNM design (selected design), Figure D-3 illustrates the FAA design, and Figure D-4 shows the modified ASTM E274. The UNM design was ultimately selected for use with the Mu-Meter. A detailed discussion of the selection process is presented in Section VII.

Figures D-5 through D-7 provide details of a suggested nozzle design which may be appropriate for adoption as a standard. (This design is noted as Model GSL.) The Model GSL has the same flow characteristics as the UNM nozzle.

Full sized prints of these nozzles are available from NMERI upon request.

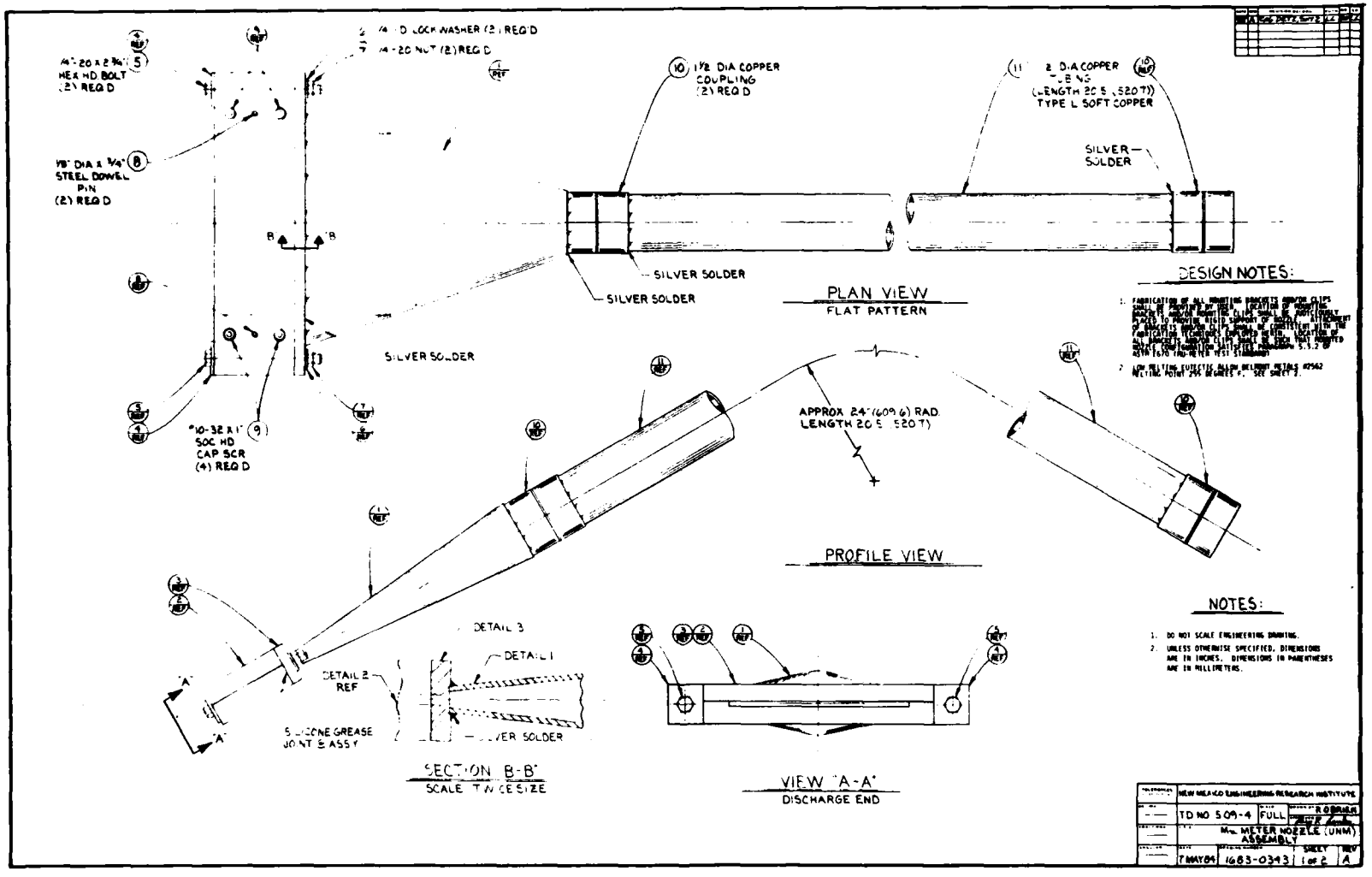

FIGURE D-1. MU-METER WATER NOZZLE (UNM)--ASSEMBLY

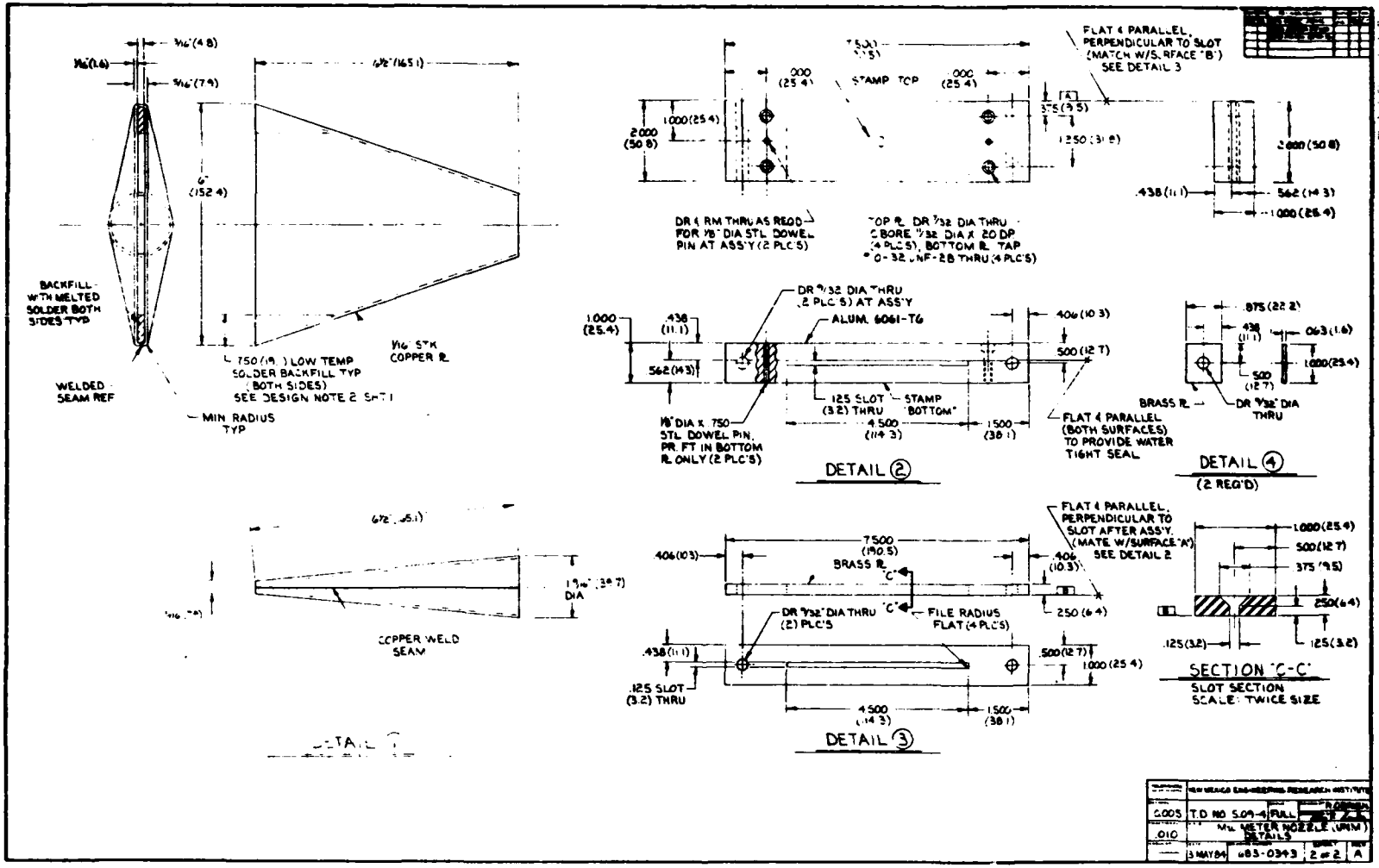

FIGURE D-2. MU-METER WATER NOZZLE (UNM)--DETAILS

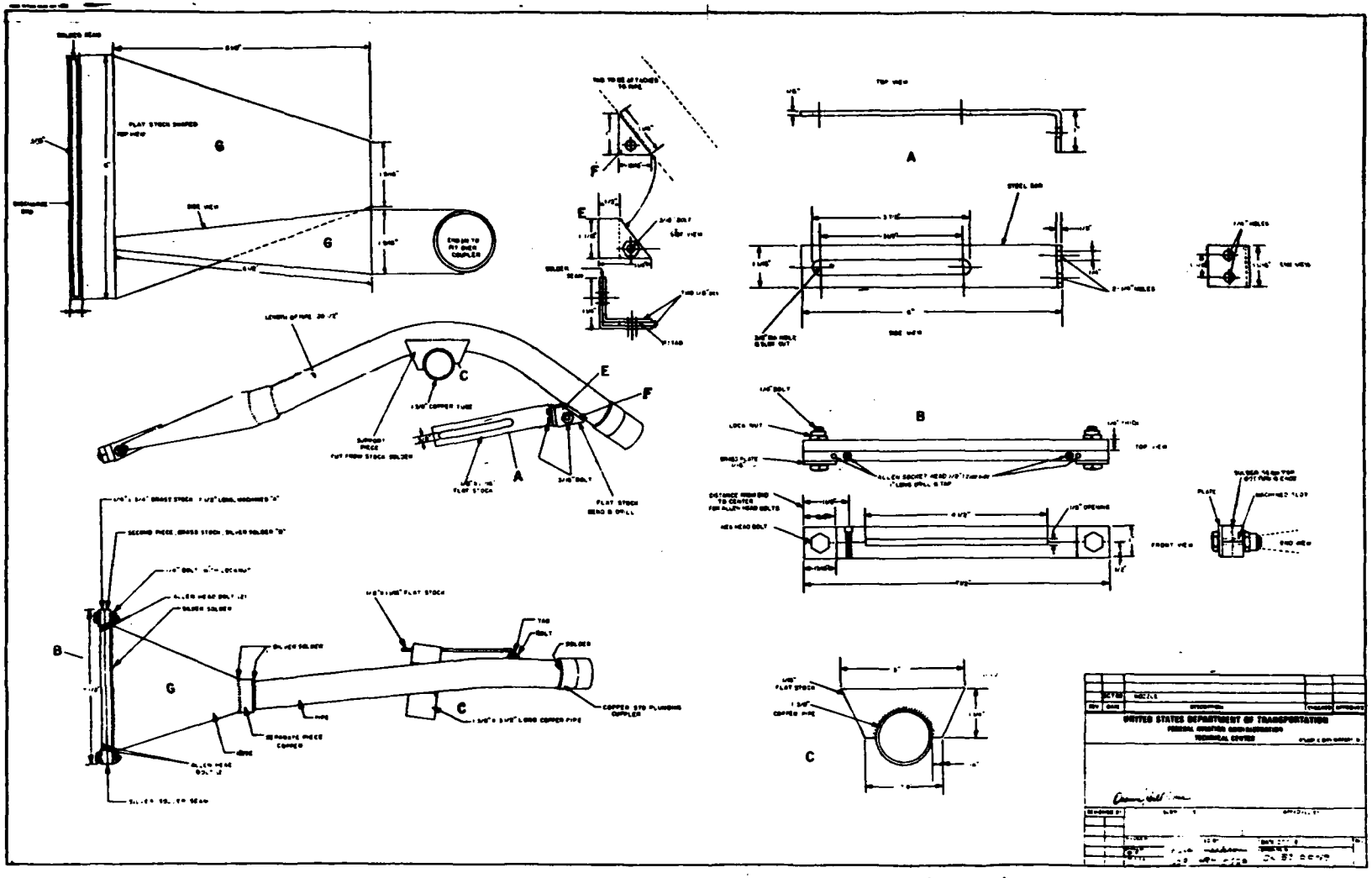

FIGURE D-3. MU-METER WATER NOZZLE--FAA DESIGN

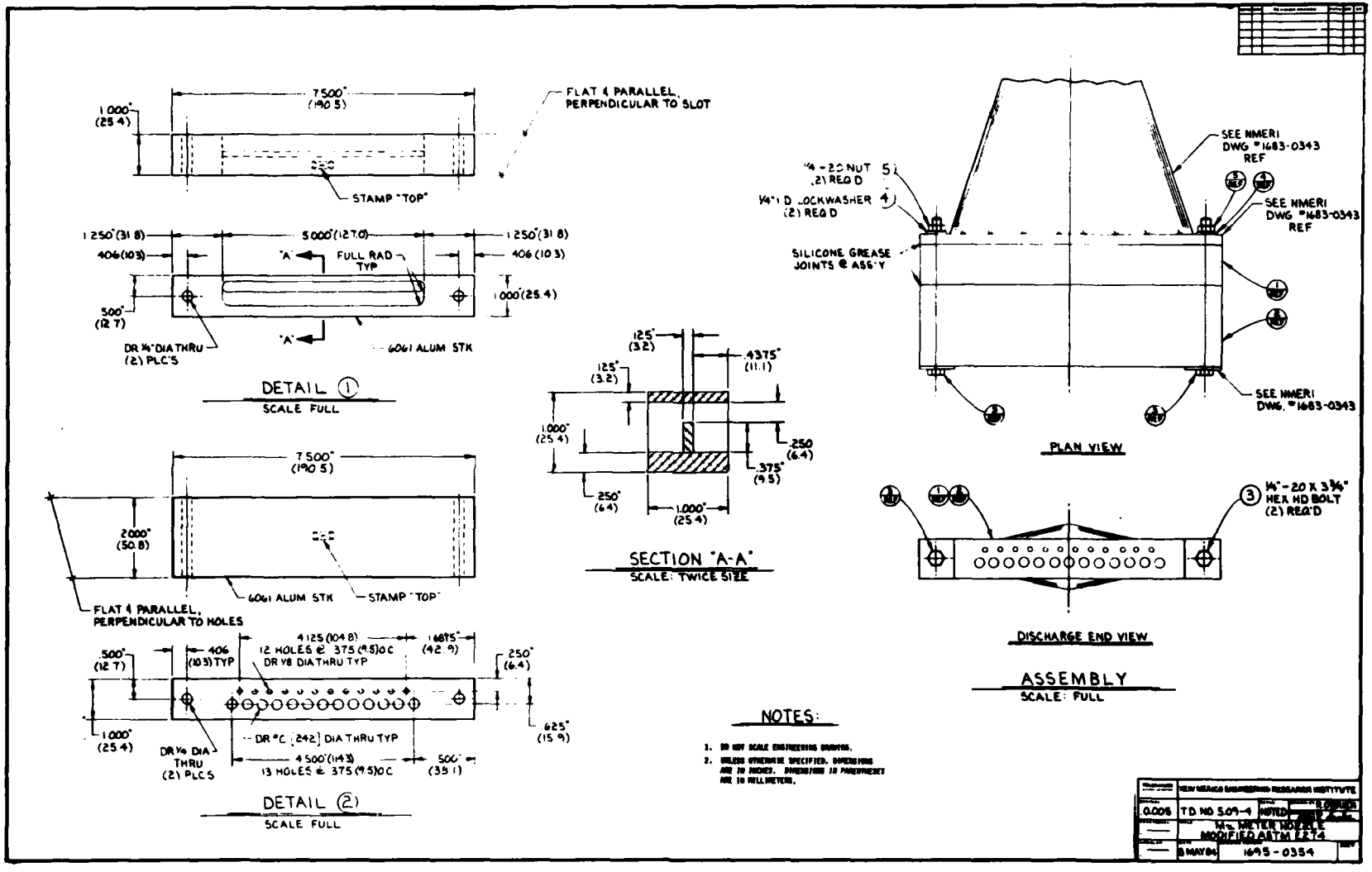

FIGURE D-4. MU-METER WATER NOZZLE--MODIFIED ASTM E274

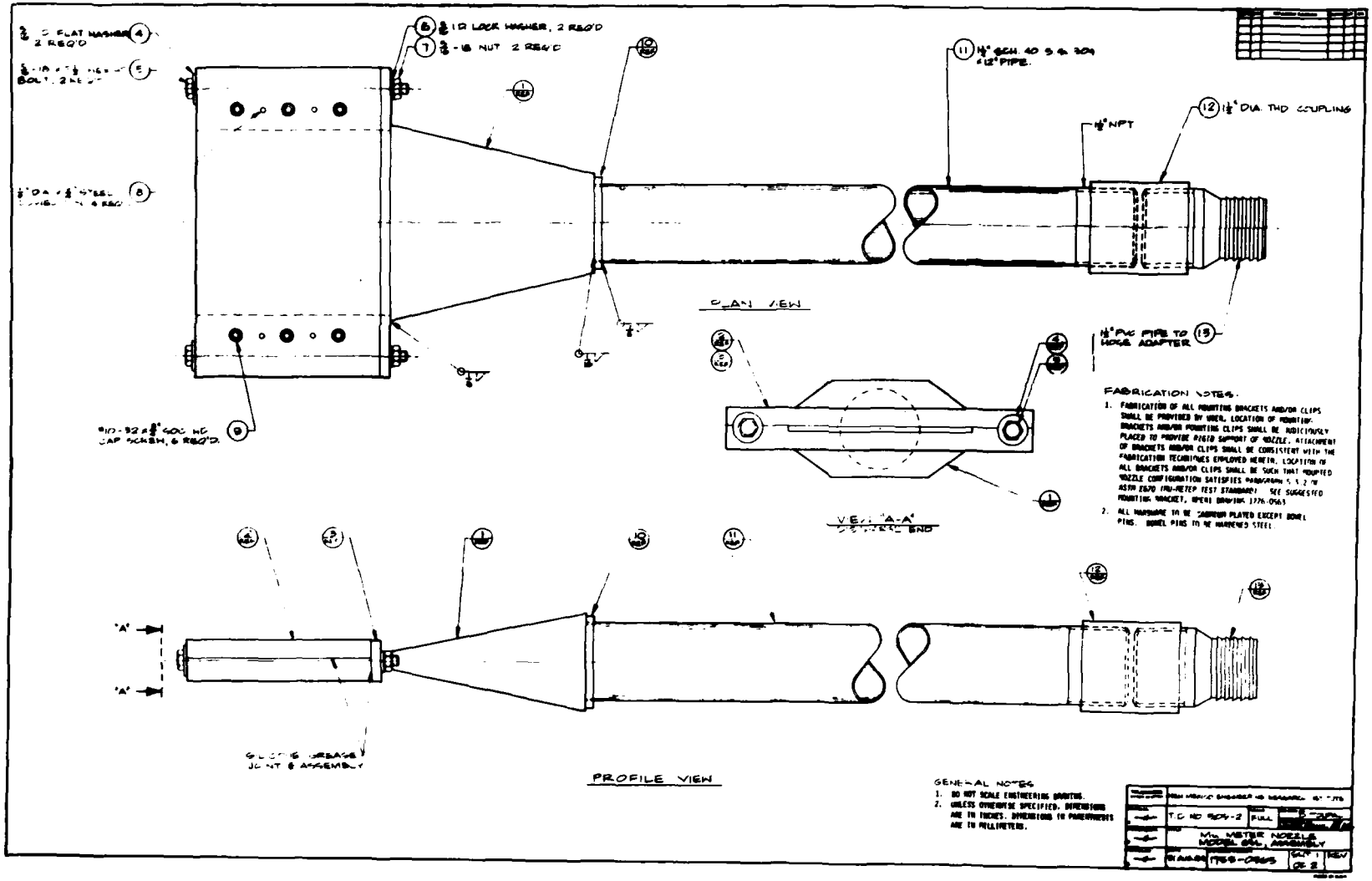

FIGURE D-5. MU-METER WATER NOZZLE, MODEL GSL--ASSEMBLY

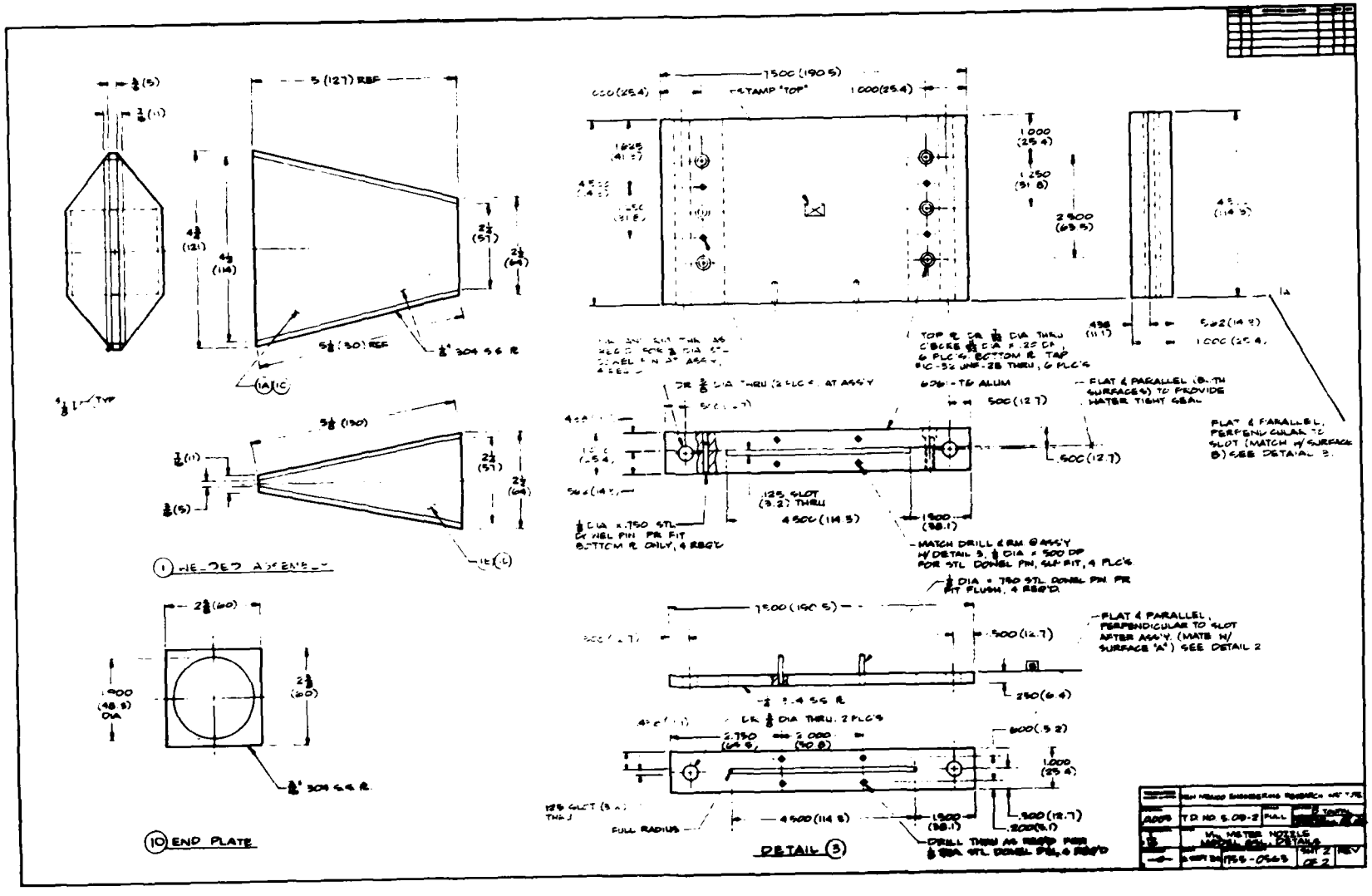

FIGURE D-6. MU-METER WATER NOZZLE, MODEL GSL--DETAILS

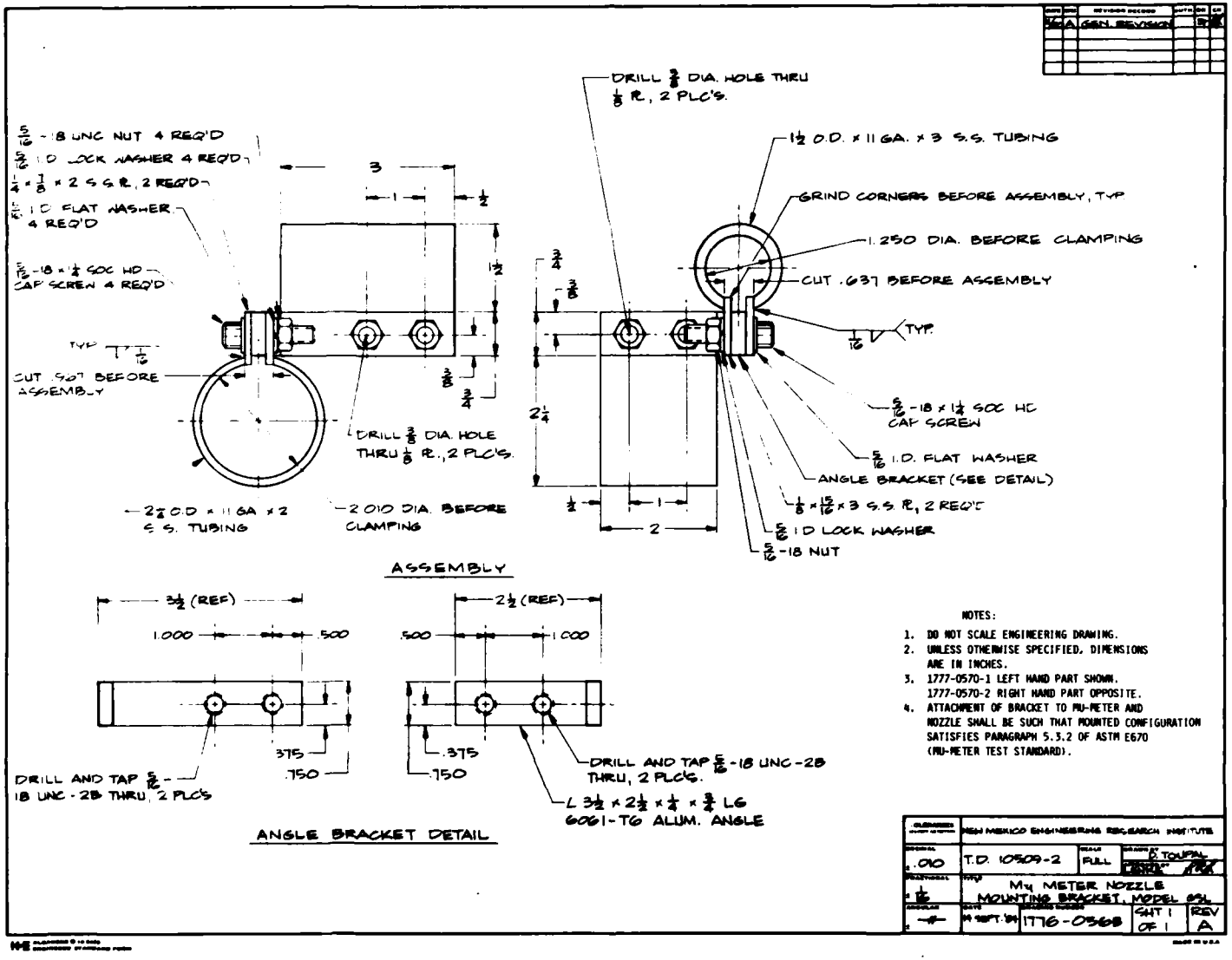

FIGURE D-7. MU-METER WATER NOZZLE, MODEL GSL--MOUNTING BRACKET

APPENDIX E

MU-METER WATER DISTRIBUTION SYSTEM ANALYSIS AND DESIGN

This appendix provides detailed computational information used in evaluating various pumping systems and nozzle designs for use during Mu-Meter testing at NMERI.

Two pump systems were evaluated for use with the FAA or UNM nozzle designs. These two pump systems were a 3/4-hp system with a 1 1/2-in pipe network (existing FAA design used during NRFMP) and a 3-hp system with a 2-in pipe network. The advantages of the larger system are clearly illustrated in this appendix, particularly for Mu-Meter testing at speeds to 60 mi/h. The larger system was eventually selected by NMERI for future field evaluation with the Mu-Meter.

An additional analysis was also conducted to ascertain the pump requirements for a nozzle capable of delivering a 1-mm water depth at a zero velocity relative to the pavement. The pump requirements were found to be quite large for such a nozzle design.

The first part of this appendix illustrates why the nozzle depth dimension must equal the specified water depth (in this case 1 mm) for zero relative velocity.

1. NOZZLE VELOCITIES

a. 40 mi/h test speed--

$$Q = V \cdot A$$

where

Q = volumetric flow rate
V = outlet velocity

and

A = cross sectional area of nozzle

$$Q = (3520 \text{ ft/min})\,(4.5 \text{ in})\,(0.04 \text{ in})\left(\frac{1 \text{ ft}}{12 \text{ in}}\right)^2$$

$$= 4.40 \text{ ft}^3/\text{min per nozzle}$$

For a nozzle 1/8 x 4.5 in

$$V = \frac{Q}{A} = \frac{4.40 \text{ ft}^3/\text{min}}{(4.5 \text{ in})(0.125 \text{ in})}\left(\frac{12 \text{ in}}{\text{ft}}\right)^2$$

$$V = 1126 \text{ ft/min} = 12.8 \text{ mi/h}$$

Velocity relative to pavement, V_R

$$V_R = 40 \text{ mi/h} - 12.8 \text{ mi/h} = 27.2 \text{ mi/h}$$

b. 60 mi/h test speed--

$Q = 6.60\ ft^3/min$

For 1/8 in nozzle

$$V = \frac{Q}{A} = \frac{6.60}{(4.5)(0.125)}(12)^2$$

$V = 1690\ ft/min = 19.2\ mi/h$

$V_R = 60 - 19.2 - 40.8\ mi/h$

For a relative velocity of zero, the nozzle depth dimension must equal the specified water depth. e.g.,

$V = 40\ mi/h,\ Q = 4.40\ ft^3/min,\ L = 4.5\ in$

$$A = \frac{Q}{V} = t \cdot L$$

$t = 0.040\ in = 1\ mm$

where
t and L = depth and width dimenison of the nozzle

2. PUMP DESIGN

To determine pump requirements, two details are needed i.e., flow requirements and system head loss characteristics.

a. Flow requirements (for FAA nozzle*)--

(1) V = 40 mi/h--

$$Q = V \cdot A$$

$$= 2(3520\ ft/min)(4.5\ in)(0.04\ in)\left(\frac{1\ ft}{12\ in}\right)^2$$

$Q_{40} = 8.8\ ft^3/min$

$= 65.82\ gal/min \sim 65\ gal/min$

(2) V = 60 mph

$$Q = 2(5280\ ft/min)(4.5\ in)(0.04\ in)\left(\frac{1\ ft}{12\ in}\right)^2$$

$Q_{60} = 13.2\ ft^3/min$

$= 98.74\ gal/min \sim 100\ gal/min$

*The UNM nozzle is similar to the FAA nozzle in terms of outlet dimensions and head loss characteristics.

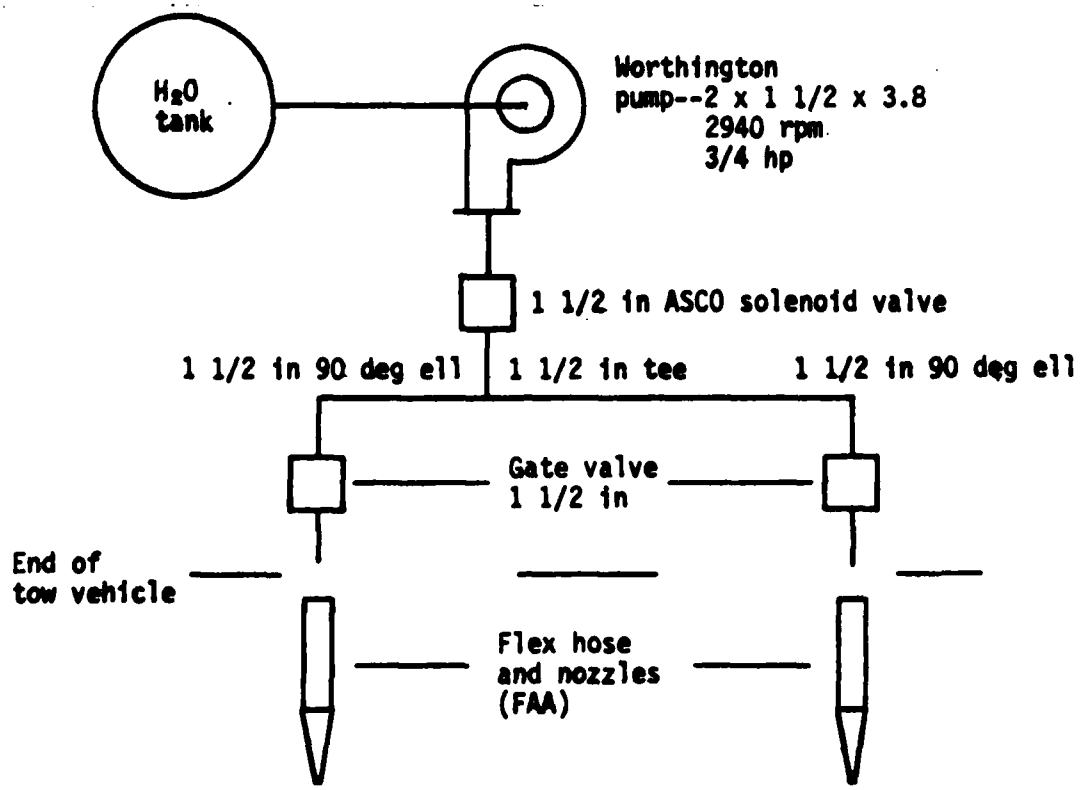

FIGURE E-1. MU-METER WATER DISTRIBUTION SYSTEM (FAA)

b. System head loss--

(1) Existing FAA system (used in NRFMP) with FAA nozzle (Fig. E-1)--

(a) Head losses at 40 mph, Q = 65 gal/min--

Solenoid valve (ASCO 1 1/2 in Series 8210)
From Table E-1

$$C_v = 22.5$$

From Figure E-2 (liquid flow graph)

$$F_{sg} = 1,\ F_t = 1$$

$$F_g = \frac{GPM}{C_v\ F_{sg}} = \frac{65}{22.5} = 2.89$$

where

C_v = coefficient of contraction (flow factor)

$F_{sg} = \frac{1}{\sqrt{S.G.}}$, S.G. being specific gravity of fluid

F_t = temperature correction factor

F_g = graph factor (Figure E-2)

Pressure drop across solenoid valve is

$$8.2\ lb/in^2 = 19.0\ ft$$

TABLE E-1. SPECIFICATIONS FOR ASCO 8210 SOLENOID VALVES

Pipe Size (ins.)	Orifice Size (ins.)	Cv Flow Factor	Operating Pressure Differential (psi) Minimum	Maximum Air-Inert Gas AC	Maximum Air-Inert Gas DC	Maximum Water AC	Maximum Water DC	Light Oil @ 300 SSU AC	Light Oil @ 300 SSU DC	Maximum Fluid Temp. °F. AC	Maximum Fluid Temp. °F. DC	Type 1 General Purpose Solenoid Enclosure Catalog Number	Constr. Ref. No. ①	UL Listing	Types 4 and 7 (C and D) Watertight and Explosion-Proof Solenoid Enclosure Catalog Number	UL Listing	Watt Rating/ Class of Coil Insulation AC	Watt Rating/ Class of Coil Insulation DC
NORMALLY CLOSED OPERATION, Forged Brass Body, Buna "N" or Teflon⑤ Seating for General Service																		
¼	5/16	1.2	5	125	—	120	—	—	—	180	—	8210B20	3D	•	—	—	6.5/B	—
⅜	¼	1.2	5	125	—	125	—	—	—	180	—	8210B21	3D	•	—	—	6.5/B	—
	⅜	1.5	①	125	40	125	40	—	—	180	150	8210C73⑤	1P	•	8211C73⑤	•	6/A	11.2/A
	⅜	3	0	100	40	100	40	—	—	180	150	8210C93	5D	●	8211C93	●	11/A	11.2/A
	⅜	3	5	200	125	135	100	135	100	180	150	8210D1	6D	●	8211D1	●	6/A	11.2/A
	⅜	3	5	300	—	300	—	300	—	175	—	8210C6	5D	●	8211C6	●	16.7/F	—
½	7/16	2.2	①	125	40	125	40	—	—	180	150	8210A15	2P	•	8211A15	•	6/A	11.2/A
	½	4	5	200	125	135	100	135	100	180	150	8210D2	6D	●	8211D2	●	6/A	11.2/A
	½	4	0	100	40	100	40	—	—	180	150	8210C94	5D	●	8211C94	o	11/A	11.2/A
	½	4	5	300	—	300	—	300	—	175	—	8210C7	5D	●	8211C7	o	16.7/F	—
¾	⅜	5	0	100	40	100	40	—	—	180	150	8210D95	8D	o	8211D95	o	11/A	11.2/A
	¾	5	5	125	100	125	90	125	75	180	150	8210D9	9D	o	8211D9	o	6/A	11.2/A
	¾	6	0	350	200	300	180	200	180	200	77	8210B26⑤	10P	⑤	8211B26⑤	⑤	15.4/A	30.6/H
	¾	6.5	5	250	125	150	125	100	125	180	150	8210D3	11D	o	8211D3	o	6/A	11.2/A
1	1	13	5	125	125	125	125	100	125	180	150	8210D4	12D	o	8211D4	o	6/A	11.2/A
	1	13.5	10	300	225	300	200	300	200	200	180	8210B78⑤	13P	⑤	8211B78⑤	⑤	16.7/F	16.8/A
	1	13.5	0	300	—	225	—	115	—	200	—	8210B27	14P	•	8211B27	•	20/F	—
	1	13	0	125	100	125	100	125	80	180	77	8210B54	31D	⑤	8211B54	⑤	15.4/A	30.6/H
1¼	1⅛	15	5	125	125	125	125	100	125	180	150	8210D8	16D	o	8211D8	o	6/A	11.2/A
	1⅛	15	10	300	225	300	200	300	200	200	180	8210B80⑤	17P	—	8211B80⑤	—	16.7/F	16.8/A
	1⅛	15	0	125	100	125	100	125	80	180	77	8210B55	32D	⑤	8211B55	⑤	15.4/A	30.6/H
1½	1⅛	22.5	5	125	125	125	125	100	125	180	150	8210D22	18D	o	8211D22	o	6/A	11.2/A
	1⅛	22.5	10	300	225	300	200	300	200	200	180	8210B82⑤	19P	—	8211B82⑤	—	16.7/F	16.8/A
	1⅛	22.5	0	125	100	125	100	125	80	180	77	8210B56	33D	⑤	8211B56	⑤	15.4/A	30.6/H
2	1⅜	43	5	125	50	125	50	90	50	180	150	8210100	20P	—	8211100	—	6/A	11.2/A
2½	1⅜	45	5	125	50	125	50	90	50	180	150	8210101	21P	—	8211101	—	6/A	11.2/A
3	3	101	10	250	—	250	—	250	—	200	—	8210B51①	22P	—	8211B51①⑤	—	28/H	—

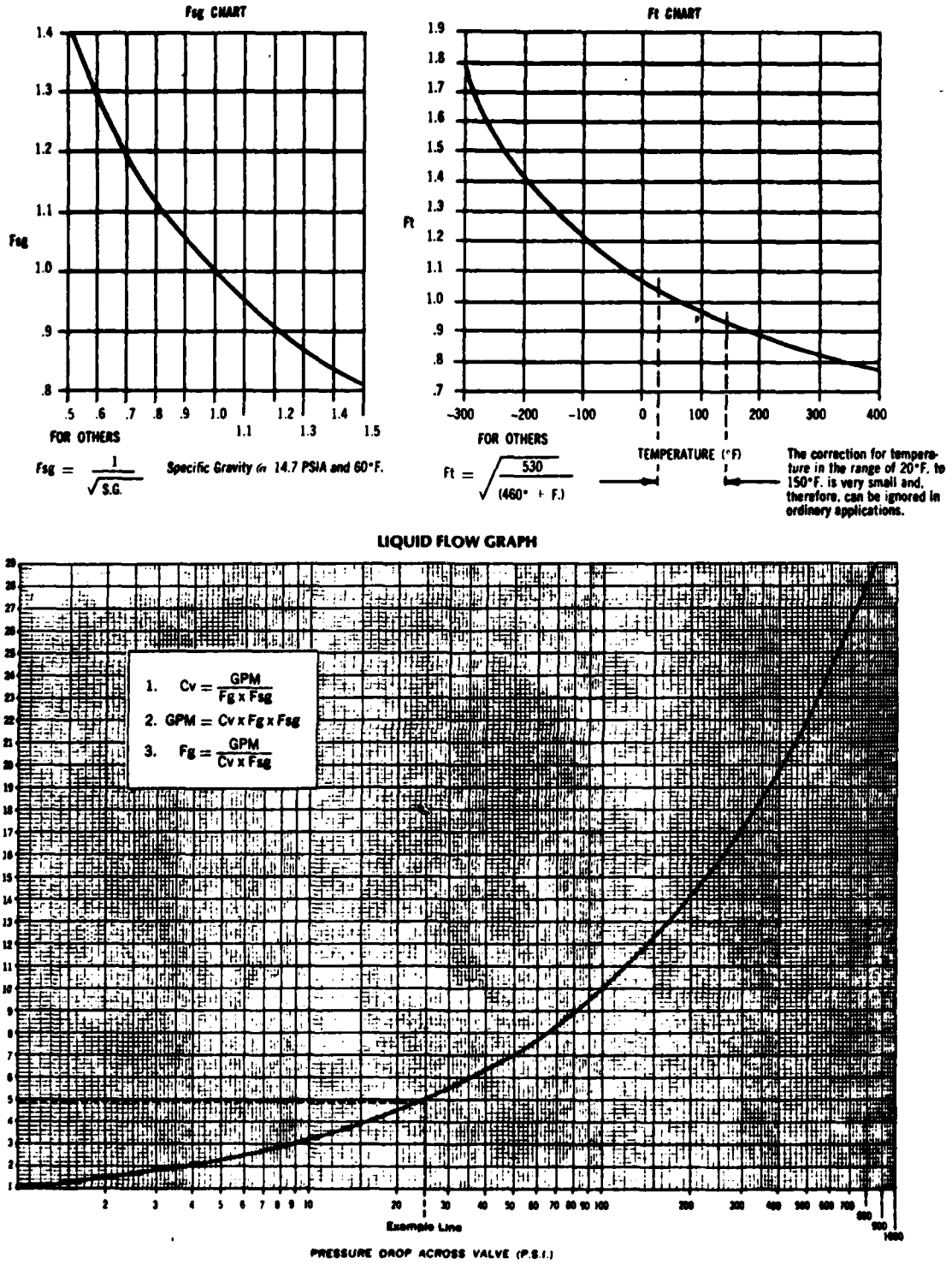

FIGURE E-2. GRAPH AND CORRECTION FACTORS FOR ASCO 8210 SOLENOID VALVE

1 1/2-in steel tee (screwed)

From Table E-2 (equivalent lengths for valves and fittings)

$\ell_{tee} = 9.9$ ft

From Table E-3 (pipe friction data)

Head loss per foot of pipe at 65 gal/min for 1 1/2-in pipe is

$$\left(0.53 \frac{ft}{ft}\right)\left(\frac{65}{70}\right)^2 = 0.457 \frac{ft}{ft}$$

Loss through tee = (9.9 ft)(0.457 ft/ft) = 4.5 ft

1 1/2-in steel 90-deg ell (screwed)

$\ell_{ell} = 7.4$ ft

1 1/2-in gate valve

$\ell_{gate} = 1.2$ ft

For flow at 35 gal/min (after tee) the head loss per foot of pipe is

$0.147 \frac{ft}{ft}$

Loss through ell and gate valve

$$= (8.6 \text{ ft})\ 0.147 \frac{ft}{ft} = 1.3 \text{ ft}$$

For an additional 15 ft (conservative extra) of 1 1/2 in pipe

$$\text{Loss} = (15 \text{ ft})\ 0.147 \frac{ft}{ft} = 2.2 \text{ ft}$$

Total head losses to the end of two vehicle for 40 mi/h = 27.0 ft

(b) Head losses at 60 mi/h, Q = 100 gal/min--

Solenoid valve

$C_v = 2.25$, $F_{sg} = 1$, $F_t = 1$

$$F_g = \frac{100 \text{ gal/min}}{22.5} = 4.44$$

Pressure drop across solenoid valve is

19 lb/in^2 = 43.9 ft

TABLE E2. EQUIVALENT LENGTH OF PIPE FOR VALVES AND FITTINGS FOR TURBULENT FLOW (Worthington Pump)

Fittings			Pipe Size, in																			
			1/4	3/8	1/2	3/4	1	1 1/4	1 1/2	2	2 1/2	3	4	5	6	8	10	12	14	16	18	20	21
Regular 90° ell	Screwed	Steel	2.3	3.1	3.6	4.4	5.2	6.6	7.4	8.5	9.3	11	13	---	---	---	---	---	---	---	---	---	---
		C.I.	---	---	---	---	---	---	---	---	---	9.0	11	---	---	---	---	---	---	---	---	---	---
	Flanged	Steel	---	---	.92	1.2	1.6	2.1	2.4	3.1	3.6	4.4	5.9	7.3	8.9	12	14	17	18	21	23	25	30
		C.I.	---	---	---	---	---	---	---	---	---	3.6	4.8	---	7.2	9.8	12	15	17	19	22	24	28
Tee (Branch Flow)	Screwed	Steel	2.4	3.5	4.2	5.3	6.6	8.7	9.9	12	13	17	21	---	---	---	---	---	---	---	---	---	---
		C.I.	---	---	---	---	---	---	---	---	---	14	17	---	---	---	---	---	---	---	---	---	---
	Flanged	Steel	---	---	2.0	2.6	3.3	4.4	5.2	6.6	7.5	9.4	12	15	18	24	30	34	37	43	47	52	62
		C.I.	---	---	---	---	---	---	---	---	---	7.7	10	---	15	20	25	30	35	39	44	49	57
Gate Valve	Screwed	Steel	.32	.45	.56	.67	.84	1.1	1.2	1.5	1.7	1.9	2.5	---	---	---	---	---	---	---	---	---	---
		C.I.	---	---	---	---	---	---	---	---	---	1.6	2.0	---	---	---	---	---	---	---	---	---	---
	Flanged	Steel	---	---	---	---	---	---	---	2.6	2.7	2.8	2.9	3.1	3.2	3.2	3.2	3.2	3.2	3.2	3.2	3.2	3.2
		C.I.	---	---	---	---	---	---	---	---	---	2.3	2.4	---	2.6	2.7	2.8	2.9	2.9	3.0	3.0	3.0	3.0

TABLE E3. FRICTION OF WATER IN PIPES (Worthington Pump)
(Loss of head in feet due to friction, per 100 feet of 15-year-old smooth iron pipe)

Gal per min.	1/8 inch pipe	1/4 inch pipe	3/8 inch pipe	1/2 inch pipe	3/4 inch pipe	1 inch pipe	1 1/4 inch pipe	1 1/2 inch pipe	2 inch pipe	2 1/2 inch pipe	3 inch pipe
1	121	28	6.4	2.1							
2		103	23.3	7.4	1.9						
3			49.0	15.8	4.1	1.26					
4			84.0	27.0	7.0	2.14	0.57	0.26			
5			126.0	41.0	10.5	3.25	0.84	0.40			
10				147.0	38.0	11.7	3.05	1.43	0.50	0.17	0.07
15					80.0	25.0	6.50	3.0	1.08	0.36	0.15
20					136.0	42.0	11.1	5.2	1.82	0.61	0.25
25						64.0	16.6	7.8	2.73	0.92	0.38
30						89.0	23.5	11.0	3.84	1.29	0.54
35						119.0	31.2	14.7	5.1	1.72	0.71
40						152.0	40.0	18.8	6.6	2.20	0.91
45							50	23.2	8.2	2.80	1.15
50							60	23.4	9.9	3.32	1.38
70							113	53.0	18.4	6.21	2.57
75								60.0	20.9	7.1	3.05
100								102	35.8	12.0	4.96
120								143	50.0	16.8	7.0
125									54	18.2	7.6
150									76	25.5	10.5
175									102	33.8	14.0
200									129	43.1	17.8
225										54.3	22.3
250										66	27.2
270											31.3
275											32.5
300											38.0

Fitting	Equivalent length	Frictional loss (ft/ft)	Head loss
Tee	9.9 ft	1.02	10.1 ft
Ell	7.4 ft	0.284	2.1 ft
Gate valve	1.2 ft	0.284	0.3 ft
Pipe (1 1/2 in)	15 ft	0.284	4.3 ft

Total head losses to the end of tow vehicle for 60 mph = 60.7

(c) Head losses in flex hose and FAA nozzle (1/8 in x 4.5 in cross section)--

The FAA calibration of the nozzle outflow volume was conducted by measuring pressure upstream for a known volumetric outflow. The pressure gages were placed after the gate valves and prior to the flexible hoses.

The FAA provided the calibration data in Table E-4 (by personal communication with Mr. Tom Morrow).

TABLE E-4. FAA WATER NOZZLE CALIBRATION

Velocity, mi/h	Pressure, lb/in^2	Flow rate (per nozzle), ft^3/min	V_2, ft/s	V_1, ft/s
20	1.5	2.2	9.4	3.0
40	4	4.4	18.8	6.0
60	9	6.6	28.2	9.0

Notes: V_2 = nozzle outlet velocity
V_1^2 = velocity at pressure gage (1 1/2 in cross section)

The calibration given in Table E-4 was found to agree favorably with later calibrations performed at NMERI.

Using Bernoulli's equation

$$\frac{p_1}{\gamma} + \frac{V_1^2}{2g} = \frac{p_2}{\gamma} + \frac{V_2^2}{2g} + h_L$$

$$h_L = \frac{p_1}{\gamma} + \frac{V_1^2 - V_2^2}{2g}$$

where

$\frac{p}{\gamma}$ = pressure-head term

$\frac{V^2}{2g}$ = velocity-head term

and

h_L = frictional-head loss term.

The head losses through the flex hose and nozzle were calculated to be

Velocity (mi/h)	h_L
60	9.7 ft
40	4.3 ft
20	2.2 ft

Therefore the frictional head losses through the existing FAA system are

40 mi/h: h_L = 27.0 ft + 4.3 ft = 31.3 ft

60 mi/h: h_L = 60.7 ft + 9.7 ft = 70.4 ft

The head losses above do not include the velocity head at the nozzle exit. The velocity head increases the total head (h_T) requirements to

40 mi/h: h_T = 31.3 ft + 5.5 ft = 36.8 ft

60 mi/h: h_T = 70.4 ft + 12.3 ft = 82.7 ft

Comparing these values with the pump rating curves (Figure E-3) at 2940 rev/min indicates the shortcomings of a 3/4 hp D.C. system. In both cases the total head requirements are greater than the pump developed head.

(2) Proposed system with FAA nozzle--Reduction of head losses can be affected by 1) enlargement of pipe network (use 2 in- instead of 1 1/2-in pipe) and 2) use of a Y instead of a Tee. The proposed system incorporates only 1) above, as 2) is difficult to incorporate due to space limitations. Also, the pump has a 4.25-in impellar and is operated at 3500 rev/min.

(a) Head losses at 40 mi/h, Q = 65 gal/min--

Solenoid valve (2 in)

C_v = 43

$$F_g = \frac{\text{gal/min}}{C_v} = \frac{65}{43} = 1.51$$

Drop across solenoid valve is

2 lb/in^2 = 4.6 ft

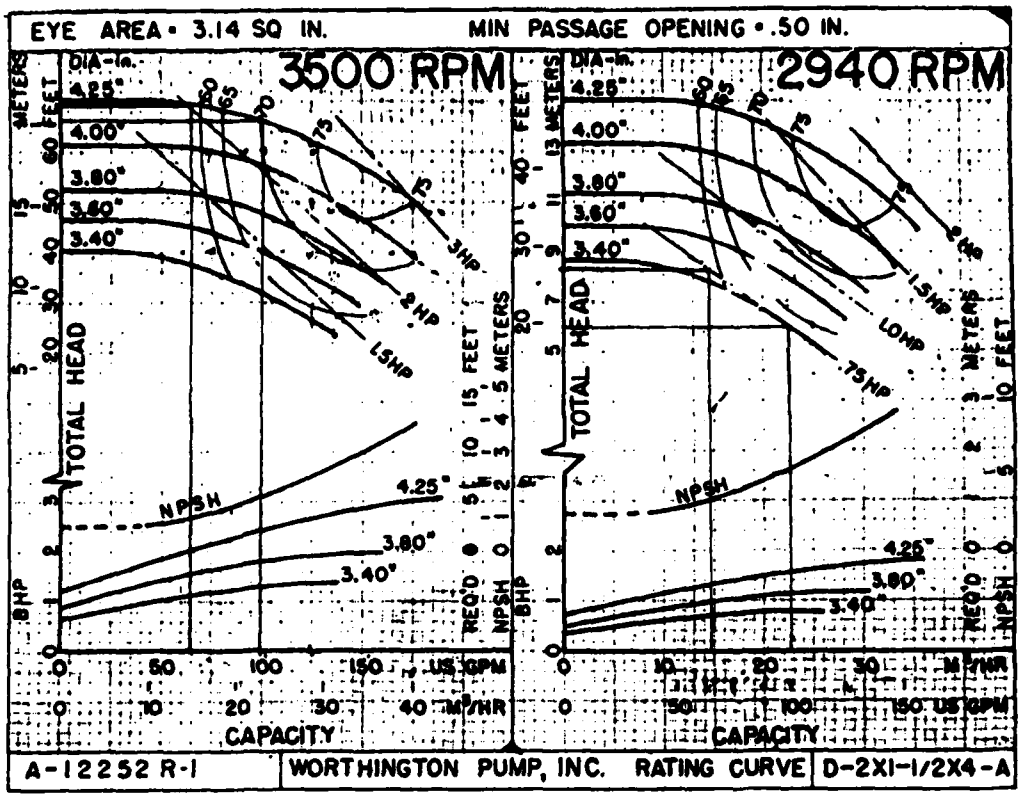

FIGURE E-3. RATING CURVE FOR WORTHINGTON PUMP

Fitting	Equivalent length	Frictional loss (ft/ft)	Head loss
Tee (2 in)	12 ft	$0.184 \left(\frac{65}{70}\right)^2$	1.9 ft
Ell (2 in)	8.5 ft	0.051	0.4 ft
Gate valve (2 in)	1.5 ft	0.051	0.1 ft
Pipe (2 in)	15 ft	0.051	0.8 ft

Head loss through flex hose and FAA nozzle = 4.3 ft

Total frictional head losses = 12.1 ft
Velocity head at 40 mi/h = 5.5 ft
Required pump head at 40 mi/h = 17.6 ft

(b) Head losses at 60 mph, Q = 100 gal/min--

Solenoid valve (2 in)

$C_v = 43$

$$F_g = \frac{100}{43} = 2.33$$

Solenoid valve head loss = 5.2 lb/in^2 = 12.0 ft

Fitting	Equivalent length	Frictional loss (ft/ft)	Head loss
Tee (2 in)	12 ft	0.358	4.3 ft
Ell (2 in)	8.5 ft	0.099	0.8 ft
Gate valve (2 in)	1.5 ft	0.099	0.1 ft
Pipe (2 in)	15 ft	0.099	1.5 ft

Head loss through flex hose and FAA nozzle = 9.7 ft

Total frictional head losses = 28.4 ft
Velocity head at 60 mi/h = 12.3 ft
Required pump head at 60 mi/h = 40.7 ft

Comparison of pump head requirements with pump rating curves shows

1) Existing 3/4 hp (D.C.) pump satisfactory for 40 mi/h

2) For 60 mi/h larger motor and/or pump are required. D.C. pumps larger than 3/4 hp are not readily available (they are usually custom designed and built); therefore, an A.C. system is required.

(3) Proposed system with 1 mm nozzle--To determine head losses through such a system the head losses of a 1-mm nozzle must be determined. The head loss at a sudden contraction (nozzle) is governed by

$$h_L = \frac{kV^2}{2g}$$

where
k = loss coefficient
V = the downstream velocity (outlet velocity)
and
g = gravitational acceleration. Rearranging this equation

$$V = \sqrt{\frac{2gh_L}{k}}$$

Recall $Q = V \cdot A$
For a rectangular nozzle

$$Q = \frac{2gh_L}{k} \cdot L \cdot t$$

where
L = nozzle width
and
t = nozzle depth

For similar nozzles (similitude)

$$\frac{Q_1}{Q_2} = \frac{\sqrt{h_1/k_1}}{\sqrt{h_2/k_2}} \frac{L_1 t_1}{L_2 t_2}$$

where subscript 1 is associated with the FAA nozzle (1/8 in depth) and subscript 2 is associated with a 1-mm nozzle.

For a required water depth of 1 mm, $Q_1 = Q_2$ and $L_1 = L_2$ for both nozzles. Therefore,

$$\sqrt{\frac{h_2}{k_2}} = \sqrt{\frac{h_1}{k_1}} \frac{t_1}{t_2}$$

or

$$h_2 = h_1 \frac{k_2}{k_1} \left(\frac{t_1}{t_2}\right)^2$$

To determine the k values a plot of reduction k value (Figure E-4) for circular pipe versus diameter ratio was used as follows. Since diameter is proportional to area to the 1/2 power, an area ratio to the 1/2 power was calculated and plotted on Figure E-4 to estimate k.

(a) 40 mi/h, Q = 65 gal/min--

Head losses exclusive of flex hose and nozzle = 7.8 ft

$$\text{Velocity head} = \frac{(58.67 \text{ ft/s})^2}{2(32.2 \text{ ft/s}^2)} = 53.4 \text{ ft}$$

Head loss through hose and nozzle

$$h = (4.3 \text{ ft})\left(\frac{0.38}{0.31}\right)\left(\frac{0.125}{0.040}\right)^2 = 51.5 \text{ ft}$$

Total pump head required for 40 mi/h at 1-mm water depth = 112.7 ft

(b) 60 mi/h, Q = 100 gal/min--

Head loss exclusive of flex hose and nozzle = 18.7 ft

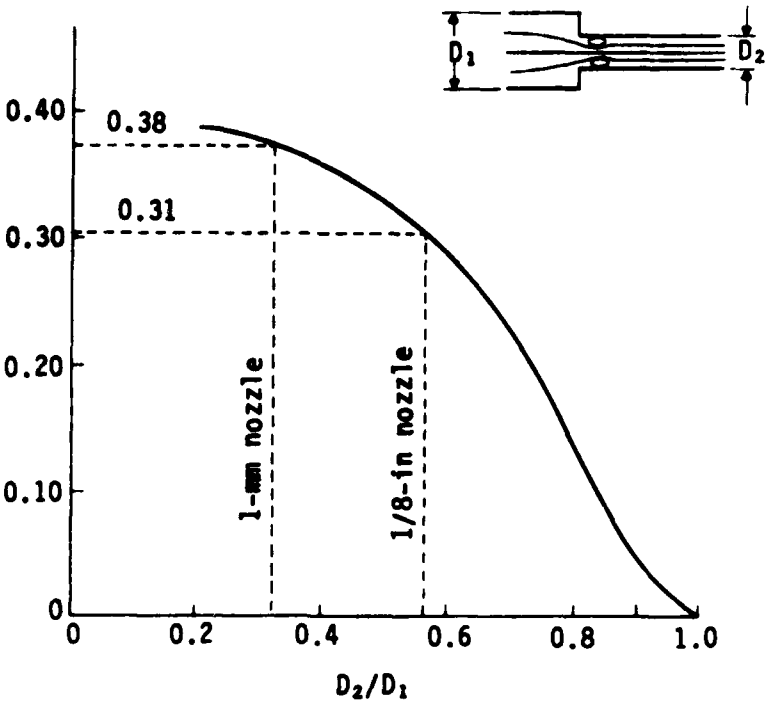

FIGURE E-4. k VERSUS SQUARE ROOT OF AREA RATIO (D_2/D_1), (Ref. 51)

$$\text{Velocity head} = \frac{(88\ \text{ft/s})^2}{2(32.2\ \text{ft/s}^2)} = 120.2\ \text{ft}$$

Head loss through hose and nozzle

$$h = (9.7\ \text{ft})\left(\frac{0.38}{0.31}\right)\left(\frac{0.125}{0.040}\right)^2 = 116.1\ \text{ft}$$

Total pump head required for 60 mi/h at 1-mm water depth = 255.0 ft

The above analysis assumes little head loss in the flex hose, i.e., most of the loss occurs at the nozzle. Other similarity analyses indicate that the power of t_1/t_2 is cubic and not square.

The above discussion shows the large head requirements for a 1-mm water depth. Although the head losses can be calculated using various assumptions, the actual head loss can only be verified by measurement.

(c) Power requirements--

$$hp = \frac{Q\gamma h}{e}$$

---

51. Olson, R. M., **Essentials of Engineering Fluid Mechanics**, Intext Educational Publishers, New York, New York, 1973.

where

hp = required horsepower
Q = flow rate
h = head required
γ = density of water
e = efficiency of pump

For

e = 1.0 (100 percent)

and

V = 40 mi/h

$$hp = \frac{(8.8\ ft^3/min)(62.4\ lb/ft^3)(112.7\ ft)}{(1.0)(33{,}000\ \frac{ft\text{-}lb}{min}\ /hp)}$$

$$hp_{40} = 1.88\ hp$$

For

V = 60 mi/h

$$hp = \frac{(13.2\ ft^3/min)(62.4\ lb/ft^3)(255\ ft)}{(1.0)(33{,}000)}$$

$$hp_{60} = 6.36\ hp$$

Efficiencies typically range from 0.5 to 0.8 depending on pump size.

(d) Affect of nozzle depth on Q and h--

Recall that

$$Q = \sqrt{\frac{2gh}{k}} \cdot L \cdot t$$

or

$$\frac{Q_1}{Q_2} = \frac{\sqrt{h_1/k_1}}{\sqrt{h_2/k_2}} \cdot \frac{L_1 t_1}{L_2 t_2}$$

If t is reduced from 1 mm to 1/2 mm, then $t_2 = 1/2\ t_1$, but Q is also affected, i.e., $Q_2 = 1/2\ Q_1$

$$\sqrt{\frac{h_2}{k_2}} = \frac{Q_2}{Q_2} \sqrt{\frac{h_1}{k_1}} \cdot \frac{L_1 t_1}{L_2 t_2}$$

For $L_1 = L_2$

$$h_2 = h_1 \left(\frac{Q_2}{Q_1}\right)^2 \frac{k_2}{k_1} \left(\frac{t_1}{t^2}\right)^2$$

$$= h_1 \frac{1}{4} \frac{k_2}{k_1} \cdot 4$$

$$h_2 = h_1 \frac{k_2}{k_1}$$

But $k_2 \cong k_1$ (Figure E-4)
So, $h_2 \cong h_1$

In other words, the head requirements for 1/2-mm nozzle are similar to the head requirements of a 1-mm nozzle.

A comparison of the three combinations of pumping systems and nozzle designs is shown in Table E-5. Two pumping systems (3/4 hp with 1 1/2-in plumbing and 3 hp with 2-in plumbing) were evaluated with two nozzle designs (0.125- and 0.040-in opening). Table E-5 shows that the large pumping system with an FAA type nozzle is the most appropriate.*

Based on this analysis a pump system with 2-in plumbing and a 3-hp pump and motor were selected for Mu-Meter testing. The power for the pump motor was supplied by a 6.5 kW A.C. generator.

---

*The UNM nozzle is very similar to the FAA nozzle in terms of head loss characteristics.

TABLE E5. COMPARISON OF EVALUATED MU-METER WATER DISTRIBUTION SYSTEMS

	FAA system with FAA nozzle		Proposed system with FAA nozzle			Proposed system with 1 mm nozzle	
	40 mph	60 mph	40 mph		60 mph	40 mph	60 mph
Flow rate, gal/min	65	100	65		100	65	100
Pipe network size	1 1/2"	1 1/2"	2 "		2"	2"	2"
Head losses, ft							
System	27.0	60.7	7.8		18.7	7.8	18.7
Nozzle and flex hose	4.3	9.7	4.3		9.7	51.5	116.1
Outlet velocity, ft/s	18.8	28.2	18.8		28.2	58.7	88.0
Velocity head, ft	5.5	12.3	5.5		12.3	53.4	120.2
Total head, ft	36.8	82.7	17.6		40.7	112.7	255.0
Pump requirements							
hp, calculated							
(100 percent efficiency)	0.61	2.06	0.29		1.02	1.88	6.36
Pump capabilities (from rating curves)							
Power, AC/DC	DC	DC	DC	AC	AC	AC	AC
Speed, rpm	2940	2940	2940	3500	3500	---	---
hp	3/4	3/4	3/4	2	2.4	[a]3.76	[a]12.72
head, ft	27	19	27	69	66	---	---

[a]Pump curves not used; calculated for 50 percent efficiency

REFERENCES

1. Horne, W. B., **Evaluation of High-Pressure Water Blast With Rotating Spary Bar for Removing Paint and Rubber Deposits From Airport Runways, and Review of Runway Slipperiness Problems Created by Rubber**, NASA TMX-72797, National Aeronautics and Space Administration, Hampton, Virginia, 1975.

2. Carpenter, S. H., and Barenberg, E. J., **Rubber Removal From Porous Friction Coarse**, DOT/FAA/PM-83/31, U.S. Department of Transportation, Federal Aviation Administration, Washington, D.C., 1983.

3. McKeen, R. G., and Lenke, L. R., **Alternatives for Rubber Removal From Porous Friction Surfaces**, DOT/FAA/PM-84/28, U.S. Department of Transportation, Federal Aviation Administration, Washington, D.C., 1984.

4. Burk, D. O., **Effectiveness of Rubber Removal Processes at Six Air Force Bases**, AFCEC Memorandum 4-77, Air Force Civil Engineering Center, Tyndall Air Force Base, Florida, 1977.

5. Grisel, C., **A Summary of Runway Friction Changes Due to High-Pressure Water-Jet Cleaning Operations at Four Airports**, FAA-RD-75-218, U.S. Department of Transportation, Federal Aviation Administration, Washington, D.C., 1976.

6. Yager, T. J., **Factors Influencing Aircraft Ground-Handling Performance**, NASA TM-85652, National Aeronautics and Space Administration, Hampton, Virginia, 1983.

7. Moore, D. F., **The Friction of Pneumatic Tyres**, Elsevier Scientific Publishing Company, New York, New York, 1975.

8. Kummer, H. W., **Unified Theory of Rubber and Tire Friction**, Engineering Research Bulletin B-94, Pennsylvania State University, College of Engineering, University Park, Pennsylvania, 1966.

9. Kummer, H. W., and Meyer, W. E., **Measurement of Skid Resistance**, Symposium on Skid Resistance, ASTM STP-326, American Society for Testing and Materials, Philadelphia, Pennsylvania, 1962, pp. 3-28.

10. Browne, A. L., **Mathematical Analysis for Pneumatic Tire Hydroplaning, Surface Texture Versus Skidding: Measurements, Frictional Aspects, and Safety Features of Tire-Pavement Interactions**, ASTM STP-583, American Society for Testing and Materials, Philadelphia, Pennsylvania, 1975, pp. 75-94.

11. Horne, W. B., and Joyner, U. T., **Pneumatic Tire Hydroplaning and Some Effects on Vehicle Performance**, International Automative Engineering Congress, Society of Automotive Engineers, Detroit, Michigan, January 1965.

12. Moore, D. F., **Prediction of Skid-Resistance Gradient and Drainage Characteristics for Pavements**,, Highway Research Record 131, Highway Research Board, Washington, D.C., 1966, pp. 181-203.

13. Horne, W. B., **Status of Runway Slipperiness Research**, Presented at NASA Conference on Aircraft Safety and Operating Problems, Hampton, Virginia, October 18-20, 1976.

14. MacLennan, J. R., Wench, N. C., Josephson, P. D., and Erdmann, J. B., **National Runway Friction Measurement Program**, FAA-AAS-80-1, U.S. Department of Transportation, Federal Aviation Administration, Washington, D.C., 1980.

15. Williams, J. H., **Analysis of the Standard USAF Runway Skid Resistance Tests**, AFCEC-TR-75-3, Air Force Civil Engineering Center, Tyndall Air Force Base, Florida, 1975.

16. **Standard Test Method for Side Force Friction on Paved Surfaces Using the Mu-Meter**, ASTM Designation E-670-79, Annual Book of ASTM Standards, Vol. 04.03, American Society for Testing and Materials, Philadelphia, Pennsylvania, 1984.

17. **Mu-Meter Instruction and Servicing Manual**, M. L. Aviation Company, Ltd., White Watham Aerodrome, Maidenhead, Berkshire, England, January 1975.

18. **Standard Specification for Smooth-Tread Standard Tire for Special-Purpose Pavement Skid-Resistance Tests**, ASTM Designation E-524-82, Annual Book of ASTM Standards, Vol. 04.03, American Society for Testing and Materials, Philadelphia, Pennsylvania, 1984.

19. **Standard Test Method for Skid Resistance of Paved Surfaces Using a Full-Scale Tire**, ASTM Designation E-274-79, Annual Book of ASTM Standards, Vol. 04.03, American Society for Testing and Materials, Philadelphia, Pennsylvania, 1984.

20. Ballentine, G. D., **The Air Force Weapons Laboratory Skid Resistance Research Program, 1969-1974**, AFWL-TR-74-181, Air Force Weapons Laboratory, Kirtland Air Force Base, New Mexico, 1975.

21. Wambold, J. C., Henry, J. J., and Heymon, R. R., **Evaluation of Pavement Surface Texture Significance and Measurement Techniques**, Wear, Vol. 83, No. 2, 1982, pp. 351-368.

22. Leu, M. C., and Henry, J. J., **Prediction of Skid Resistance as a Function of Speed From Pavement Texture Measurements**, Transportation Research Record 666, Transportation Research Board, Washington, D.C., 1978, pp. 7-13.

23. Smith, L. L., and Fuller, S. L., **Florida Skid Correlation Study of 1967 Skid Testing With Trailers**, ASTM-STP-456, Highway Skid Resistance, American Society for Testing and Materials, Philadelphia, Pennsylvania, 1968, pp. 4-101.

24. Leland, T.J.W., Yager, T. J., and Joyner, U. T., **Effects of Pavement Texture on Wet-Runway Braking Performance**, NASA TN D-4323, National Aeronautics and Space Administration, 1968.

25. Gallaway, B. M., Epps, J. A., and Tomita, H., **Effects of Pavement Surface Characteristics and Textures on Skid Resistance**, Report No. 138-4, Texas Transportation Institute, Texas A&M University, College Station, Texas, 1971.

26. Henry, J. J., and Dahir, S. H., **Effects of Textures and the Aggregates that Produce Them on the Performance of Bituminous Surfaces**, Transportation Research Record 712, Transportation Research Board, Washington, D.C., 1979, pp. 44-50.

27. Olson, R. M., Johnson, J. H., and Gallaway, B. M., **Vehicle-Pavement Interaction Study**, Report No. 138-7F, Texas Transportation Institute, Texas A&M University, College Station, Texas, 1974.

28. Ashkar, B. H., **Development of a Texture Profile Recorder**, Research Report No. 133-2, Texas Highway Department, 1970.

29. Rose, J. G., Hutchinson, J. W., and Gallaway, B. M., **Summary and Analysis of the Attributes of Methods of Surface Texture Measurement**, ASTM STP-530, American Society for Testing and Materials, Philadelphia, Pennsylvania, 1973.

30. **Standard Test Method for Measuring Surface Macrotexture Depth Using a Sand Volumetric Technique**, ASTM Designation E-965-83, Annual Book of ASTM Standards, Vol. 04.03, American Society for Testing and Materials, Philadelphia, Pennsylvania, 1984.

31. Forster, S. W., **Aggregate Microtexture: Profile Measurement and Related Frictional Levels**, FHWA/RD-81/107, U.S. Department of Transportation, Federal Highway Administration, Washington, D.C., 1981.

32. Scrivner, F. H., and Hudson, W. R., **A Modification of the AASHO Read Test Serviceability Index Formula**, Record No. 46, Highway Research Board, Washington, D.C., 1964.

33. Schonfeld, R., **Photo-Interpretation of Pavement Skid Resistance in Practice**, Transportation Research Record 523, Transportation Research Board, Washington, D.C., 1974, pp. 65-75.

34. **Standard Test Method for Classifying Pavement Surface Textures**, ASTM Designation E-770-80, Annual Book of ASTM Standards, Vol. 04.03, American Society for Testing and Materials, Philadelphia, Pennsylvania, 1984.

35. Howerter, E. D., and Rudd, J. T., **Automation of the Schonfeld Method for Highway Surface Texture Classification**, Maryland State Highway Administration, Brooklandville, Maryland, 1975.

36. Holt, F. B., and Musgrove, G. R., **Surface Texture Classification: A Guide to Pavement Skid Resistance**, ASTM STP-763, Pavement Surface Characteristics and Materials, American Society for Testing and Materials, Philadelphia, Pennsylvania, 1982, pp. 31-44.

37. Cechetini, J. A., **The Effects of Studded Tires on Pavement Surfaces in California**, CA-TL-79-04, California Department of Transportation, Sacramento, California, 1979.

38. **Standard Method for Measuring Surface Frictional Properties Using the British Pendulum Tester**, ASTM Designation E-303-83, Annual Book of ASTM Standards, Vol. 04.03, American Society for Testing and Materials, Philadelphia, Pennsylvania, 1984.

39. Kummer, H. W., **The Penn State Drag Tester**, Report No. 7, Joint Road Friction Program, Pennsylvania Department of Highways, Pennsylvania State University, Department of Mechanical Engineering, University Park, Pennsylvania, 1963.

40. Kummer, H. W., **Correlation Tests With the Penn State Drag Tester**, Report No. 9, joint Road Friction Program, Pennsylvania Department of Highways, Pennsulvania State University, Department of Mechanical Engineering, University Park, Pennsylvania, 1964.

41. Her, I., Henry, J. J., and Wambold, J. C., **Development of a Data Acquisition Method for Noncontact Pavement Macrotexture Measurement**, Presented at the 63rd Annual Meeting of the Transportation Research Board, Washington, D.C., 1984.

42. Gee, S., King, W. L., Jr., and Hegmon, R. R., **Pavement Texture Measurement by Laser, A Feasiblity Study, Surface Texture Versus Skidding: Measurements, Frictional Aspects, and Safety Features of Tire-Pavement Interactions**, STP-583, American Society for Testing and Materials, Philadelphia, Pennsylvania, 1975, pp. 29-40.

43. Harr, M. E., and Elton, D. J., **Non-Contact, Non-Destructive Airport Pavement Profile, Texture, and Deflection Measurements**, DOT/FAA/PM-83/14, U.S. Department of Transportation, Federal Aviation Administration, Washington, D.C., 1983.

44. Veres, R. E., Henry, J. J., and Lawther, J. M., **Use of Tire Noise as a Measure of Pavement Macrotexture, Surface Texture Versus Skidding: Measurements, Frictional Aspects, and Safety Features of Tire-Pavement Interactions**, STP-583, American Society for Testing and Materials, Philadelphia, Pennsylvania, 1975, pp. 18-27.

45. Yager, T. J., and Bühlmann, F., **Macrotexture and Drainage Measurements on a Variety of Concrete and Asphalt Surfaces**, ASTM STP-763, Pavement Surface Characteristics and Materials, American Society for Testing and Materials, Philadelphia, Pennsylvania, 1982, pp. 16-30.

46. Gallaway, B. M., and Rose, J. G., **Macro-Texture, Friction, Cross Slope, and Wheel Track Depression Measurements on 41 Typical Texas Highway Pavements**, Report No. 138-2, Texas Transportation Institute, Texas A&M University, College Station, Texas, 1970.

47. Henry, J. J., and Hegmon, R. R., **Pavement Texture Measurement and Evaluation, Surface Texture Versus Skidding: Measurements, Frictional Aspects, and Safety Features of Tire-Pavement Interactions**, STP-583, American Society for Testing and Materials, Philadelphia, Pennsylvania, 1975, pp. 3-17.

48. Hill, B. J., and Henry, J. J., **Surface Materials and Properties Related to Seasonal Variations in Skid Resistance**, ASTM STP-763, Pavement Surface Characteristics and Materials, American Society for Testing and Materials, Philadelphia, Pennsylvania, 1982, pp. 45-60.

49. Hearst, P. J., **Reflective Coatings for Hangar Floors--Laboratory Studies and Initial Field Test Results**, TM No. 52-84-06, Naval Civil Engineering Laboratory, Port Hueneme, California, 1983.

50. Anderson, V. L., and McLean, R. A., **Design of Experiments, A Realistic Approach**, Marcel Dekker, Inc., New York, New York, 1974.

51. Olson, R. M., **Essentials of Engineering Fluid Mechanics**, Intext Educational Publishers, New York, New York, 1973.

END

FILMED

5-85

DTIC